R. & M. No. 3760

R. & M. No. 3760

PROCUREMENT EXECUTIVE, MINISTRY OF DEFENCE

AERONAUTICAL RESEARCH COUNCIL
REPORTS AND MEMORANDA

A Lifting Surface Theory Method for Treating Swept or Slender Wings in Attached Subsonic Flow

By W. Kellaway
British Aircraft Corporation Limited

LONDON: HER MAJESTY'S STATIONERY OFFICE
1975

PRICE £4·55 NET

A Lifting Surface Theory Method for Treating Swept or Slender Wings in Attached Subsonic Flow

By W. Kellaway

British Aircraft Corporation Limited

Reports and Memoranda No. 3760*
December, 1973

Summary

A lifting surface theory method is described, capable of calculating the loading distribution on swept or slender planforms in attached, subsonic flow. Preliminary numerical results are presented which demonstrate that the method produces accurate, convergent loading solutions.

* Replaces A.R.C. 35 352

LIST OF CONTENTS

1. Introduction

In the subsonic design of lifting wings, three-dimensional linearised theory makes a significant contribution. Within the framework of linearised theory, a major problem is the accurate solution of the integral equation for the loading on a thin lifting wing, i.e. the classical problem of lifting surface theory. In the classical lifting surface problem, the downwash at any point in the plane of the wing is given as an integral involving the (unknown) loading over the wing planform. There are two major problems involved in the solution of this equation,

(a) the choice of a suitable representation for the loading distribution, and

(b) the accurate evaluation of the integral involving the loading representation.

For planforms with smooth edge shapes, i.e. without slope discontinuities of leading or trailing edges, suitable loading representations are well defined (except in the neighbourhood of tip corners), and numerous lifting surface methods exist based on the pioneer method of Multhopp.[1] The method due to Garner[2] and the N.L.R. method[3] in particular, show considerable improvement over the basic Multhopp method but both these methods suffer from a loss of accuracy in evaluating the integral of the loading representation for downwash points in the neighbourhood of the leading edge.

The B.A.C. method[4] incorporates basically the same form of loading representation as used in the methods due to Multhopp,[1], Garner,[2] N.L.R.,[3] etc.... but achieves superior accuracy, particularly for downwash points in the neighbourhood of the leading edge, through the use of an integration technique in which the spanwise integration (along local chordwise coordinate lines) is performed before the chordwise integration. The accuracy that is achieved through this integration technique has been demonstrated in several documents, *see* e.g. Refs. 4, 5 and 6 for results from the B.A.C. method. Also, the datum method for rectangular planforms due to Ray and Miller[7] and the accurate method due to Sells[8] both employ this integration technique. However, the methods of Ray and Miller[7] and Sells[8] are confined to the evaluation of the downwash for a *known* loading; although recently Sells[9,10] has shown that his method can be combined with a lifting surface method of moderate accuracy to iterate to an accurate solution of the lifting-surface equation for a restricted class of wing geometries.

The lifting-surface theory methods developed for planforms with smooth edge shapes may be applied to planforms with edge slope discontinuities, i.e. cranked planforms, if the discontinuities are first removed by a suitable smoothing (or rounding) procedure. In fact, the B.A.C. method incorporating a rounding procedure is in regular use in wing design and loading calculations on current aircraft projects.[11] Although the use of a rounding procedure is a satisfactory compromise in the treatment of swept wings, i.e. wings of moderate aspect ratio, it is inappropriate to the treatment of slender wings, i.e. wings of small aspect ratio with pointed apexes.

These slender wings are relevant to the design of supersonic transport aircraft, quiet airbuses for high subsonic speeds, and possibly strike/fighter aircraft with supersonic capability, and would operate normally with wing flow which separates along the whole or part of the leading edge. Thus any theoretical technique for treating the wing flow must take account of the formation of detached vortex sheets. However, a lifting-surface theory method for treating the subsonic attached-flow problem would form an important stepping stone towards a more involved theory incorporating the modelling of free leading-edge vortex sheets and their interaction with the wing-loading distribution. Furthermore, if the flow is attached at some particular incidence, as current design philosophy[28] postulates it should be, the attached flow theory gives the lift slope and aerodynamic centre at this incidence.

The integration technique introduced in the B.A.C. method[4] for planforms with smooth edge shapes can be applied equally well for planforms with edge slope discontinuities; however, the choice of a suitable loading representation is a major problem. Although recent work by Brown and Stewartson,[12] Taylor,[13] Rossiter,[14] and Davies[15] (*nee* Rossiter), which followed the pioneer work of Germain[16] and Legendre,[17] succeeded in accurately defining the local loading behaviour in the neighbourhood of a leading or trailing-edge crank, the incorporation of the local behaviour into a suitable overall loading representation remained a major problem.

A lifting-surface theory method that incorporates the correct loading behaviour at the leading-edge centreline (apex) crank was developed at B.A.C. and is described in Ref. 18. The method was developed initially to assess the feasibility of incorporating the correct apex loading behaviour into the lifting-surface integral equation. In order to obtain results within a reasonable time scale the class of planforms originally treated was restricted to the cropped-delta type, and for a cropped-delta of aspect ratio 3 with 45 degrees leading edge sweep, covergent loading solutions are presented in Ref. 18. The successful treatment of the cropped-delta planform provided encouragement to extend the method to treat a wider class of planforms, and this extension is described in the present report.

Section 2 presents the classical integral equation of subsonic lifting-surface theory and discusses in general terms the method of solution. Section 3 discusses the derivation of a suitable loading representation and

highlights some inadequacies in the representation used in Ref. 18 which necessitated a change of coordinate system in the present work. Section 4 describes in some detail the integration techniques employed and Section 5 presents results for a range of planforms.

The results presented in Section 5 were obtained using a suite of computer programs written in standard FORTRAN and run on an IBM 360/65 computer. The programs are capable of treating symmetric pointed planforms of general apex angle, with curved leading edges and smooth trailing edges, with or without a finite tip chord. The leading and trailing edge geometry is defined through user-supplied subroutines, so that quite general planforms (within the restrictions of the last sentence) can be treated. However, the results presented in Section 5 are all for slender planforms, i.e. with the trailing edge normal to the free-stream direction; results for swept planforms will be presented in a future report.

The work described in this report was carried out at B.A.C. Military Aircraft Division, Preston, under research contract K5A/82 for the Procurement Executive, Ministry of Defence, and was monitored by Mr. J. H. B. Smith of the Aerodynamics Department, Royal Aircraft Establishment, Farnborough.

2. The Basic Integral Equation

The basic integral equation of subsonic lifting-surface theory relates the normal velocity distribution (downwash) to the pressure difference distribution on a thin wing and may be written in the form,

$$\frac{w}{U}(x_r, y_s) = -\frac{1}{8\pi}\iint_S \Delta Cp(x, y)\,.\,K(X, Y; M)\,dx\,dy. \tag{1}$$

The coordinate system is defined in Fig. 1, $w(x_r, y_s)$ is the normal velocity distribution (downwash), $\Delta Cp(x, y)$ is the distribution of pressure difference coefficient, (or loading), $\Delta Cp = (p_{\text{lower}} - p_{\text{upper}})/(\frac{1}{2}\rho U^2)$,

S is the projected wing planform in the plane $z = 0$,

U is the free stream velocity

and

M is the free stream Mach no.

The kernel function, K, is defined by,

$$K(X, Y; M) = \frac{1}{Y^2}\left(1 - \frac{X}{R}\right), \tag{2}$$

with

$$X = (x - x_r),$$
$$Y = (y - y_s),$$
$$R = \sqrt{X^2 + \beta^2 Y^2},$$

and where $\beta^2 = (1 - M^2)$.

The classical lifting-surface problem is the evaluation of the loading from equation (1) for a prescribed downwash distribution. Analytic solutions exist only for circular or elliptic planforms,[19] so that for arbitrary planforms numerical solutions must be sought. Only numerical solutions of the collocation type are considered here.

2.1. Collocation Solution

In the collocation solution of the basic integral equation, the loading distribution is represented by the sum of a finite number of known functions with unknown coefficients, i.e.,

$$\Delta Cp = \sum_{i=0}^{n-1}\sum_{j=0}^{m-1} a_{ij} C_{ij}(x, y). \tag{3}$$

Substituting the loading representation into equation (1) there results,

$$\frac{w}{U}(x_r, y_s) = -\frac{1}{8\pi}\sum_{i=0}^{n-1}\sum_{j=0}^{m-1} a_{ij} W_{ij}(x_r, y_s) \tag{4}$$

where

$$W_{ij}(x_r, y_s) = \int_S \int C_{ij}(x, y) \,.\, K(X, Y; M)\, dx\, dy, \tag{5}$$

The functions $C_{ij}(x, y)$ will be termed 'loading modes' and the corresponding integrals defined by equation (5) will be termed 'downwash modes'. The problem has been reduced to solving for the unknown coefficients a_{ij} by satisfying equation (4) at mn suitably chosen collocation points, (x_r, y_s). The two major problems that remain are:

(a) the choice of the loading modes, $C_{ij}(x, y)$, and

(b) the numerical evaluation of the downwash modes, $W_{ij}(x_r, y_s)$.

2.2. Loading Modes

In general, the downwash distribution on the planform is regular, i.e. it does not exhibit discontinuities or infinities in value or derivatives. (Wings with deflected control surfaces are excluded here.) Thus, referring to equation (4), either the downwash modes $W_{ij}(x_r, y_s)$ must be regular; or else the sum of the modes must be regular, i.e. if discontinuities or infinities are contained in the modes then the coefficients a_{ij} must be chosen such that the overall coefficients of the irregularities are identically zero. An approach involving the latter alternative was proposed in Ref. 20 but was found to be impractical to implement.

The first alternative, i.e. that the individual downwash modes $W_{ij}(x_r, y_s)$ are regular, is naturally preferable. Thus the loading modes $C_{ij}(x, y)$ must be chosen such that the downwash modes, defined through equation (5), are regular.

For planforms with smooth edge shapes, (i.e. without slope discontinuities of leading or trailing edges), with finite tip chord, suitable loading modes are readily defined. If $x = x_l(y)$, $x = x_t(y)$ are the equations of the leading and trailing edge respectively, and $y = s$ is the wing semispan (it is assumed that the planform is symmetric about $y = 0$), then to ensure that the downwash modes are regular, the following conditions must be satisfied:

$$\text{near} \quad x = x_l(y), \qquad C_{ij}(x, y) \sim \frac{1}{\sqrt{x - x_l(y)}}, \tag{6a}$$

$$\text{near} \quad x = x_t(y), \qquad C_{ij}(x, y) \sim \sqrt{x_t(y) - x} \tag{6b}$$

$$\text{near} \quad y = \pm s, \qquad C_{ij}(x, y) \sim \sqrt{s - |y|}, \tag{6c}$$

and for

$$-s \leqslant y \leqslant s, \qquad \frac{\partial C_{ij}(x, y)}{\partial y} \quad \text{is continuous.} \tag{6d}$$

Equations (6a) and (6b) may be inferred from two-dimensional thin aerofoil theory and (6c) from lifting-line theory. Recently equations (6a), (6b) and (6c) have been verified three-dimensionally by matched asymptotic expansion techniques.[21,5] Equation (6d) expresses the physical requirement that kinked isobars cannot exist. Defining the variables,

$$\xi = \left\{\frac{x - x_l(y)}{x_t(y) - x_l(y)}\right\}, \qquad \eta = \frac{y}{s}, \tag{7}$$

then suitable loading modes may be defined as,

$$C_{ij}(x, y) = \sqrt{\frac{1 - \xi}{\xi}}\sqrt{1 - \eta^2}\, P_i(\xi) Q_j(\eta^2), \tag{8}$$

where $P_i(\xi)$, $Q_j(\eta^2)$ represent polynomials; e.g. in the B.A.C. regular planform method,[4]

$$P_i(\xi) = T_i(2\xi - 1), \qquad Q_j(\eta^2) = T_{2j}(\eta),$$

where $T_k(x)$, $-1 \leqslant x \leqslant 1$, is the Chebyshev polynomial of the first kind.

For regular planforms, the downwash modes defined by equation (5) for the loading modes in equation (8) are regular almost everywhere on the wing planform. However, Ref. 4 (and more recently Ref. 22) has shown that the downwash modes exhibit a radial logarithmic singularity at the leading-edge-tip corners. To remove this singularity, it is necessary to modify the definition of the loading modes in the neighbourhood of the leading-edge-tip corners. The required behaviour of the loading modes in the leading-edge-tip corner-region has been analytically inferred in Ref. 5 and verified by numerical experimentation in Ref. 23. However, the wealth of results obtained by lifting-surface methods using loading modes of the form in equation (8) (*see* e.g. Refs. 2, 3 and 4) indicates that the implicit local singularity in the downwash modes at the tip corners can exist without serious detriment to the prediction of the loading elsewhere on the planform.

For planforms with slope discontinuities of leading or trailing edges inboard of the tip, the conditions on the loading modes defined by equations (6a) to (6d) must still be satisfied. The variable ξ defined in equation (7) cannot be used in the definition of loading modes, since if $x_l(y)$ or $x_t(y)$ have slope discontinuities then so have $(\partial\xi/\partial y)_x$ and $\partial C_{ij}(x, y)/\partial y$. Thus the condition given by equation (6d) is not satisfied and hence the downwash modes defined through equation (5) have implicit logarithmic singularities along the spanwise locations of the edge slope discontinuities. Thus either the planform edges must be artificially rounded to remove the slope discontinuities or else an alternative chordwise loading variable must be sought.

If the planform edges are not to be rounded, then it is prudent to analyse the loading variation in the neighbourhood of the edge cranks. Through the concept of matched asymptotic expansions, the 'inner' problem of finding the linearised theory cross-flow potential in the neighbourhood of a centreline crank can be reduced to an eigenvalue problem for the incompressible cross-flow around an infinite sector. This latter problem was initially investigated by Germain[16] who showed that the equation for the velocity potential has eigensolutions of the form

$$\phi_m = r^{\nu_m} f_m(\theta, \omega),$$

with $\nu_m \geqslant 0$, where r is the distance from the apex of the sector, f_m is a function of the polar angles θ and ω, and ν_m depends only on the apex angle of the sector. The flow at the apex of a wing is dominated by the eigensolution with smallest exponent, ν_0.

Several authors[12,13,14,15] have studied the problem of calculating the values ν_m for various apex angles. The most comprehensive set of results is given by Davies.[15]

Thus for a centreline apex crank, the loading, which is proportional to the streamwise derivative of the potential, exhibits a variation of the form $\Delta Cp \sim r^{\nu_0 - 1} F_0(\theta, \omega, r)$ and this special functional behaviour must be incorporated into the loading modes to ensure the regular behaviour of the downwash modes in the neighbourhood of the crank. For a centreline trailing edge crank and for cranks situated between the centreline and the tips of a planform, the necessity for the incorporation of other special functional behaviours can be inferred.

To correctly treat planforms with leading and/or trailing edge cranks, the definition of the loading modes thus requires the introduction of an alternative chordwise variable and the introduction of local functional behaviours at the crank stations. For complex planforms with several cranks, it is difficult to envisage loading modes of the global type, (i.e. each mode extends over the whole planform area), as being suitable to define the loading distribution. Rather, loading modes of the local type would be better suited. Local modes extend over limited areas of the planform and hence can represent local behaviours accurately without affecting the loading behaviour in remote areas. Example of local modes are the fundamental cubic spline or *B* spline modes. Roberts[24] has successfully used these spline modes to represent both surface shape and surface source distributions in the Neumann problem, and has demonstrated how to incorporate required singular edge behaviours into the modes. However, for the limited class of planforms considered in the present lifting-surface-theory method, global modes will be adequate.

2.3. Downwash Modes

The downwash modes are defined by equation (5), for a particular choice of loading modes. Referring to equation (4), the downwash distribution on the planform for a particular collocation order is represented by a sum of downwash modes. In general (ignoring local singularities) the form of the downwash modes is similar

to the form of the loading modes, i.e. if the loading modes are based on global polynomials then the downwash modes exhibit a similar behaviour. Since the downwash distribution is, by definition, the local incidence distribution on the planform, then for wings with complex twist or camber distributions a large number of downwash modes, (i.e. a high order of collocation solution) may be necessary to represent the downwash distribution. If the twist or camber distribution exhibits rapid variations in local regions, then global modes may be unsuitable and local modes, as mentioned in the last section, may be necessary to represent the loading distribution.

It is required that the double integral in equation (5) is evaluated at the collocation point (x_r, y_s). To obtain accurate solutions of the lifting-surface problem, high orders of collocation may be required (especially for complex downwash distributions). In general, as the order of collocation is increased, the collocation points approach the edges of the planform so that to obtain accurate solutions it is essential that the accuracy of evaluation of equation (5) is unimpaired for collocation points in the vicinity of the planform edges. To maintain accuracy for collocation points in the vicinity of the leading and trailing edges, it is essential that the first integration in evaluating equation (5) be performed along coordinate lines that do not intersect these edges. This integration technique was introduced in the B.A.C. method for regular planforms,[4] and is the fundamental reason for the success of that method. The technique has since been successfully applied by Ray and Miller[7] and Sells[8] to evaluate the downwash integral for a given loading. The accuracy that is achieved with the B.A.C. method is well illustrated in Ref. 6, whilst Refs. 22 and 25 illustrate the inadequacies of conventional lifting-surface-theory methods that do not incorporate this necessary integration technique.

3. The Loading Representation for a Particular Class of Planform

Section 2.2 above highlighted the problems associated with the definition of loading modes capable of correctly representing the loading distribution for planforms with leading and/or trailing-edge cranks. For complex planforms with several cranks the definition of the loading modes presents a formidable task. However, if a restricted class of planforms is considered then the definition of the loading modes can be a practical proposition.

The lifting-surface-theory method described in the current report is restricted to treating symmetric pointed planforms of general apex angle, with curved leading edges and smooth trailing edges, with or without a finite tip-chord. Thus a centreline apex crank is treated, but leading edge cranks outboard of the centreline and trailing-edge cranks are not treated. These latter cranks can of course be approximately treated by the incorporation of an artificial rounding.

Mathematically, the class of planforms is defined by,

$$x_l(y) = |y| f(y^2), \tag{9a}$$

and

$$x_t(y) = g(y^2), \tag{9b}$$

where $f(y^2)$, $g(y^2)$ denote even functions of the spanwise coordinate, y. In practice, the requirement in equation (9a) can be relaxed, and leading edges of the form $x_l(y) = |y| f(|y|)$ have been treated.

The class of planforms includes most slender wings, e.g. gothics, mild gothics, cropped deltas, etc.... Swept wings are included in the class if trailing-edge cranks are artificially rounded.

3.1. The Chordwise Loading Variable

Referring to equation (7), for regular planforms a suitable chordwise loading variable is given by,

$$\xi = \frac{x - x_l(y)}{x_t(y) - x_l(y)},$$

so that lines of constant ξ are defined by,

$$x = \xi x_t(y) + (1 - \xi) x_l(y). \tag{10}$$

It was pointed out in Section 2.2 above that this chordwise coordinate is unsuitable for cranked planforms since for such planforms the lines of constant ξ have discontinuous derivative with respect to y at the spanwise

locations of the cranks. For the class of planforms defined by equation (9), a suitable ξ coordinate analogous to the ξ coordinate above may be defined as

$$\xi = \frac{x^2 - x_l^2(y)}{x_t^2(y) - x_l^2(y)}. \tag{11}$$

From equation (9a), $x_l^2(y) = y^2 f^2(y^2)$, and is an even function of y, hence the lines of constant ξ defined by,

$$x = \{\xi x_t^2(y) + (1 - \xi)x_l^2(y)\}^{\frac{1}{2}} \tag{12}$$

have continuous derivative across the centreline crank-station, unless $\xi = 0$. The line $\xi = 0$ corresponds to $x = x_l(y)$ and defines the planform leading-edge.

The chordwise coordinate defined by equation (11) for the class of planforms defined by equation (9) was successfully employed in the B.A.C. lifting-surface-theory method for cropped delta planforms.[18] A comparison of the ξ coordinates defined by equations (7), (10) and (11), (12) for the cropped delta of aspect ratio 3 with 45 degrees leading-edge sweep is given in Fig. 2.

The results presented in Ref. 18 proved that the method of solution of the lifting-surface-theory problem was successful, but certain inadequacies were apparent in the results. In particular, the downwash distribution, obtained by substituting the loading solutions into the integral for the downwash equation (1), exhibited relatively large discrepancies (compared with the defined incidence distribution) at the leading edge of the planform near the centreline. Also, an apparent infinity in the downwash distribution was observed along the centreline of the planform. This apparent centreline infinity (which is not of the logarithmic type associated with kinked isobars) has been analytically isolated and is associated with the special local functional behaviour assumed for the loading in the apex region. It is discussed in Section 3.2 below.

The loading solutions presented for the cropped delta in Ref. 18 were obtained using the standard Multhopp chordwise distribution of collocation stations, i.e.

$$\xi_r = \frac{1}{2}\left\{1 - \cos\left(\frac{2r\pi}{2n+1}\right)\right\}, \qquad r = 1, 2, \ldots, n \tag{13}$$

where n is the number of chordwise terms in the loading representation, and ξ is the coordinate defined by equation (11). For $n = 5$, Fig. 2 compares these collocation stations with the usual Multhopp stations with ξ defined by equation (7). It is seen that near the centreline, the first chordwise collocation station defined by equations (11) and (13) is relatively a considerable distance from the leading edge and hence the downwash representation may be expected to be poor in that region. Several alternative collocation distributions have been investigated subsequent to the work reported in Ref. 18, but the downwash discrepancy could not be improved at the leading edge without introducing large downwash discrepancies elsewhere.

The fundamental reason for the leading-edge-downwash discrepancy is the choice of the ξ variable in equation (11). The chordwise loading variation is represented by polynomial modes in this ξ variable (factored by the appropriate singular edge variations) and hence, as discussed in Section 2.3 above, the downwash distribution is represented by similar modes. At the centreline, from equation (11),

$$\xi = \frac{x^2}{x_t^2(0)},$$

and thus the loading (and hence the downwash) is represented by polynomial-type modes in the variable x^2, i.e. odd powers of x do not appear. These modes are clearly unsuitable for representing general downwash distributions.

Since the ξ variable defined in equations (7) and (10) is known to be perfectly suitable for defining the loading modes for regular planforms, then for cranked planforms it is prudent to seek a chordwise variable that does not diverge greatly from the regular planform ξ variable but which satisfies the criterion of continuous y derivative. For the class of planforms defined by equation (9), a suitable ξ variable may be derived by analogy with equation (10), through the definition of lines of constant ξ as,

$$x = \xi x_t(y) + (1 - \xi)\{x_l^2(y) + \xi h(\xi, y^2)\}^{\frac{1}{2}} \tag{14a}$$

where $h(\xi, y^2)$ is an even function of y (as yet arbitrary). It is readily seen that the lines $\xi = 0$, $\xi = 1$ define

the planform leading and trailing edges respectively, and that the constant ξ lines (apart from $\xi = 0$) have continuous derivative across the centreline crank station. It should be noted that, in general, the ξ in equation (14) cannot be defined explicitly as a function of x and y.

It is reasonable to require that $\partial x/\partial\xi$ is finite at $\xi = 0$, and it may be shown that this implies that $h(\xi, y^2) = \xi h^*(\xi, y^2)$, where $h^*(\xi, y^2)$ is finite at $\xi = 0$. Thus the lines of constant ξ are defined by,

$$x = \xi x_t(y) + (1 - \xi)\{x_l^2(y) + \xi^2 h^*(\xi, y^2)\}^{\frac{1}{2}} \tag{14b}$$

or

$$x = [\xi x_t(y) + (1 - \xi)x_l(y)] + \frac{\xi^2(1 - \xi)h^*(\xi, y^2)}{x_l(y) + \sqrt{x_l(y) + \xi^2 h^*(\xi, y^2)}} \tag{14c}$$

In equation (14c) the term in square brackets defines the constant ξ lines as used for regular planforms (*see* (10) above), hence the second term may be regarded as a perturbation on those lines and through the choice of the function $h^*(\xi, y^2)$, the form of perturbation can be controlled.

The present lifting-surface method employs a chordwise loading variable of the form defined implicitly in equations (14b) or (14c), for $|y| \leqslant \bar{y}$, where $\bar{y}$ is a station in the range $0 < \bar{y} \leqslant s$. For $|y| > \bar{y}$, the chordwise loading variable of the form defined explicitly in equation (7) and implicitly in equation (10) is used. The function $h^*(\xi, y^2)$ is chosen so that at $y = \bar{y}$ the two sets of lines of constant ξ are continuous in value and derivative up to any required order. Thus the lines of constant ξ are defined by, for $|y| > \bar{y}$

$$x = [\xi x_t(y) + (1 - \xi)x_l(y)] \tag{15a}$$

and for $|y| \leqslant \bar{y}$

$$x = \xi x_t(y) + (1 - \xi)\sqrt{x_l^2(y) + \xi^2 A(\bar{y}^2 - y^2)^k} \tag{15b}$$

or

$$x = [\xi x_t(y) + (1 - \xi)x_l(y)] + \frac{\xi^2(1 - \xi)A(\bar{y}^2 - y^2)^k}{x_l(y) + \sqrt{x_l^2(y) + \xi^2 A(\bar{y}^2 - y^2)^k}}. \tag{15c}$$

At $|y| = \bar{y}$, the lines of constant ξ are continuous in value and derivatives up to order $(k - 1)$. The maximum displacement of the lines defined by equations (15b) or (15c) from the usual percentage chord lines of equation (15a) occurs at the centreline $y = 0$, for $\xi = \frac{1}{2}$, and is given by,

$$\Delta x = \frac{\sqrt{A}\bar{y}^k}{4}.$$

Thus the value of the constant A regulates the maximum displacement. A comparison of the ξ coordinates defined by equation (15), with $A = 16{\cdot}0$, $\bar{y} = 0{\cdot}6s$ and $k = 4$, and by (7), for the cropped delta of aspect ratio 3 with 45 degree leading edge sweep, is given in Fig. 3.

3.2. The Loading Representation

It is convenient to non-dimensionalise all coordinates by dividing by the semispan, s, and henceforth x, x_l, x_t etc.... will refer to the non-dimensional values, (i.e. $x/s, x_l/s, x_t/s$ etc....).

The variable $\eta = y/s$ will denote the non-dimensional spanwise coordinate, and $x = x_l(\eta)$, $x = x_t(\eta)$ will define the leading and trailing edges of the planform.

The loading representation is constructed from polynomial modes in the variables ξ, η (ξ defined by equation (15)) factored by appropriate singular functions to give the required functional behaviour at the edges of the planform. At the leading edge (away from the apex) and at the trailing edge, the required behaviour is given by,

$$\text{near} \quad x = x_l(\eta), \qquad \Delta Cp \sim \frac{1}{\sqrt{x - x_l(\eta)}}, \tag{16a}$$

and

$$\text{near} \quad x = x_t(\eta), \qquad \Delta Cp \sim \sqrt{x_t(\eta) - x}, \tag{16b}$$

respectively. However, the functional form given in equation (16a) cannot be incorporated directly because $x_t(\eta)$ is not an even function and thus $\partial/\partial\eta\{1/\sqrt{x - x_t(\eta)}\}$ is discontinuous across the centreline. Since, by definition, $x_t(\eta) = |\eta| f(\eta^2)$, then the alternative form,

$$\text{near} \quad x = x_t(\eta), \qquad \Delta Cp \sim \frac{1}{\sqrt{x^2 - x_t^2(\eta)}}, \tag{16c}$$

may be incorporated.

For planforms with finite tip chord, the required loading behaviour at the tips is given by

$$\text{near} \quad |\eta| = 1, \qquad \Delta Cp \sim \sqrt{1 - \eta^2}. \tag{16d}$$

However, for planforms with zero tip chord, the required loading behaviour at the tips has not been analytically defined at the present time. The planforms with zero tip chord treated in the current report have streamwise tips, i.e.

$$\text{near} \quad |\eta| = 1, \qquad x_t(\eta) = X_T - a\sqrt{1 - \eta^2},$$

where $(x, \eta) = (X_T, \pm 1)$ are the coordinates of the tips. For these planforms, the constant ξ lines, defined by equation (15a), (excepting the trailing-edge line, $\xi = 1$), have infinite streamwise derivative at the tips. Numerical experimentation, reported in Ref. 23, implies that the loading varies in a regular manner as the tips are approached along such ξ lines. In the current method therefore, no special functional behaviour for the loading representation in the tip regions is incorporated for planforms with streamwise tips and zero tip chord.

The required special functional behaviour of the loading in the apex region was briefly discussed in Section 2.2 above. Using Legendre's[17] formulation of the basic cross flow solution given by Germain,[16] Hewitt[26] has shown that the required local loading behaviour associated with the first eigensolution may be expressed in the form,

$$\Delta Cp \sim r^{\nu_0 - 1} \cdot \frac{F_0(u; \gamma)}{u^{\frac{1}{2}}}, \tag{17}$$

where

$$u = \left| \frac{\cos\theta - \cos\gamma}{1 - \cos\theta\cos\gamma} \right|, \tag{18}$$

γ is the semi-apex angle of the infinite sector, with $\cos\theta = x/r$, and where $F_0(u; \gamma)$ is a regular function of u. The coordinate u varies in value from zero at the leading edge to unity at the centreline; the factor $u^{-\frac{1}{2}}$ is the familiar square root singularity in the loading at the leading edge.

Davies[15] gives tables of values of ν_0 and also of the coefficients of a cubic polynomial approximation to $F_0(u; \gamma)$ for a range of semi-apex angle, γ. Also given in Davies[15] are polynomial approximations to the variations with γ of ν_0 and the coefficients of the polynomial approximation to $F_0(u; \gamma)$, so that these approximations, ν_0 and $F_0(u; \gamma)$ may be computed for arbitrary apex angle.

Since $F_0(u; \gamma)$ is a regular function of u, it would appear that it need not be explicitly included in a representation for the loading. In the lifting-surface-theory method for cropped delta planforms,[18] alternative loading representations including and excluding $F_0(u; \gamma)$ were investigated, and it was shown that the loading representation excluding $F_0(u; \gamma)$ is unsatisfactory. In Appendix A of the current report it is shown that a local loading behaviour in the apex region of the form,

$$\Delta Cp \sim r^{\nu_0 - 1} \frac{G(u)}{u^{\frac{1}{2}}}$$

results in an algebraic infinity in the downwash on the centreline of the form,

$$w \sim \eta^{\nu_0 - 1},$$

unless $G(u)$ is identically the function $F_0(u;\gamma)$. Thus, the function $F_0(u;\gamma)$ must be included explicitly in the loading representation. In practice, it is impossible to represent the function $F_0(u;\gamma)$ exactly in a numerical method using a computer of finite word length, so that the singularities in downwash of the form $w \sim \eta^{\nu_0 - 1}$ cannot be avoided in the current numerical method. However, by including the representation for $F_0(u;\gamma)$ from Ref. 15 the singular effect in the downwash is so localised that it can effectively be ignored in collocation solutions, *provided that no collocation point is placed on the planform centreline.*

The loading form in equation (17) was derived for an infinite sector in incompressible flow and represents the local loading behaviour at the apex of a planform with linear edges. In order to generalise the form of equation (17) for use with planforms with curved edges in compressible flow, the Prandtl–Glauert factor is introduced into the definition of r, and the coordinate u is generalised as follows: redefine,

$$\cos\theta = \frac{x}{r} = \frac{x}{\sqrt{x^2 + \beta^2\eta^2}},$$

$$\cos\gamma = \frac{x_l(\eta)}{r_l(\eta)} = \frac{x_l(\eta)}{\sqrt{x_l^2(\eta) + \beta^2\eta^2}},$$

then, after manipulation,

$$u = \left\{ \frac{x^2 - x_l^2(\eta)}{rx + x_l(\eta)\sqrt{x_l^2(\eta) + \beta^2\eta^2}} \right\}. \tag{19}$$

The definition of u in equation (19) is used in the current method, it reduces to the definition in equation (18) for a planform with linear edges, in incompressible flow.

It will be noted that the leading-edge singularity of the form $u^{-\frac{1}{2}}$ includes the required leading-edge behaviour expressed in equation (16c), so that the latter is automatically included if the special apex form is incorporated in the loading representation.

The loading representation in the current method is finally defined as,

$$\Delta Cp(x,\eta) = r^{\nu_0 - 1}\frac{F_0(u;\gamma)}{u^{\frac{1}{2}}}\sqrt{x_t(\eta) - x}\left\{\begin{matrix}\sqrt{1-\eta^2} \\ \text{or} \\ 1\end{matrix}\right\}\Delta Cp^*(x,\eta), \tag{20}$$

with

$$\Delta Cp^*(x,\eta) = \sum_{i=0}^{(n-1)}\sum_{j=0}^{(\bar{m}-1)} a_{ij}T_i(2\xi - 1)T_{2j}(\eta), \tag{21}$$

where $T_k(z)$, $-1 \leqslant z \leqslant 1$, is the Chebyshev polynomial of the first kind. The variable u is defined by equation (19), and the variable ξ through equation (15). The value ν_0, and the function $F_0(u;\gamma)$ are defined by the polynomial equations (26) of Ref. 15; γ the semi-apex angle is defined as arc cotangent $\{dx_l(\eta)/d\eta\}$ at $\eta = 0$. The $\sqrt{1-\eta^2}$ term is included only for planforms with finite tip chord. It should be noted that for such planforms, no local functional behaviour is included to cater for the leading-edge tip corner and thus a radial logarithmic singularity exists in the downwash calculated for the loading in equation (20). However, as mentioned in Section 2.2 above, this local singular effect can exist without serious detriment to the convergence of the loading solution.

4. Numerical Evaluation of the Downwash Modes

For convenience, relevant formulae are repeated here.

With all dimensions based in semispan, the basic integral equation is,

$$\frac{w}{U}(x_r,\eta_s) = -\frac{1}{8\pi}\int_{-1}^{1}\int_{x_l(\eta)}^{x_t(\eta)}\Delta Cp(x,\eta)\cdot\frac{1}{(\eta-\eta_s)^2}\left[1 - \frac{(x-x_r)}{R}\right]dx\,d\eta \tag{22}$$

with

$$R = \sqrt{(x - x_r)^2 + \beta^2(\eta - \eta_s)^2},$$

and where $\eta = y/s$.

The variable ξ is defined implicitly through the definition of lines of constant ξ as, for $|\eta| > \bar{\eta}$,

$$x = [\xi x_t(\eta) + (1 - \xi)x_l(\eta)] \tag{23a}$$

and for $|\eta| \leqslant \bar{\eta}$,

$$x = \{\xi x_t(\eta) + (1 - \xi)\sqrt{x_l^2(\eta) + \xi^2 A(\bar{\eta}^2 - \eta^2)^k}\} \tag{23b}$$

or

$$x = \left\{[\xi x_t(\eta) + (1 - \xi)x_l(\eta)] + \frac{\xi^2(1 - \xi)A(\bar{\eta}^2 - \eta^2)^k}{x_l(\eta) + \sqrt{x_l^2(\eta) + \xi^2 A(\bar{\eta}^2 - \eta^2)^k}}\right\}. \tag{23c}$$

Introducing the ξ variable into (22), the basic integral equation becomes,

$$\frac{w}{U}(x_r, \eta_s) = -\frac{1}{8\pi}\int_0^1 \oint_{-1}^{1} \Delta Cp(x, \eta) \cdot \frac{1}{(\eta - \eta_s)^2}\left[1 - \frac{(x - x_r)}{R}\right]\left(\frac{\partial x}{\partial \xi}\right) d\eta\, d\xi \tag{24}$$

with $(\partial x/\partial \xi)$ defined as follows, for $|\eta| > \bar{\eta}$

$$\left(\frac{\partial x}{\partial \xi}\right) = [x_t(\eta) - x_l(\eta)] \tag{25a}$$

and for $|\eta| \leqslant \bar{\eta}$

$$\left(\frac{\partial x}{\partial \xi}\right) = \left\{x_t(\eta) - \sqrt{x_l^2(\eta) + \xi^2 f(\eta)} + \frac{\xi(1 - \xi)f(\eta)}{\sqrt{x_l^2(\eta) + \xi^2 f(\eta)}}\right\} \tag{25b}$$

or

$$\left(\frac{\partial x}{\partial \xi}\right) = \left\{[x_t(\eta) - x_l(\eta)] + \frac{\xi f(\eta)[(1 - \xi)x_l(\eta) + (1 - 2\xi)\sqrt{x_l^2(\eta) + \xi^2 f(\eta)}]}{\sqrt{x_l^2(\eta) + \xi^2 f(\eta)}[x_l(\eta) + \sqrt{x_l^2(\eta) + \xi^2 f(\eta)}]}\right\} \tag{25c}$$

where

$$f(\eta) = A(\bar{\eta}^2 - \eta^2)^k. \tag{25d}$$

It should be noted that the spanwise (η) integral in the basic integral equation is a finite part integral. In equation (24) this finite part integration is to be performed first along the constant ξ lines, which do not intersect the leading or trailing edges of the planform. This integration technique was mentioned in Section 2.3 above and is essential if the double integral is to be evaluated accurately for collocation points in the vicinity of the leading or trailing edges.

The loading is represented by a sum of loading modes in the form,

$$\Delta Cp(x, \eta) = \sum_{i=0}^{(n-1)} \sum_{j=0}^{(\bar{m}-1)} a_{ij} C_{ij}(x, \eta), \tag{26a}$$

with

$$C_{ij}(x,\eta) = r^{\nu_0 - 1}\frac{F_0(u:\gamma)}{u^{\frac{1}{2}}}\sqrt{x_t(\eta) - x}\left\{\begin{matrix}\sqrt{1-\eta^2}\\ \text{or}\\ 1\end{matrix}\right\}T_i(2\xi - 1)T_{2j}(\eta), \tag{26b}$$

where

$$r = \sqrt{x^2 + \beta^2\eta^2},$$

and

$$u = \left\{\frac{x^2 - x_l^2(\eta)}{rx + x_l(\eta)\sqrt{x_l^2(\eta) + \beta^2\eta^2}}\right\}. \tag{27}$$

The term $\sqrt{1-\eta^2}$ is included only for planforms with finite tip chord.

Substituting the representation (26a) into equation (24), the basic integral equation may be written as,

$$\frac{w}{U}(x_r,\eta_s) = -\frac{1}{8\pi}\sum_{i=0}^{(n-1)}\sum_{j=0}^{(\bar{m}-1)} a_{ij}W_{ij}(x_r,\eta_s) \tag{28a}$$

with

$$W_{ij}(x_r,\eta_s) = \int_0^1 \oint_{-1}^{1} C_{ij}(x,\eta)\cdot\frac{1}{(\eta-\eta_s)^2}\left[1 - \frac{(x-x_r)}{R}\right]\left(\frac{\partial x}{\partial \xi}\right)d\eta\, d\xi. \tag{28b}$$

The accurate numerical evaluation of the downwash modes $W_{ij}(x_r,\eta_s)$ is a difficult task. The techniques employed in the current method are described in this Section.

From equations (23a), (23c) the following relationships are defined,

$$\{x - x_l(\eta)\} = \xi x_l^*(\xi,\eta) \tag{29a}$$

and

$$\{x_t(\eta) - x\} = (1-\xi)x_t^*(\xi,\eta), \tag{29b}$$

where, for $|\eta| > \bar{\eta}$,

$$x_l^*(\xi,\eta) = [x_t(\eta) - x_l(\eta)] \tag{29c}$$

and

$$x_t^*(\xi,\eta) = [x_t(\eta) - x_l(\eta)], \tag{29d}$$

and, for $|\eta| \leqslant \bar{\eta}$,

$$x_l^*(\xi,\eta) = \left\{[x_t(\eta) - x_l(\eta)] + \frac{\xi(1-\xi)f(\eta)}{x_l(\eta) + \sqrt{x_l^2(\eta) + \xi^2 f(\eta)}}\right\} \tag{29e}$$

and

$$x_t^*(\xi,\eta) = \left\{[x_t(\eta) - x_l(\eta)] - \frac{\xi^2 f(\eta)}{x_l(\eta) + \sqrt{x_l^2(\eta) + \xi^2 f(\eta)}}\right\}, \tag{29f}$$

with $f(\eta)$ defined by equation (25d).

Thus from equation (27),

$$u = \xi\left\{\frac{x_l^*(\xi,\eta)[x + x_l(\eta)]}{rx + x_l(\eta)\sqrt{x_l^2(\eta) + \beta^2\eta^2}}\right\}, \tag{30}$$

and hence from equation (26b), the loading modes are written in the form,

$$C_{ij}(x,\eta) = H(x,\eta)\sqrt{\frac{1-\xi}{\xi}}\sqrt{1-\eta^2}T_i(2\xi - 1)T_{2j}(\eta), \tag{31a}$$

where,

$$H(x,\eta) = \frac{r^{\nu_0 - 1}F_0(u;\gamma)\sqrt{rx + x_l(\eta)\sqrt{x_l^2(\eta) + \beta^2\eta^2}}}{\sqrt{x + x_l(\eta)}}\sqrt{\frac{x_l^*(\xi,\eta)}{x_l^*(\xi,\eta)}}. \tag{31b}$$

Thus the downwash modes are written in the form,

$$W_{ij}(x_r,\eta_s) = \int_0^1 \sqrt{\frac{1-\xi}{\xi}}T_i(2\xi - 1)L_{rs,j}(\xi)\,d\xi, \tag{32a}$$

with $L_{rs,j}(\xi)$, the spanwise integral, defined by,

$$L_{rs,j}(\xi) = \oint_{-1}^{1}\sqrt{1-\eta^2}T_{2j}(\eta)H(x,\eta)\left(\frac{\partial x}{\partial\xi}\right)\cdot\frac{1}{(\eta-\eta_s)^2}\left[1 - \frac{(x-x_r)}{R}\right]d\eta. \tag{32b}$$

N.B. In equations (31a) and (32b) and in any expressions that follow, the term $\sqrt{1-\eta^2}$ is to be omitted for planforms with zero tip chord.

The integrals defined in equations (32a) and (32b) are analogous to the integrals that occur in the lifting-surface-theory treatment of regular planforms and which are extensively analysed in Ref. 4. Thus many of the techniques employed in treating the regular planform problem may be applied to the current problem. The main extra complication is due to the presence of the term $H(x,\eta)\cdot(\partial x/\partial\xi)$ which precludes an analytic extraction of the finite part contribution to the spanwise integral.

4.1. The Spanwise Integration

It is convenient to divide the range of the spanwise integral into three parts. Thus write,

$$L_{rs,j}(\xi) = {}_1L_{rs,j}(\xi) + {}_2L_{rs,j}(\xi) + {}_3L_{rs,j}(\xi), \tag{33a}$$

where

$${}_1L_{rs,j}(\xi) = \int_{-1}^{\eta_1}\sqrt{1-\eta^2}T_{2j}(\eta)H(x,\eta)\left(\frac{\partial x}{\partial\xi}\right)\cdot\frac{1}{(\eta-\eta_s)^2}\left[1 - \frac{(x-x_r)}{R}\right]d\eta, \tag{33b}$$

$${}_2L_{rs,j}(\xi) = \int_{\eta_2}^{1}\sqrt{1-\eta^2}T_{2j}(\eta)H(x,\eta)\left(\frac{\partial x}{\partial\xi}\right)\cdot\frac{1}{(\eta-\eta_s)^2}\left[1 - \frac{(x-x_r)}{R}\right]d\eta \tag{33c}$$

and

$${}_3L_{rs,j}(\xi) = \oint_{\eta_1}^{\eta_2}\sqrt{1-\eta^2}T_{2j}(\eta)H(x,\eta)\left(\frac{\partial x}{\partial\xi}\right)\cdot\frac{1}{(\eta-\eta_s)^2}\left[1 - \frac{(x-x_r)}{R}\right]d\eta, \tag{33d}$$

and where $0 < \eta_1 < \eta_s < \eta_2 \leqslant 1$. (If $\eta_2 = 1$, then the integral ${}_2L_{rs,j}$ does not exist.)

In the integrals ${}_1L_{rs,j}$, ${}_2L_{rs,j}$, the term $(\eta - \eta_s)^2$ is non-zero and hence straightforward numerical quadrature techniques may be applied. However, the term $H(x, \eta)(\partial x/\partial \xi)$ exhibits rapid variations across $\eta = 0$ for ξ small, so that to economise on order of quadrature it is necessary to further subdivide the integral ${}_1L_{rs,j}$.

Let,

$$ {}_1L_{rs,j}(\xi) = \int_{-1}^{\eta_1} G_{rs,j}(\xi, \eta)\, d\eta, $$

where

$$ G_{rs,j}(\xi, \eta) = \sqrt{1 - \eta^2}\, T_{2j}(\eta) H(x, \eta) \left(\frac{\partial x}{\partial \xi}\right) \cdot \frac{1}{(\eta - \eta_s)^2} \left[1 - \frac{(x - x_r)}{R}\right], $$

then write

$$ {}_1L_{rs,j}(\xi) = {}_{11}L_{rs,j}(\xi) + {}_{12}L_{rs,j}(\xi), \tag{34a} $$

where

$$ {}_{11}L_{rs,j}(\xi) = \int_{-1}^{-\eta_1} G_{rs,j}(\xi, \eta)\, d\eta, \tag{34b} $$

and

$$ \begin{aligned} {}_{12}L_{rs,j}(\xi) &= \int_{-\eta_1}^{\eta_1} G_{rs,j}(\xi, \eta)\, d\eta \\ &= \int_{0}^{\eta_1} \{G_{rs,j}(\xi, \eta) + G_{rs,j}(\xi, -\eta)\}\, d\eta. \end{aligned} $$

In ${}_{12}L_{rs,j}(\xi)$, the transformation $\eta = p^2$ stretches the variable of integration in the region of $\eta = 0$ and renders the expression more amenable to numerical quadrature.

Thus

$$ {}_{12}L_{rs,j}(\xi) = \int_{0}^{\sqrt{\eta_1}} 2p\{G_{rs,j}(\xi, \eta) + G_{rs,j}(\xi, -\eta)\}\, dp, \tag{34c} $$

where $\eta = p^2$.

The integrals ${}_{11}L_{rs,j}$, ${}_{12}L_{rs,j}$, ${}_2L_{rs,j}$ are evaluated from the expressions (34b), (34c), (33c) respectively using 8 point Gauss–Legendre quadrature, with subdivision of the range if necessary. In the intervals adjacent to $\eta = \pm 1$, the transformations $\eta = \pm(1 - p^2)$ are first applied to remove the infinite derivative due to the term $\sqrt{1 - \eta^2}$ (if present).

Consider the remaining spanwise integral, ${}_3L_{rs,j}$, defined in expression (33d). Let $\{\xi = \xi_r, \eta = \eta_s\}$ correspond to the point $\{x = x_r, \eta = \eta_s\}$, then the term $(x - x_r)/R$ is written in the form,

$$ \frac{(x - x_r)}{R} = \operatorname{sgn}(\xi - \xi_r) - \frac{\beta^2(\eta - \eta_s)^2}{R[(x - x_r) + R \operatorname{sgn}(\xi - \xi_r)]}. \tag{35} $$

Therefore

$$ \frac{1}{(\eta - \eta_s)^2}\left[1 - \frac{(x - x_r)}{R}\right] = \frac{\{1 - \operatorname{sgn}(\xi - \xi_r)\}}{(\eta - \eta_s)^2} + \frac{\beta^2}{R[(x - x_r) + R \operatorname{sgn}(\xi - \xi_r)]}, $$

and thus ${}_3L_{rs,j}$ is written in the form,

$$ {}_3L_{rs,j} = \{1 - \operatorname{sgn}(\xi - \xi_r)\}\, {}_{31}L_{s,j}(\xi) + {}_{32}L_{rs,j}(\xi) \tag{36a} $$

where

$$ {}_{31}L_{s,j}(\xi) = \oint_{\eta_1}^{\eta_2} \sqrt{1-\eta^2}\, T_{2j}(\eta) H(x,\eta) \left(\frac{\partial x}{\partial \xi}\right) \frac{d\eta}{(\eta-\eta_s)^2} \tag{36b} $$

and

$$ {}_{32}L_{rs,j}(\xi) = \int_{\eta_1}^{\eta_2} \sqrt{1-\eta^2}\, T_{2j}(\eta) H(x,\eta) \left(\frac{\partial x}{\partial \xi}\right) \frac{\beta^2\, d\eta}{R[(x-x_r) + R\,\mathrm{sgn}\,(\xi-\xi_r)]}. \tag{36c} $$

The finite part integral is isolated in the integral ${}_{31}L_{s,j}$. The integrand of the integral ${}_{32}L_{rs,j}$ is regular but exhibits rapid variations across $\eta = \eta_s$ for $|\xi - \xi_r|$ small.

In the integral ${}_{31}L_{s,j}$, let

$$ G(\xi,\eta) = \sqrt{1-\eta^2} H(x,\eta) \left(\frac{\partial x}{\partial \xi}\right). $$

Expanding $G(\xi,\eta)$ in a Taylor series about $\eta = \eta_s$,

$$ G(\xi,\eta) = G(\xi,\eta_s) + (\eta-\eta_s)\left\{\frac{\partial}{\partial\eta} G(\xi,\eta)\right\}_{\eta_s} + (\eta-\eta_s)^2 R(\xi,\eta;\eta_s) $$

where

$$ R(\xi,\eta;\eta_s) = \frac{[G(\xi,\eta) - G(\xi,\eta_s) - (\eta-\eta_s)\{(\partial/\partial\eta)G(\xi,\eta)\}_{\eta_s}]}{(\eta-\eta_s)^2}, \tag{37a} $$

is a regular function of η, amenable to numerical quadrature. Thus the integral ${}_{31}L_{s,j}$ is written as,

$$ {}_{31}L_{s,j}(\xi) = G(\xi,\eta_s) \oint_{\eta_1}^{\eta_2} T_{2j}(\eta) \frac{d\eta}{(\eta-\eta_s)^2} + \left\{\frac{\partial}{\partial\eta} G(\xi,\eta)\right\}_{\eta_s} \oint_{\eta_1}^{\eta_2} T_{2j}(\eta) \frac{d\eta}{(\eta-\eta_s)} + \int_{\eta_1}^{\eta_2} T_{2j}(\eta) R(\xi,\eta;\eta_s)\, d\eta. \tag{37b} $$

The first two integrals in equation (37b) are evaluated by recurrence formulae, given in Appendix B, which also contains an expression for $(\partial/\partial\eta)G(\xi,\eta)$.

The last integral in equation (37b) is evaluated using 8 point Gauss–Legendre quadrature, with subdivision of the range if necessary. To ensure at least single length accuracy in the numerical quadrature, the expression for $R(\xi,\eta;\eta_s)$ in expression (37a) is evaluated using double length arithmetic throughout, and the integration range is split at $\eta = \eta_s$ to ensure that $|\eta - \eta_s|$ does not become indefinitely small. If an interval extends to $\eta = 1$, the transformation $(1-\eta) = p^2$ is first applied to remove the infinite derivative due to the term $\sqrt{1-\eta^2}$ (if present).

It may be shown that the function ${}_{32}L_{rs,j}(\xi)$ contains terms of the form, $1/(\xi-\xi_r)$ and $(\xi-\xi_r)^p \log|\xi-\xi_r|$, $p \geqslant 0$. Thus in evaluating ${}_{32}L_{rs,j}(\xi)$ from equation (36c) it is convenient to consider the integral,

$$ (\xi-\xi_r)\,{}_{32}L_{rs,j}(\xi) = \int_{\eta_1}^{\eta_2} T_{2j}(\eta) G(\xi,\eta) \left\{\frac{\beta^2(\xi-\xi_r)}{R[(x-x_r) + R\,\mathrm{sgn}\,(\xi-\xi_r)]}\right\} d\eta, \tag{38} $$

where

$$ G(\xi,\eta) = \sqrt{1-\eta^2} H(x,\eta) \left(\frac{\partial x}{\partial \xi}\right). $$

The function $\beta^2(\xi-\xi_r)/R[(x-x_r) + R\,\mathrm{sgn}\,(\xi-\xi_r)]$ occurring in the integrand of equation (38) is extensively analysed in Ref. 4. It is shown in Ref. 4 that to achieve an accurate numerical integration of an integrand including this function, then a stretching transformation of a particular type must first be applied if the order

of numerical quadrature is not to be prohibitively high. An analogous transformation is applied in the current problem, details of which are given in Appendix C. The transformed integral is in the form,

$$(\xi - \xi_r)_{32}L_{rs,j}(\xi) = \int_{t_1}^{t_2} T_{2j}(\eta)G(\xi, \eta)P_{rs}(\xi, t)\, dt \tag{39}$$

where

$$(\eta - \eta_s) = E_{rs}(\xi)\sinh t - D_{rs}(\xi),$$

and where $P_{rs}(\xi, t)$, $E_{rs}(\xi)$, $D_{rs}(\xi)$ are defined in Appendix C. The values t_1, t_2 correspond to η_1, η_2 respectively. The integral in equation (39) is evaluated using 8 point Gauss–Legendre quadrature, with subdivision of the range if necessary. Since the function $P_{rs}(\xi, t)$ includes certain divided differences, the range of integration is split at the t point corresponding to $\eta = \eta_s$, so that $|\eta - \eta_s|$ does not become indefinitely small. If the upper η limit corresponds to the tip, i.e. $\eta_2 = 1$, then the transformation $(t_2 - t) = p^2$ is applied to remove the infinite derivative due to the term $\sqrt{1 - \eta^2}$ (if present).

4.2. The Chordwise Integration

The chordwise integral is defined by equation (32a), i.e.

$$W_{ij}(x_r, \eta_s) = \int_0^1 \sqrt{\frac{1 - \xi}{\xi}}\, T_i(2\xi - 1)L_{rs,j}(\xi)\, d\xi,$$

and $L_{rs,j}(\xi)$ is defined from equations (33a), (34a), and (36a) in the form,

$$L_{rs,j}(\xi) = {}_{11}L_{rs,j}(\xi) + {}_{12}L_{rs,j}(\xi) + {}_{2}L_{rs,j}(\xi) + \{1 - \operatorname{sgn}(\xi - \xi_r)\}{}_{31}L_{s,j}(\xi) + \frac{\{(\xi - \xi_r)_{32}L_{rs,j}(\xi)\}}{(\xi - \xi_r)}, \tag{40}$$

the integrals ${}_{11}L_{rs,j}$, ${}_{12}L_{rs,j}$, ${}_{2}L_{rs,j}$, ${}_{31}L_{s,j}$, $(\xi - \xi_r)_{32}L_{rs,j}$ being evaluated from the expressions (34b), (34c), (33c), (37b), and (39) respectively.

As was noted in Section 4.1 above, the function ${}_{32}L_{rs,j}(\xi)$ contains terms of the form $1/(\xi - \xi_r)$ and $(\xi - \xi_r)^p \log|\xi - \xi_r|$, $p \geqslant 0$. Thus $(\xi - \xi_r)_{32}L_{rs,j}(\xi)$ is of the form,

$$(\xi - \xi_r)_{32}L_{rs,j}(\xi) = {}_{32}\bar{L}_{rs,j} + S_{rs,j}.(\xi - \xi_r)\log|\xi - \xi_r| + O\{(\xi - \xi_r)^2 \log|\xi - \xi_r|\}$$

where ${}_{32}\bar{L}_{rs,j} = \lim_{\xi \to \xi_r}\{(\xi - \xi_r)_{32}L_{rs,j}(\xi)\}$, and $S_{rs,j}$ are given in Appendix C.

Thus $L_{rs,j}(\xi)$ is written in the form,

$$L_{rs,j}(\xi) = L^*_{rs,j}(\xi) + \frac{{}_{32}\bar{L}_{rs,j}}{(\xi - \xi_r)} + S_{rs,j}\log|\xi - \xi_r|, \tag{41a}$$

where $L^*_{rs,j}(\xi)$ is evaluated from,

$$\begin{aligned} L^*_{rs,j}(\xi) = {}&{}_{11}L_{rs,j}(\xi) + {}_{12}L_{rs,j}(\xi) + {}_{2}L_{rs,j}(\xi) + \{1 - \operatorname{sgn}(\xi - \xi_r)\}{}_{31}L_{s,j}(\xi) + \\ &+ \frac{[\{(\xi - \xi_r)_{32}L_{rs,j}(\xi)\} - {}_{32}\bar{L}_{rs,j}]}{(\xi - \xi_r)} - S_{rs,j}\log|\xi - \xi_r|. \end{aligned} \tag{41b}$$

The chordwise integral (32a) is written as,

$$\begin{aligned} W_{ij}(x_r, \eta_s) = {}&\int_0^1 \sqrt{\frac{1 - \xi}{\xi}}\, T_i(2\xi - 1)L^*_{rs,j}(\xi)\, d\xi + {}_{32}\bar{L}_{rs,j}\oint_0^1 \sqrt{\frac{1 - \xi}{\xi}}\, T_i(2\xi - 1)\frac{d\xi}{(\xi - \xi_r)} + \\ &+ S_{rs,j}\int_0^1 \sqrt{\frac{1 - \xi}{\xi}}\, T_i(2\xi - 1)\log|\xi - \xi_r|\, d\xi. \end{aligned} \tag{42}$$

The last two integrals in (42) are evaluated analytically using the formulae in Appendix D. In the first integral

in equation (42), the function $L^*_{rs,j}(\xi)$ contains a term of the form $(\xi - \xi_r)\log|\xi - \xi_r|$, and also because of th limiting form in equation (41b) cannot be evaluated for $|\xi - \xi_r|$ arbitrarily small. However, if the range o integration is split at $\xi = \xi_r$ then 'open ended' quadrature formulae (i.e. formulae that do not require integratio points at the ends of the range), may be applied to the intervals $0 \leqslant \xi \leqslant \xi_r$ and $\xi_r \leqslant \xi \leqslant 1$.

The integrals

$$\int_0^{\xi_r} \sqrt{\frac{1-\xi}{\xi}}\, T_i(2\xi - 1) L^*_{rs,j}(\xi)\, d\xi \quad \text{and} \quad \int_{\xi_r}^{1} \sqrt{\frac{1-\xi}{\xi}}\, T_i(2\xi - 1) L^*_{rs,j}(\xi)\, d\xi$$

are evaluated using 8 point Gauss–Legendre quadrature, with subdivision of the range if necessary. In the interval with lower limit $\xi = 0$, the transformation $\xi = p^2$ is first applied to remove the singular term $1/\sqrt{\xi}$. In the interval with upper limit $\xi = 1$, the transformation $(1 - \xi) = p^2$ is applied to remove the infinite derivative due to the term $\sqrt{1 - \xi}$.

5. Solution of the Integral Equation and a Discussion of the Results

The solution of the basic integral equation has been reduced to the evaluation of the $\bar{m}n$ coefficients a_{ij} that define the loading representation, by satisfying equation (28a) at suitably chosen collocation points. For the loading solutions presented here, the collocation points (x_r, η_s) are chosen as,

$$(x_r, \eta_s) = \{x(\xi_r, \eta_s), \eta_s\}, \qquad r = 1, 2, \ldots, n; \qquad s = 1, 2, \ldots, \bar{m}, \tag{43a}$$

where

$$\xi_r = \frac{1}{2}\left\{1 - \cos\left(\frac{2r\pi}{2n+1}\right)\right\} \tag{43b}$$

and

$$\eta_s = \cos\left(\frac{s\pi}{2\bar{m}+1}\right), \tag{43c}$$

are the standard Multhopp distributions, and where $x(\xi, \eta)$ is defined by definition (23). The spanwise collocation stations $(\eta_s, s = 1, 2, \ldots, \bar{m})$ all lie on the half planform $\eta > 0$ and do not include the centreline, $\eta = 0$.

With the collocation points defined by expressions (43) the coefficients a_{ij} are evaluated from the integral equation (28a) using a Gaussian elimination technique for the solution of simultaneous linear equations. To facilitate comparison with previous solutions of the lifting surface problem, the loading solutions for particular values of $\bar{m}$, n will be identified by the values (m, n) where $m = 2\bar{m}$.

Results are presented below for the following planforms, all at zero Mach number.

1. A cropped delta planform aspect ratio 3, 45 degree leading edge sweep, with unit downwash distribution. Extensive results for this planform are presented in Ref. 18. Comparison of the results from the present method with the results from Ref. 18 demonstrates that the present method gives correct results, and also that it is an improvement over the method of Ref. 18.
2. Gothic planforms, aspect ratio $\frac{1}{2}$, 1, 2, 3, with unit downwash distribution. Extensive results are presented for the planform of aspect ratio 1 to demonstrate the convergence of the present method with increasing number of chordwise and spanwise terms. Results are compared with the results of slender-wing theory for the four aspect ratios.
3. A cambered wing of mild gothic planform. This is the wing denoted 'wing 1' in Ref. 28. Its camber surface is designed to support a given loading distribution at the attachment condition, when the load vanishes along the leading edge. Results from the present method are compared with the design loading-distribution.

5.1. The Cropped Delta Planform

Figs. 5 to 10 compare the chordwise loading-distributions calculated by the present method and by the method of Ref. 18 with $(m, n) = (14, 4)$. Also included is the loading distribution calculated by the method of Ref. 18 with $(m, n) = (14, 9)$, which is a 'converged solution' in the chordwise sense for $m = 14$ spanwise terms.

Outboard of $\eta = 0{\cdot}2$, the results from the two methods are virtually identical. Inboard of $\eta = 0{\cdot}2$, the (14, 4) results from the present method are closer to the converged solution than the corresponding results from Ref. 18.

The superiority of the present method is due to the improved loading and downwash representations through the choice of chordwise loading variable. Fig. 11 compares the chordwise downwash variation, along the first spanwise collocation station ($\eta_s = 0{\cdot}1045$), calculated from loading solutions with $(m, n) = (14, 5)$. Fig. 12 compares the spanwise downwash variation, along the first chordwise collocation station ($\xi_r = 0{\cdot}0794$), calculated from loading solutions with $(m, n) = (16, 5)$. The distributions of collocation points are compared in Figs. 13 and 14 respectively. The spanwise downwash variations from the two methods are very similar and are dominated by the effect of the singularity in the downwash at the leading-edge tip corner.

However, in the chordwise sense the present method shows a considerable improvement over the method of Ref. 18 in that the downwash discrepancy at the leading edge is greatly reduced.

5.2. The Gothic Planforms

The family of gothic planforms are defined by the leading and trailing edge equations,

$$x_l(\eta) = c_R\{1 - \sqrt{1 - \eta^2}\}, \tag{44a}$$

and

$$x_t(\eta) = c_R, \tag{44b}$$

respectively, where c_R is the root chord. The leading edge may be expressed in the alternative form,

$$\eta = \eta_l(x) = \left(\frac{x}{c_R}\right)\left\{2 - \left(\frac{x}{c_R}\right)\right\}. \tag{44c}$$

The geometric mean chord and aspect ratio are,

$$\bar{c} = \frac{2}{3}c_R, \qquad AR = \frac{3}{c_R}.$$

The planforms of aspect ratio $\frac{1}{2}$, 1, 2, 3 are illustrated in Fig. 15.

(a) *Convergence Demonstration for AR = 1, planform*

Loading solutions have been calculated with $m = 8, 12, 16$ to demonstrate the convergence with increasing spanwise terms, and with $n = 5, 8, 9$ to demonstrate the convergence with increasing chordwise terms. Table 1 presents a summary of the overall lift coefficients, C_L, chordwise centre of pressure, $Xac/\bar{c}$, and spanwise centre of pressure, $\bar{\eta}$, calculated from the loading solutions. For a fixed value of m, chordwise convergence to within 0·03 per cent is achieved with $n = 5$. For a fixed value of n, the spanwise convergence is slower, but convergence to within 1 per cent is achieved by $m = 16$.

Figs. 16 and 17 illustrate the spanwise loading variation and the cross loading variation respectively, calculated from the loading solutions. The spanwise loading and cross loading are defined as,

$$\frac{c(\eta)C_{LL}(\eta)}{\bar{c}C_L} = \frac{1}{\bar{c}C_L}\int_{x_l(\eta)}^{x_t(\eta)} \Delta Cp(x, \eta)\, dx \tag{45}$$

and

$$D^*(x) = \frac{1}{2\bar{c}}\int_{-\eta_l(x)}^{\eta_l(x)} \Delta Cp(x, \eta)\, d\eta, \tag{46}$$

respectively, where $c(\eta)$ is the local chord. For a fixed value of m the results for different values of n are virtually indistinguishable and are plotted with the same symbol. For increasing m the results show a stable convergence trend.

Figs. 18 to 21 illustrate the chordwise convergence of the loading distribution at four spanwise stations with $m = 8$, and Figs. 22 to 25 illustrate the chordwise convergence with $m = 16$. The loading distributions with $n = 9$ and $m = 8, 12, 16$ are compared in Figs. 26 to 29.

Fig. 30 illustrates the spanwise convergence of the loading distribution at three chordwise stations with $n = 5$, and Fig. 31 illustrates the spanwise convergence with $n = 9$. The results are plotted against the variable η^* defined as,

$$\eta^* = \frac{\eta}{\eta_l(x)}, \tag{47}$$

for constant values of x. The loading distributions with $m = 16$ and $n = 5, 8, 9$ are compared in Fig. 32.

The results presented in Figs. 18 to 32 demonstrate the excellent convergence characteristics of the method. As is the case with regular planform solutions (*see* e.g. Refs. 4, 5), spanwise convergence trends are slower than chordwise convergence trends, but the results presented show a stable trend towards full convergence.

(b) *Comparison with Slender Wing Theory*

According to Slender Wing Theory, the loading distribution on a slender planform at uniform incidence, α, in incompressible flow is given by,

$$\frac{\Delta Cp}{\alpha} = \frac{4\eta_l(x)\, d\eta_l/dx}{\sqrt{\eta_l^2(x) - \eta^2}}, \tag{48}$$

where $\eta = \eta_l(x)$ is the leading-edge equation. From the loading distribution given in equation (48), the lift coefficient and spanwise centre of pressure can be derived, independent of planform shape, as

$$C_L = \frac{\pi}{2} AR, \qquad \bar{\eta} = \frac{4}{3\pi}. \tag{49}$$

For the gothic planforms, with η_l defined by equation (44c), the chordwise centre of pressure can be derived as

$$\frac{Xac}{\bar{c}} = 0{\cdot}7. \tag{50}$$

From equation (48), the cross loading can be derived as,

$$D^*(x) = \frac{2\pi}{\bar{c}} \eta_l(x) \frac{d\eta_l}{dx}. \tag{51}$$

The slender-wing results equations (48) to (51) are compared below with the results calculated by the present method for the gothic planforms of aspect ratio $\frac{1}{2}$, 1, 2, 3. The results from the present method may be considered as exact results if the collocation order is sufficiently large. From the convergence results on the aspect ratio 1 planform, the collocation order $(m, n) = (16, 5)$ is sufficient. This order should be sufficient also for the higher aspect ratios. For the aspect ratio $\frac{1}{2}$, less spanwise terms and more chordwise terms should be required to obtain a reasonable degree of convergence, since for equal semispans the planform is twice the length of the aspect ratio 1 planform. To ensure a reasonable degree of convergence, the collocation order $(m, n) = (12, 16)$ has been chosen. Thus the collocation orders of the solutions presented are as follows:

Aspect Ratio	Collocation Order (m, n)
$\frac{1}{2}$	(12, 16)
1	(16, 5)
2	(16, 5)
3	(16, 5)

Table 2 compares the values of lift coefficient, chordwise centre of pressure, and spanwise centre of pressure. The variation of lift coefficient with aspect ratio is illustrated in Fig. 33. The total lift is overestimated by slender-wing theory but the results indicate that the spanwise distribution of lift is estimated quite accurately, the chordwise distribution not so accurately.

The chordwise distributions of lift (cross loading) are compared for the four aspect ratios in Fig. 34. The quantity compared is $\bar{c}^2 D^*(x)$, which according to slender-wing theory is independent of aspect ratio.

Finally, Figs. 35 and 36 compare the slender-wing loading-distributions with the lifting-surface results at three chordwise stations for the two smallest aspect ratios.

Clearly, the smaller the aspect ratio, the more accurate are the slender-wing-theory results, so that the results presented can be taken as illustrating both the limitations of slender-wing theory with increasing aspect ratio and the accuracy of the present method for small aspect ratios.

5.3. The Cambered Mild Gothic

The mild gothic planform is defined by the leading and trailing-edge equations,

$$\eta_l(x) = \frac{1}{4}\left\{5\left(\frac{x}{c_R}\right) - \left(\frac{x}{c_R}\right)^5\right\}, \tag{52a}$$

$$x_t(\eta) = c_R, \tag{52b}$$

respectively, where c_R is the root chord. The particular planform treated here has $c_R = 2{\cdot}476167$, which corresponds to an aspect ratio of 1·385, and is shown in Fig. 37. A curve fit to express the leading-edge equation in the form $x = x_l(\eta)$ is incorporated in the method since (52a) cannot be inverted in closed form.

For this planform, warped (i.e. cambered and twisted), mean surfaces have been derived for specified loading distributions, using the method of Ref. 29, and are described in Ref. 28. The loading (c) of Ref. 28 is chosen as a datum here and loading solutions have been calculated for the corresponding warp distribution. The downwash values $(-\partial z/\partial x)$ were taken from Ref. 30.

Table 3 compares the overall lift coefficient, chordwise centre of pressure and spanwise centre of pressure for the datum loading distribution and for the loading solutions obtained from the present method with $m = 8, 16$ and $n = 8, 9$. Figures 38 and 39 compare the spanwise loadings and cross loadings respectively. For a fixed value of m, the results indicate a reasonable trend towards chordwise convergence. However, large differences are apparent between the results with $m = 8$ and $m = 16$, and between those results and the datum.

Figures 40 to 43 compare the datum loading distribution with the (16, 9) loading distribution at four spanwise stations, and Figs. 44 to 48 compare the distributions at five chordwise stations. The results indicate that the present method cannot reproduce the datum loading distribution in the neighbourhood of the centre-line or apex, although the results in other regions are quite good. (It should be noted that the datum loading distribution vanishes along the edges of the planform and that the present method assumes an explicit infinity along the leading edge.)

Results obtained for this planform with unit downwash distribution have shown that with $(m, n) = (16, 9)$ the loading solution obtained is very close to full convergence. Thus, in the present case, the poor convergence is due to the form of downwash distribution.

The downwash values from Ref. 30 are plotted in Fig. 49 against x/c_R along lines of constant η^*, defined by equation (47). The variable η^* is an angular coordinate in the apex region, with the apex corresponding to $x/c_R = 0$ and $-1 \leqslant \eta^* \leqslant 1$. Thus Fig. 49 shows that the warp surface has conical form in the apex region.

In the present method the downwash distribution is represented by polynomial-like modes in the variables ξ, η. The variations along lines of constant η are shown superimposed on the downwash plots in Fig. 49. Along these lines the downwash distribution exhibits increasingly rapid chordwise variations in the leading-edge region as η becomes progressively smaller. The form of these chordwise variations is not amenable to representation by the downwash modes employed in the present method. To illustrate this point, Fig. 50 compares the datum downwash distribution and the downwash calculated from the (16, 9) loading solution, along the most inboard spanwise collocation station for $m = 16$. If the order of spanwise collocation is increased, so that the most inboard spanwise collocation station is closer to the centreline, then the downwash representation will deteriorate further.

In order to treat downwash distributions due to conically cambered surfaces, it would be necessary to explicitly couch the loading representation (and hence implicitly the downwash representation) in terms of modes which are functions of conical-type variables. Although such an approach is possible, it would of course require a considerable revision of the present method.

6. Concluding Remarks

The lifting-surface-theory method described above has been shown to produce accurate, convergent loading solutions for plane wings with pointed apices, curved leading edges and smooth trailing edges. The method is less successful for wings with conical camber. The problems described in defining a suitable loading representation inhibit the extension of the method to treat more general planforms, e.g. with trailing-edge cranks or with more than one leading-edge crank, although such an extension is theoretically possible following the guidelines described above.

Numerical results have been presented for a limited range of planforms of the slender type, sufficient to demonstrate the accuracy of the method. Further results and applications of the method, including results for swept wings will be presented in a future report.

LIST OF SYMBOLS

A Parameter in definition of ξ coordinate, *see* equations (15), (23).

$A_{rs}(\xi)$ $\{x(\xi, \eta_s) - x(\xi_r, \eta_s)\}/(\xi - \xi_r)$, *see* Appendix C.

AR Aspect ratio.

a_{ij} Unknown coefficients in loading representation

$a_s(\xi)$ $\{B_s^2(\xi, \eta_s) + \beta^2\}$, *see* Appendix C.

$B_s(\xi, \eta)$ $\{x(\xi, \eta) - x(\xi_r, \eta_s)\}/(\eta - \eta_s)$, *see* Appendix C.

$C_{ij}(x, \eta)$ Loading mode.

$C_p(x, \eta)$ Pressure coefficient. The loading,

$$\Delta C_p = \{C_{p\ \text{lower surface}} - C_{p\ \text{upper surface}}\}.$$

C_L Lift coefficient.

$C_{LL}(\eta)$ Local lift coefficient, *see* equation (45).

$c(\eta)$ Chord function.

$\bar{c}$ Geometric mean chord

c_R Root chord.

$D^*(x)$ Cross loading coefficient, *see* equation (46).

$D_{rs}(\xi)$ *See* equation (C10).

$E_{rs}(\xi)$ *See* equation (C11).

$F_0(u; \gamma)$ Regular part of loading behaviour in apex region, *see* equation (17).

$F_{rs}(\xi)$ *See* equation (C12).

$f(\eta)$ Function in definition of ξ coordinate.

$$f(\eta) = A(\bar{\eta}^2 - \eta^2)^k, \text{ see equation (25).}$$

$f(y^2)$ Function defining leading edge.

$$x_l(y) = |y| f(y^2), \text{ see equation (9).}$$

$f_0(\theta)$ Function defining velocity potential behaviour in apex region, *see* equation (A-7).

$f_m(\theta, \omega)$ Eigenfunctions of cross flow solution.

$G(\xi, \eta)$ $\sqrt{1 - \eta^2} H(x, \eta) \left| \frac{\partial x}{\partial \xi} \right|$.

$G_{rs,j}(\xi, \eta)$ Integrand of spanwise integral.

$$G_{rs,j}(\xi, \eta) = G(\xi, \eta) \frac{T_{2j}(\eta)}{(\eta - \eta_s)^2} \left[1 - \frac{(x - x_r)}{R} \right].$$

$H(x, \eta)$ Function in definition of loading modes, *see* equation (31).

$h(\xi, y^2)$ General function in definition of ξ coordinate, *see* equation (14).

$h^*(\xi, y^2)$ $h(\xi, y^2) = \xi h^*(\xi, y^2)$.

$K(X, Y; M)$ Kernel function in basic integral equation.

k Parameter in definition of ξ coordinate, *see* equations (15), (23).

$L_{rs,j}(\xi)$ The spanwise integral, *see* equation (32).

Prefixes, e.g. ${}_1L_{rs,j}(\xi)$, denote splitting of range of integration into sub regions.

$L^*_{rs,j}(\xi)$ Regular part of spanwise integration, *see* equation (41).

${}_{32}\bar{L}_{rs,j}$ Coefficient of $1/(\xi - \xi_r)$ arising from spanwise integration, *see* equation (41).

M Mach number.

m Number of spanwise collocation stations on the full planform.

$\bar{m}$ Number of spanwise terms in loading representation. Number of spanwise collocation stations on the half planform.

n Number of chordwise terms in loading representation. Number of chordwise collocation stations.

$P_{rs}(\xi, t)$ Function arising from stretching transformation of spanwise integration variable, *see* Appendix C.

R $\sqrt{X^2 + \beta^2 Y^2}$.

$R(\xi, \eta; \eta_s)$ Regular part of integrand of finite part integral, *see* equation (37).

r Radial distance from apex in incompressible flow. $\sqrt{x^2 + \beta^2\eta^2}$ in compressible flow.

r_l $\sqrt{x_l^2(\eta) + \beta^2\eta^2}$.

S Projected wing planform area in plane $z = 0$.

$S_{rs,j}$ Coefficient of $\log|\xi - \xi_r|$ arising from spanwise integration, *see* equation (41).

s Wing semispan.

$T_k(x)$ Chebyshev polynomial of first kind, $-1 \leqslant x \leqslant 1$.

t Variable of integration of transformed spanwise integral.

$$(\eta - \eta_s) = E_{rs}(\xi)\sinh t - D_{rs}(\xi).$$

t_1, t_2 Integration range of transformed spanwise integral, *see* equations (39), (C-18), (C-19).

t_s Value of t corresponding to $\eta = \eta_s$.

U Free stream velocity.

u Angular variable used in definition of apex loading behaviour, *see* equations (18), (19).

$W_{ij}(x_r, \eta_s)$ Downwash mode.

w Downwash.

x, y, z Right handed set of cartesian coordinates, with origin at the wing apex.

(x_r, y_s) Collocation point.

X $(x - x_r)$.

$x_l(y), x_l(\eta)$ Leading edge coordinate.

$x_t(y), x_t(\eta)$ Trailing edge coordinate.

$x_l^*(\eta), x_t^*(\eta)$ *See* equation (29).

Xac Chordwise centre of pressure.

Y $(y - y_s)$.

$\bar{y}$ Parameter in definition of ξ coordinate, *see* equation (15).

α Wing incidence.

β $\sqrt{1 - M^2}$.

LIST OF SYMBOLS (continued)

γ Semi-apex angle in incompressible flow.

$\cos^{-1}\{x_l(\eta)/\sqrt{x_l^2(\eta) + \beta^2\eta^2}\}$ in compressible flow.

η Non-dimensional spanwise coordinate, $\eta = y/s$.

η_s Spanwise collocation station.

η_1, η_2 Parameters defining split of spanwise integration range, *see* equation (33).

$\eta_l(x)$ Leading-edge coordinate.

η^* $\eta/\eta_l(x)$.

$\bar{\eta}$ Parameter in definition of ξ coordinate, *see* equation (23).

$\bar{\bar{\eta}}$ Spanwise centre of pressure.

θ Angular variable, $\cos\theta = x/r$.

ν_m Eigenvalues associated with the infinite sector problem.

ν_0 Smallest ν_m which gives dominant term of loading in apex region, *see* equation (17).

ξ Non-dimensional chordwise variable. $\xi = 0$, $\xi = 1$ define the wing leading- and trailing-edges respectively. Several alternative definitions are given in the text. The definition incorporated in the current method is defined by equation (23).

ξ_r Chordwise collocation station.

ρ Free stream density.

ϕ Velocity potential.

ϕ_m Eigensolutions for velocity potential in cross flow.

REFERENCES

No.	*Author(s)*	*Title, etc.*
1	H. Multhopp	Methods for calculating the lift distribution of wings (Subsonic lifting surface theory). A.R.C. R. & M. 2884. (1950).
2	H. C. Garner and D. A. Fox . .	Algol 60 programme for Multhopp's low-frequency subsonic lifting-surface theory. A.R.C. R. & M. 3517 (1966).
3	P. J. Zandbergen, T. E. Labrujere and J. G. Wouters	A new approach to the numerical solution of the equation of subsonic lifting surface theory. N.L.R. Report TR G.49 (1967).
4	B. L. Hewitt and W. Kellaway . .	A new treatment of the subsonic lifting surface problem using curvilinear coordinates. Part I: Details of the method as applied to regular surfaces with finite tip chords and a preliminary set of numerical results. B.A.C. (Preston Division) Report Ae. 290. S. and T. Memo 2/69 (1968).
5	B. L. Hewitt and W. Kellaway . .	A new treatment of the subsonic lifting surface problem using curvilinear coordinates. Part II: Numerical convergence tests and comments related to possible future development. B.A.C. (Preston Division) Report Ae. 290. S. and T. Memo 6/69 (1969).
6	W. Kellaway	Evaluation of the downwash integral for rectangular planforms by the B.A.C. subsonic lifting-surface method. Aeronautical Quarterly, Vol. XXIII, p. 181, August, 1972.
7	Valerie A. Ray and G. F. Miller . .	Numerical evaluation of the downwash integral for a lifting rectangular planform N.P.L. Report Maths 90 (1970).
8	C. C. L. Sells	Calculation of the downwash on the centre line of a swept wing with given load distribution. A.R.C. R. & M. 3725 (1970).
9	C. C. L. Sells	An iterative method for the calculation of the loading on a thin unswept wing. A.R.C. R. & M. 3719 (1972).
10	C. C. L. Sells	Iterative solution for thick symmetrical wings at incidence in incompressible flow. R.A.E. Technical Report 73047 (1973), A.R.C. 34959.
11	B. L. Hewitt, D. Marland and D. W. Armstrong	The use of small perturbation techniques in subsonic wing design procedures. Part I: Determination of surface velocity distributions on thick, lifting, three-dimensional wings in inviscid potential flow. B.A.C. (Military Aircraft Division) Report Ae. 309 (1973).
12	S. N. Brown and K. Stewartson . .	Flow near the apex of a plane delta wing. Jl. I.M.A., **5**, 206–216 (1969).

REFERENCES (continued)

No.	Author(s)	Title, etc.
13	R. S. Taylor	A new approach to the delta wing problem. Jl. I.M.A., 7, 337–347 (1971).
14	Patricia J. Rossiter	The linearised subsonic flow over the centre-section of a lifting swept wing. A.R.C. R. & M. 3630 (1969).
15	Patricia J. Davies	The load near the apex of a lifting swept wing in linearised subsonic flow. R.A.E. Technical Report 72031, A.R.C. R. & M. 3716 (1972).
16	P. Germain	Sur l'écoulement subsonique au voisinage de la pointe avante d'une aile delta. La Recherche Aéronautique 44, 3–8 (1955).
17	R. Legendre	Écoulement subsonique transversal a' un secteur angulaire plan. C.R. Acad. Sci., 1716–18, 26 November, 1956.
18	B. L. Hewitt and W. Kellaway ..	Developments in the lifting surface theory treatment of symmetric planforms with a leading edge crank in subsonic flow. B.A.C. (Military Aircraft Division) Report Ae. 313. S. and T. Memo 4/71 (1971).
19	E. van Spiegel	Boundary value problems in lifting surface theory. N.L.L. Technical Report W.I. (1959).
20	B. L. Hewitt	Comments on a numerical treatment of the subsonic lifting surface theory problem for wings with a centre-section crank. B.A.C. (Preston Division) Technical Note Ae./A/315 (1968).
21	M. T. Landahl	On the pressure loading functions for oscillating wings with control surfaces. Proceedings AIAA/ASME 8th Structures, Structural Dynamics and Material Conference, Palm Springs, March, 1967.
22	H. C. Garner and G. F. Miller ..	Analytical and numerical studies of downwash over rectangular planforms. Aeronautical Quarterly, Vol. XXIII, p. 169, August, 1972.
23	B. L. Hewitt and D. Marland ..	Numerical investigation of potential variations in the vicinity of the tip corners of lifting wings in linearised incompressible flow. To be issued as: B.A.C. (Military Aircraft Division) Technical Note Ae./A/384.
24	A. Roberts and K. Rundle	Computation of incompressible flow about bodies and thick wings using the spline mode system. B.A.C. (Commercial Aircraft Division) Report Aero MA19 (1972).
25	Doris E. Lehrian and H. C. Garner	Convergence of current routines for evaluating downwash at a lifting surface. N.P.L. Aero Note 1095 (1970).

REFERENCES (continued)

No.	*Author(s)*	*Title, etc.*
26	B. L. Hewitt	A reassessment of the numerical treatment of the lifting surface theory problem for wings with centre-section cranks in subsonic flow. B.A.C. (Preston Division) Technical Note Ae./A/306 (1968).
27	—	Tables of Chebyshev Polynomials $S_n(x)$ and $C_n(x)$. National Bureau of Standards, Applied Mathematics Series 9, U.S. Government Printing Office, Washington (1952).
28	Patricia J. Davies	The design of a series of warped slender wings for subsonic speeds. A.R.C. C.P. 1263 (1971).
29	M. P. Carr	The calculation of warp to produce a given load and pressures due to a given thickness on thin slender wings in subsonic flow. Handley Page APRO Report 99 (1968).
30	J. H. B. Smith	Private communication.

APPENDIX A

The Downwash on the Centreline due to the Loading at the Apex

For a planform with straight leading edges and pointed apex, let the loading in the apex region be defined by,

$$\Delta Cp = r^{\nu_0 - 1} \frac{G(u)}{u^{\frac{1}{2}}}. \tag{A-1}$$

where

$$r = \sqrt{x^2 + \eta^2},$$

$$u = \left\{ \frac{\cos\theta - \cos\gamma}{1 - \cos\theta\cos\gamma} \right\},$$

γ is the semi-apex angle and $\cos\theta = x/r$.

ν_0 depends on γ, and $G(u)$ is an arbitrary function of the variable u. (The zero Mach number case is considered here.)

The downwash due to the loading (A-1) is, from equation (1),

$$\frac{w}{U}(x_r, \eta_s) = -\frac{1}{8\pi} \oint_S \int r^{\nu_0 - 1} \frac{G(u)}{u^{\frac{1}{2}}} \frac{1}{(\eta - \eta_s)^2} \left\{ 1 - \frac{X}{R} \right\} dx\, d\eta. \tag{A-2}$$

It may be shown that the contribution to the downwash from X/R term in equation (A-2) is regular, so this term is ignored in the present analysis. Consider the integral,

$$W(x_r, \eta_s) = \oint_S \int r^{\nu_0 - 1} \frac{G(u)}{u^{\frac{1}{2}}} \frac{dx\, d\eta}{(\eta - \eta_s)^2},$$

which by definition is,

$$W(x_r, \eta_s) = -\frac{\partial^2}{\partial \eta_s^2} \int_S \int r^{\nu_0 - 1} \frac{G(u)}{u^{\frac{1}{2}}} \log|\eta - \eta_s|\, dx\, d\eta. \tag{A-3}$$

Let S be limited to a region symmetric about the centreline, including the station $\eta = \eta_s\ (\geqslant 0)$, bounded by the value $x = B$; i.e. S is defined by,

$$x_l(\eta) \leqslant x \leqslant B, \qquad -A \leqslant \eta \leqslant A.$$

The region S is illustrated in Fig. 4. Since r, u are symmetric about $\eta = 0$, then from equation (A-3),

$$W(x_r, \eta_s) = -\frac{\partial^2}{\partial \eta_s^2} \int_0^A \int_{x_l(\eta)}^B r^{\nu_0 - 1} \frac{G(u)}{u^{\frac{1}{2}}} \log|\eta^2 - \eta_s^2|\, dx\, d\eta, \tag{A-4}$$

and transforming to (r, θ) coordinates, (*see* Fig. 4),

$$W(x_r, \eta_s) = -\frac{\partial^2}{\partial \eta_s^2} \int_0^\gamma \frac{G(u)}{u^{\frac{1}{2}}} \int_0^{R(\theta)} r^{\nu_0} \log|r^2 \sin^2\theta - \eta_s^2|\, dr\, d\theta, \tag{A-5}$$

where, for

$$0 \leqslant \theta \leqslant \tan^{-1}\left(\frac{A}{B}\right), \qquad R(\theta) = \frac{B}{\cos\theta},$$

and for

$$\tan^{-1}\left(\frac{A}{B}\right) \leqslant \theta \leqslant \gamma, \qquad R(\theta) = \frac{A}{\sin\theta}.$$

Expanding the term $\log|r^2 \sin^2\theta - \eta_s^2|$ appropriately for $r\sin\theta \leqslant \eta_s$ and $r\sin\theta \geqslant \eta_s$, it may be shown from equation (A-5) that,

$$W(x_r, \eta_s) = C_1 \frac{\partial^2}{\partial \eta_s^2} \eta_s^{\nu_0+1} \int_{\theta_s}^{\gamma} \frac{G(u)\, d\theta}{u^{\frac{1}{2}} \sin^{\nu_0+1}\theta} + \text{(Regular terms)},$$

$$= C_2 \frac{\partial}{\partial \eta_s} \eta_s^{\nu_0} \int_{\theta_s}^{\gamma} \frac{G(u)\, d\theta}{u^{\frac{1}{2}} \sin^{\nu_0+1}\theta} + \text{(Regular terms)}, \tag{A-6}$$

where $\theta_s = \tan^{-1}(\eta_s/B)$, and C_1, C_2 are constants.

Thus for arbitrary $G(u)$ the function $W(x_r, \eta_s)$ contains a singularity of the form $\eta_s^{\nu_0-1}$, $(\nu_0 < 1)$, for $\eta_s = 0$. This singularity may be observed in the downwash modes given in Ref. 18 for the loading modes that exclude the function $F_0(u;\gamma)$. It is not apparent in the downwash modes given in Ref. 18 for the loading modes that include the function $F_0(u;\gamma)$, but further numerical results obtained since the publication of Ref. 18 indicate that the singularity is present although its effect is noticeable only in a very small region surrounding $\eta_s = 0$.

The load in the apex region is related to the potential on the upper surface by,

$$\Delta Cp = 4\frac{\partial \phi}{\partial x}.$$

Davies[14] shows that for the potential corresponding to the first eigensolution of the infinite sector problem, which is of the form,

$$\phi = r^{\nu_0} f_0(\theta), \tag{A-7}$$

if the loading is written in the form,

$$\Delta Cp = r^{\nu_0-1} \frac{F_0(u;\gamma)}{u^{\frac{1}{2}}},$$

then,

$$\frac{F_0(u;\gamma)}{u^{\frac{1}{2}}} = \left\{ \frac{r}{\nu_0} \frac{\partial f_0(\theta)}{\partial x} + \frac{x}{r} f_0(\theta) \right\}. \tag{A-8}$$

Now,

$$\frac{\partial f_0(\theta)}{\partial x} = -\frac{\sin\theta}{r} \frac{df_0(\theta)}{d\theta}$$

Therefore

$$\frac{F_0(u;\gamma)}{u^{\frac{1}{2}}} = \left\{ f_0(\theta)\cos\theta - \frac{\sin\theta}{\nu_0} \frac{df_0(\theta)}{d\theta} \right\}.$$

If $G(u)$ in equation (A-6) is replaced by $F_0(u;\gamma)$, then

$$W(x_r, \eta_s) = C_2 \frac{\partial}{\partial \eta_s} \eta_s^{\nu_0} \int_{\theta_s}^{\gamma} \left\{ \frac{f_0(\theta)\cos\theta}{\sin^{\nu_0+1}\theta} - \frac{1}{\nu \sin^{\nu_0}\theta} \frac{df_0(\theta)}{d\theta} \right\} d\theta + \text{(Regular terms)},$$

$$= C_2 \frac{\partial}{\partial \eta_s} \eta_s^{\nu_0} \int_{\theta_s}^{\gamma} -\frac{d}{d\theta}\left(\frac{f_0(\theta)}{\nu \sin^{\nu_0}\theta} \right) d\theta + \text{(Regular terms)}$$

$$= -C_2 \frac{\partial}{\partial \eta_s} \eta_s^{\nu_0} \left[\frac{f_0(\theta)}{\nu \sin^{\nu_0} \theta} \right]_{\theta_s}^{\gamma} + \text{(Regular terms)},$$

$$= C_2 \frac{\partial}{\partial \eta_s} \left\{ \frac{\eta_s^{\nu_0} f_0(\theta_s)}{\nu \sin^{\nu_0} \theta_s} \right\} + \text{(Regular terms)},$$

since $f_0(\gamma) = 0$.

Therefore

$$W(x_r, \eta_s) = \frac{C_2 \cos^2 \theta_s}{B} \frac{\partial}{\partial \theta_s} \left\{ \frac{B^{\nu_0} \tan \theta_s f_0(\theta_s)}{\nu_0 \sin^{\nu_0} \theta_s} \right\} + \text{(Regular terms)}$$

$$= \frac{C_2 B^{\nu_0 - 1}}{\nu_0} \left\{ \frac{1}{\cos^{\nu_0} \theta_s} \frac{df_0(\theta_s)}{d\theta_s} + \frac{\nu_0 f_0(\theta_s) \sin \theta_s}{\cos^{\nu_0 + 1} \theta_s} \right\} + \text{(Regular terms)}. \tag{A-9}$$

Now from Ref. 14,

$$f_0(0) = 1, \quad \text{and} \quad \frac{df_0}{d\theta} = 0 \quad \text{for} \quad \theta = 0.$$

Hence for $\theta_s = 0$, i.e. on the centreline $\eta_s = 0$, the first term in equation (A-7) vanishes and thus $W(x_r, \eta_s)$ is regular at $\eta_s = 0$.

Thus if the loading in the apex region is chosen to be of the form in equation (A-1) then the function $G(u)$ must be identically the function $F_0(u; \gamma)$, which has the special form defined in equation (A-8), if the inferred downwash distribution is to be regular at the centreline. Since in the method of Ref. 18, and in the current method, a numerical approximation for $F_0(u; \gamma)$ is incorporated, it is impossible to ensure that the relationship defined in equation (A-8) is exactly satisfied and hence to ensure that the first term in equation (A-6) vanishes. Thus in the method of Ref. 18 and the current method, a singularity of the form $\eta_s^{\nu_0 - 1}$ is predicted in the downwash at the centreline. However, as noted above, if the term $F_0(u; \gamma)$ is included in the loading representation then the effect of the singularity is noticeable only over a very small region surrounding $\eta_s = 0$. The effect on collocation solutions is negligible, provided that no collocation point is positioned on the centreline.

APPENDIX B

Expressions Required in the Evaluation of the Finite Part Integral

From equation (37b), the evaluation of the finite part integral requires the evaluation of the integrals,

$$P_j(\eta_s) = \oint_{\eta_1}^{\eta_2} T_{2j}(\eta)\frac{d\eta}{(\eta - \eta_s)^2}, \tag{B-1}$$

$$Q_j(\eta_s) = \oint_{\eta_1}^{\eta_2} T_{2j}(\eta)\frac{d\eta}{(\eta - \eta_s)}, \tag{B-2}$$

and of the function,

$$\frac{\partial}{\partial \eta}G(\xi, \eta),$$

where

$$G(\xi, \eta) = \sqrt{1 - \eta^2}H(x, \eta)\left(\frac{\partial x}{\partial \xi}\right),$$

with

$$H(x, \eta) = \frac{r^{\nu_0 - 1}F_0(u; \gamma)\sqrt{rx + x_t(\eta)}\sqrt{x_t^2(\eta) + \beta^2\eta^2}}{\sqrt{x + x_t(\eta)}}\sqrt{\frac{x_t^*(\xi, \eta)}{x_t^*(\xi, \eta)}},$$

$r = \sqrt{x^2 + \beta^2\eta^2}$, $F_0(u; \gamma)$ is defined as a cubic in the variable

$$u = \left\{\frac{x^2 - x_t^2(\eta)}{rx + x_t(\eta)\sqrt{x_t^2(\eta) + \beta^2\eta^2}}\right\},$$

and x_t^*, x_t^* are defined in equations (29). For planforms with zero tip chord, the term $\sqrt{1 - \eta^2}$ is omitted.

B.1. Evaluation of $P_j(\eta_s)$, $Q_j(\eta_s)$

Using the recurrence relation for the Chebyshev polynomials,

$$T_{2j}(\eta) = 2(2\eta^2 - 1)T_{2(j-1)}(\eta) - T_{2(j-2)}(\eta), \tag{B-3}$$

the following recurrence relations may be derived,

$$P_j(\eta_s) = 2(2\eta_s^2 - 1)P_{j-1}(\eta_s) - P_{j-2}(\eta_s) + 8\eta_s Q_{j-1}(\eta_s) + 4R_{j-1}, \tag{B-4}$$

$$Q_j(\eta_s) = 2(2\eta_s^2 - 1)Q_{j-1}(\eta_s) - Q_{j-2}(\eta_s) + 4S_{j-1}(\eta_s), \tag{B-5}$$

where

$$R_j = \int_{\eta_1}^{\eta_2} T_{2j}(\eta)\, d\eta, \tag{B-6}$$

and

$$S_j(\eta_s) = \int_{\eta_1}^{\eta_2} (\eta + \eta_s)T_{2j}(\eta)\, d\eta. \tag{B-7}$$

The expressions (B-4), (B-5) are valid for $j \geqslant 2$, with initial values,

$$P_0(\eta_s) = \oint_{\eta_1}^{\eta_2} \frac{d\eta}{(\eta - \eta_s)^2} = -\left\{\frac{1}{(\eta_2 - \eta_s)} + \frac{1}{(\eta_s - \eta_1)}\right\}, \tag{B-8}$$

$$Q_0(\eta_s) = \oint_{\eta_1}^{\eta_2} \frac{d\eta}{(\eta - \eta_s)} = \log\left|\frac{\eta_2 - \eta_s}{\eta_s - \eta_1}\right|, \tag{B-9}$$

$$P_1(\eta_s) = (2\eta_s^2 - 1)P_0(\eta_s) + 4\eta_s Q_0(\eta_s) + 2(\eta_2 - \eta_1), \tag{B-10}$$

and

$$Q_1(\eta_s) = (2\eta_s^2 - 1)Q_0(\eta_s) + 2\eta_s(\eta_2 - \eta_1) + (\eta_2^2 - \eta_1^2). \tag{B-11}$$

The integrals in definitions (B-6), (B-7) are readily derived using the properties of Chebyshev polynomials (*see* e.g. Ref. 27).

$$R_j = \frac{1}{2}\left[\frac{T_{2j+1}(\eta)}{2j+1} - \frac{T_{2j-1}(\eta)}{2j-1}\right]_{\eta_1}^{\eta_2} \quad \text{for} \quad j \geqslant 1, \tag{B-12a}$$

with

$$R_0 = (\eta_2 - \eta_1). \tag{B-12b}$$

$$S_j(\eta_s) = \eta_s R_j + \frac{1}{4}\left[\frac{T_{2j+2}(\eta)}{2j+2} - \frac{T_{2j-2}(\eta)}{2j-2}\right]_{\eta_1}^{\eta_2} \quad \text{for} \quad j \geqslant 2, \tag{B-13a}$$

with

$$S_0(\eta_s) = \eta_s R_0 + \tfrac{1}{2}(\eta_2^2 - \eta_1^2), \tag{B-13b}$$

and

$$S_1(\eta_s) = \eta_s R_1 + \tfrac{1}{16}[T_4(\eta)]_{\eta_1}^{\eta_2}. \tag{B-13c}$$

B.2. Evaluation of $\partial/\partial\eta\, G(\xi, \eta)$

To evaluate $(\partial/\partial\eta)G(\xi, \eta)$, it is convenient to write,

$$G(\xi, \eta) = g_1(\eta)g_2(\eta)g_3(\eta)g_4(\eta)g_5(\eta)g_6(\eta) \tag{B-14}$$

where,

$$g_1(\eta) = \sqrt{1 - \eta^2} \quad \text{(or 1 for zero tip chord)}, \tag{B-15}$$

$$g_2(\eta) = r^{\nu_0 - 1}, \tag{B-16}$$

$$g_3(\eta) = F_0(u; \gamma), \tag{B-17}$$

$$g_4(\eta) = \sqrt{\frac{rx + x_l(\eta)\sqrt{x_l^2(\eta) + \beta^2\eta^2}}{x + x_l(\eta)}}, \tag{B-18}$$

$$g_5(\eta) = \sqrt{\frac{x_t^*(\xi, \eta)}{x_t^*(\xi, \eta)}} \tag{B-19}$$

and

$$g_6(\eta) = \left|\frac{\partial x}{\partial \xi}\right|. \tag{B-20}$$

Then, if $g_i(\eta)$ and $\partial g_i(\eta)/\partial\eta$ have been evaluated, $G(\xi, \eta)$ and $(\partial/\partial\eta)G(\xi, \eta)$ are defined by the following algorithm:

(a) Set $G_0 = 1$, Set $G_1 = 0$.

(b) For $i = 1, 2, \ldots, 6$

$$\text{Set} \quad G_1 = G_0 \frac{\partial g_i(\eta)}{\partial \eta} + G_1 g_i(\eta), \qquad \text{Set} \quad G_0 = G_0 g_i(\eta).$$

(c) $$G(\xi, \eta) = G_0, \qquad \frac{\partial G(\xi, \eta)}{\partial \eta} = G_1.$$

Expressions for $\partial g_i(\eta)/\partial\eta$ are given below.

$$g_1(\eta) = \sqrt{1 - \eta^2} \quad \text{or} \quad 1, \qquad \frac{\partial g_1(\eta)}{\partial \eta} = \frac{-\eta}{\sqrt{1 - \eta^2}} \quad \text{or} \quad 0. \tag{B-21}$$

$$g_2(\eta) = r^{\nu_0 - 1}, \qquad \frac{\partial g_2(\eta)}{\partial \eta} = (\nu_0 - 1) r^{\nu_0 - 1} \frac{\partial r}{\partial \eta}, \tag{B-22}$$

where

$$\frac{\partial r}{\partial \eta} = \frac{1}{r}\left(x \frac{\partial x}{\partial \eta} + \beta^2 \eta\right). \tag{B-23}$$

x is defined by equation (23), from which, for $|\eta| > \bar{\eta}$,

$$\frac{\partial x}{\partial \eta} = \left[\xi \frac{dx_t(\eta)}{d\eta} + (1 - \xi) \frac{dx_l(\eta)}{d\eta}\right] \tag{B-24a}$$

and for $|\eta| \leqslant \bar{\eta}$,

$$\frac{\partial x}{\partial \eta} = \left\{\left[\xi \frac{dx_t(\eta)}{d\eta} + (1 - \xi) \frac{dx_l(\eta)}{d\eta}\right] + \frac{-\xi^2(1 - \xi)}{2\sqrt{x_l^2(\eta) + \xi^2 f(\eta)}} \times \left[\frac{2f(\eta)[dx_l(\eta)/d\eta]}{\{x_l(\eta) + \sqrt{x_l^2(\eta) + \xi^2 f(\eta)}\}} - \frac{df(\eta)}{d\eta}\right]\right\}, \tag{B-24b}$$

where

$$f(\eta) = A(\bar{\eta}^2 - \eta^2)^k, \tag{B-25a}$$

and

$$\frac{df(\eta)}{d\eta} = -2kA\eta(\bar{\eta}^2 - \eta^2)^{k-1}. \tag{B-25b}$$

$$g_3(\eta) = F_0(u; \gamma), \qquad \frac{\partial g_3(\eta)}{d\eta} = \frac{dF_0(u; \gamma)}{du} \cdot \frac{\partial u}{\partial \eta}. \tag{B-26}$$

The expression used for $F_0(u; \gamma)$ is of the form,

$$F_0(u; \gamma) = a_0(\gamma) + a_1(\gamma)u + a_2(\gamma)u^2 + a_3(\gamma)u^3, \tag{B-27a}$$

where the $a_i(\gamma)$ are taken from Ref. 15.

Therefore

$$\frac{dF_0(u; \gamma)}{du} = a_1(\gamma) + 2a_2(\gamma)u + 3a_3(\gamma)u^2. \tag{B-28a}$$

It is convenient to introduce

$$r_t(\eta) = \sqrt{x_t^2(\eta) + \beta^2\eta^2}, \tag{B-29a}$$

with

$$\frac{dr_t(\eta)}{d\eta} = \frac{1}{r_t(\eta)}\left\{x_t(\eta)\frac{dx_t(\eta)}{d\eta} + \beta^2(\eta)\right\}, \tag{B-29b}$$

then

$$u = \left\{\frac{x^2 - x_t^2(\eta)}{rx + r_t(\eta)x_t(\eta)}\right\}, \tag{B-30a}$$

and,

$$\frac{\partial u}{\partial \eta} = \frac{[\{2x(\partial x/\partial\eta) - 2x_t(\eta)[dx_t(\eta)/d\eta]\} - u\{r(\partial x/\partial\eta) + x(\partial r/\partial\eta) + r_t(\eta)[dx_t(\eta)/d\eta] + x_t(\eta)[dr_t(\eta)/d\eta]\}]}{\{rx + r_t(\eta)x_t(\eta)\}} \tag{B-30b}$$

$$g_4(\eta) = \sqrt{\frac{rx + r_t(\eta)x_t(\eta)}{x + x_t(\eta)}},$$

$$\frac{\partial g_4(\eta)}{\partial \eta} = \frac{\left[\dfrac{\{r(\partial x/\partial\eta) + x(\partial r/\partial\eta) + r_t(\eta)[dx_t(\eta)/d\eta] + x_t(\eta)[dr_t(\eta)/d\eta]\}}{\sqrt{rx + r_t(\eta)x_t(\eta)}} - g_4(\eta)\dfrac{\{\partial x/\partial\eta + dx_t(\eta)/d\eta\}}{\sqrt{x + x_t(\eta)}}\right]}{2\sqrt{x + x_t(\eta)}} \tag{B-31}$$

$$g_5(\eta) = \sqrt{\frac{x_t^*(\xi,\eta)}{x_t^*(\xi,\eta)}},$$

$$\frac{\partial g_5(\eta)}{\partial \eta} = \frac{1}{2}\frac{\{x_t^*(\xi,\eta)[\partial x_t^*(\xi,\eta)/\partial\eta] - x_t^*(\xi,\eta)[\partial x_t^*(\xi,\eta)/\partial\eta\}}{\sqrt{x_t^*(\xi,\eta)}\{x_t^*(\xi,\eta)\}^{\frac{3}{2}}} \tag{B-32}$$

$x_t^*(\xi,\eta)$, $x_t^*(\xi,\eta)$ are defined by equation (29), from which, for $|\eta| > \bar{\eta}$,

$$\frac{\partial x_t^*(\xi,\eta)}{\partial\eta} = \frac{\partial x_t^*(\xi,\eta)}{\partial\eta} = \left[\frac{dx_t(\eta)}{d\eta} - \frac{dx_t(\eta)}{d\eta}\right]$$

therefore

$$g_5(\eta) \equiv 1, \qquad \frac{\partial g_5(\eta)}{\partial\eta} \equiv 0, \tag{B-33a}$$

and for $|\eta| \leqslant \bar{\eta}$

$$\frac{\partial x_t^*(\xi,\eta)}{\partial\eta} = \left[\frac{dx_t(\eta)}{d\eta} - \frac{dx_t(\eta)}{d\eta}\right] - \frac{\xi(1-\xi)}{2\sqrt{x_t^2(\eta) + \xi^2 f(\eta)}}\left\{\frac{2f(\eta)[dx_t(\eta)/d\eta]}{\{x_t(\eta) + \sqrt{x_t^2(\eta) + \xi^2 f(\eta)}\}} - \frac{df(\eta)}{d\eta}\right\} \tag{B-33b}$$

$$\frac{\partial x_t^*(\xi,\eta)}{\partial\eta} = \left[\frac{dx_t(\eta)}{d\eta} - \frac{dx_t(\eta)}{d\eta}\right] - \frac{\xi^2}{2\sqrt{x_t^2(\eta) + \xi^2 f(\eta)}}\left\{\frac{2f(\eta)[dx_t(\eta)/d\eta]}{\{x_t(\eta) + \sqrt{x_t^2(\eta) + \xi^2 f(\eta)}\}} - \frac{df(\eta)}{d\eta}\right\} \tag{B-33c}$$

$$g_6(\eta) = \left(\frac{\partial x}{\partial\xi}\right), \qquad \frac{\partial g_6(\eta)}{\partial\eta} = \left(\frac{\partial^2 x}{\partial\xi\,\partial\eta}\right). \tag{B-34}$$

$(\partial x/\partial\xi)$ is defined by equation (25), from which, for $|\eta| > \bar{\eta}$,

$$\left(\frac{\partial^2 x}{\partial\xi\,\partial\eta}\right) = \left[\frac{dx_t(\eta)}{d\eta} - \frac{dx_t(\eta)}{d\eta}\right], \tag{B-35a}$$

and for $|\eta| \leqslant \bar{\eta}$

$$\left(\frac{\partial^2 x}{\partial \xi\, \partial \eta}\right) = \left[\frac{dx_t(\eta)}{d\eta} - \frac{dx_l(\eta)}{d\eta}\right] + \frac{\xi}{2\sqrt{x_l^2(\eta) + \xi^2 f(\eta)}} \times$$

$$\times \left\{(2 - 3\xi)\frac{df(\eta)}{d\eta} + \frac{2\xi f(\eta)[dx_t(\eta)/d\eta]}{[x_t(\eta) + \sqrt{x_l^2(\eta) + \xi^2 f(\eta)}]} - \frac{(1 - \xi) f(\eta)}{[x_l^2(\eta) + \xi^2 f(\eta)]}\left[2x_t(\eta)\frac{dx_t(\eta)}{d\eta} + \xi^2 \frac{df(\eta)}{d\eta}\right]\right\} \qquad \text{(B-35b)}$$

APPENDIX C

The Transformation of the Spanwise Integral, and the Singular Terms Arising from the Spanwise Integral

C.1. The Transformation of the Spanwise Integral

The integral considered here is defined in equation (38),

$$(\xi - \xi_r)_{32}L_{rs,j}(\xi) = \int_{\eta_1}^{\eta_2} T_{2j}(\eta)G(\xi,\eta)\left\{\frac{\beta^2(\xi - \xi_r)}{R[(x - x_r) + R\,\mathrm{sgn}\,(\xi - \xi_r)]}\right\} d\eta. \tag{C-1}$$

Let x, as defined by equation (23), be denoted as $x(\xi, \eta)$, so that $x_r = x(\xi_r, \eta_s)$. Define,

$$A_{rs}(\xi) = \frac{x(\xi, \eta_s) - x(\xi_r, \eta_s)}{(\xi - \xi_r)}, \tag{C-2}$$

and

$$B_s(\xi, \eta) = \frac{x(\xi, \eta) - x(\xi, \eta_s)}{(\eta - \eta_s)}. \tag{C-3}$$

$A_{rs}(\xi)$, $B_s(\xi, \eta)$ are regular functions and explicit formulae may be derived for their evaluation using the analytic definition of $x(\xi, \eta)$ from equation (23). However, for $|\xi - \xi_r|$, $|\eta - \eta_s|$ not extremely small the functions may be evaluated to single length accuracy if $x(\xi, \eta)$, $x(\xi, \eta_s)$, $x(\xi_r, \eta_s)$ are evaluated to double length accuracy. For $|\xi - \xi_r| = 0$, and $|\eta - \eta_s| = 0$, the limiting values are,

$$A_{rs}(\xi_r) = \left\{\frac{\partial x(\xi, \eta_s)}{\partial \xi}\right\}_{\xi = \xi_r}, \tag{C-4}$$

and

$$B_s(\xi, \eta_s) = \left\{\frac{\partial x(\xi, \eta)}{\partial \eta}\right\}_{\eta = \eta_s}. \tag{C-5}$$

Incorporating equations (C-2) and (C-3), $(x - x_r)$ may be written in the form,

$$(x - x_r) = (\eta - \eta_s)B_s(\xi, \eta) + (\xi - \xi_r)A_{rs}(\xi),$$

and writing.

$$B_s(\xi, \eta) = B_s(\xi, \eta_s) + (\eta - \eta_s)C_s(\xi, \eta),$$

then

$$(x - x_r) = \{(\eta - \eta_s)B_s(\xi, \eta_s) + (\xi - \xi_r)A_{rs}(\xi)\} + (\eta - \eta_s)^2 C_s(\xi, \eta), \tag{C-6}$$

with $C_s(\xi, \eta)$ by definition,

$$C_s(\xi, \eta) = \frac{B_s(\xi, \eta) - B_s(\xi, \eta_s)}{(\eta - \eta_s)}. \tag{C-7}$$

Incorporating equation (C-6), R may be rewritten,

$$\begin{aligned} R &= \{(x - x_r)^2 + \beta^2(\eta - \eta_s)^2\}^{\frac{1}{2}} \\ &= \{B_s^2(\xi, \eta_s) + \beta^2\}^{\frac{1}{2}}\left\{\frac{[(\eta - \eta_s) + (\xi - \xi_r)B_s(\xi, \eta_s)A_{rs}(\xi)]^2}{B_s^2(\xi, \eta_s) + \beta^2} + \left[\frac{\beta|\xi - \xi_r|A_{rs}(\xi)}{B_s^2(\xi, \eta_s) + \beta^2}\right]^2 + \right. \\ &\quad \left. + \frac{(\eta - \eta_s)^2 C_s(\xi, \eta)[(x - x_r) + (\eta - \eta_s)B_s(\xi, \eta_s) + (\xi - \xi_r)A_{rs}(\xi)]}{B_s^2(\xi, \eta_s) + \beta^2}\right\}^{\frac{1}{2}}, \end{aligned}$$

or

$$R = \sqrt{a_s(\xi)}\{[(\eta - \eta_s) + D_{rs}(\xi)]^2 + E_{rs}^2(\xi) + (\eta - \eta_s)^2 F_{rs}(\xi, \eta)\}^{\frac{1}{2}}, \tag{C-8}$$

where

$$a_s(\xi) = B_s^2(\xi, \eta_s) + \beta^2, \tag{C-9}$$

$$D_{rs}(\xi) = \frac{(\xi - \xi_r)B_s(\xi, \eta_s)A_{rs}(\xi)}{a_s(\xi)}, \tag{C-10}$$

$$E_{rs}(\xi) = \frac{|\xi - \xi_r|\beta A_{rs}(\xi)}{a_s(\xi)} \tag{C-11}$$

and

$$F_{rs}(\xi, \eta) = \frac{C_s(\xi, \eta)[(x - x_r) + (\eta - \eta_s)B_s(\xi, \eta_s) + (\xi - \xi_r)A_{rs}(\xi)]}{a_s(\xi)}. \tag{C-12}$$

With $(x - x_r)$, and R expressed in the form of equations (C-6), (C-8), respectively, a stretching transformation for the integral (C-1) is defined by direct comparison with the corresponding transformation used in Ref. 4. Thus the transformation is,

$$(\eta - \eta_s) = E_{rs}(\xi)\sinh t - D_{rs}(\xi), \tag{C-13}$$

and the integral becomes,

$$(\xi - \xi_r)_{32}L_{rs,j}(\xi) = \int_{t_1}^{t_2} T_{2j}(\eta)G(\xi, \eta)P_{rs}(\xi, t)\,dt, \tag{C-14}$$

with

$$t_1 = \sinh^{-1}\left\{\frac{(\eta_1 - \eta_s) + D_{rs}(\xi)}{E_{rs}(\xi)}\right\}, \tag{C-15}$$

$$t_2 = \sinh^{-1}\left\{\frac{(\eta_2 - \eta_s) + D_{rs}(\xi)}{E_{rs}(\xi)}\right\} \tag{C-16}$$

and where,

$$P_{rs}(\xi, t) = \frac{\beta^2(\xi - \xi_r)E_{rs}(\xi)\cosh t}{R[(x - x_r) + R\,\mathrm{sgn}\,(\xi - \xi_r)]}. \tag{C-17}$$

The expressions for t_1, t_2 can be written in the following forms which are better for numerical evaluation.

$$t_1 = -\log\left\{\frac{1}{\beta|\xi - \xi_r|}\left[\left\{(\eta_s - \eta_1)\frac{a_s(\xi)}{A_{rs}(\xi)} - (\xi - \xi_r)B_s(\xi, \eta_s)\right\} + \right.\right.$$

$$\left.\left. + \sqrt{\left\{(\eta_s - \eta_1)\frac{a_s(\xi)}{A_{rs}(\xi)} - (\xi - \xi_r)B_s(\xi, \eta_s)\right\}^2 + \beta^2(\xi - \xi_r)^2}\right]\right\}, \tag{C-18}$$

$$t_2 = \log\left\{\frac{1}{\beta|\xi - \xi_r|}\left[\left\{(\eta_2 - \eta_s)\frac{a_s(\xi)}{A_{rs}(\xi)} + (\xi - \xi_r)B_s(\xi, \eta_s)\right\} + \right.\right.$$

$$\left.\left. + \sqrt{\left\{(\eta_2 - \eta_s)\frac{a_s(\xi)}{A_{rs}(\xi)} + (\xi - \xi_r)B_s(\xi, \eta_s)\right\}^2 + \beta^2(\xi - \xi_r)^2}\right]\right\}. \tag{C-19}$$

In evaluating the integral in equation (C-14) the range is split at the t point corresponding to $\eta = \eta_s$. Denoting this point by $t = t_s$, from the transformation (C-13),

$$t_s = \sinh^{-1}\left\{\frac{D_{rs}(\xi)}{E_{rs}(\xi)}\right\} = \log\left[\frac{\operatorname{sgn}(\xi - \xi_r)B_s(\xi, \eta_s) + \sqrt{a_s(\xi)}}{\beta}\right]. \tag{C-20}$$

The function $P_{rs}(\xi, t)$ can be written in the following form which is better for numerical evaluation,

$$P_{rs}(\xi, t) = \frac{\beta^3 a_s(\xi)\{B_s^2(\xi, \eta) + \beta^2\}\cosh t}{A_{rs}(\xi)R^*[X^*\sqrt{B_s^2(\xi, \eta) + \beta^2} + R^*]}, \tag{C-21}$$

where,

$$X^* = \beta B_s(\xi, \eta)\operatorname{sgn}(\xi - \xi_r)\sinh t + a_s(\xi) - B_s(\xi, \eta)B_s(\xi, \eta_s), \tag{C-22}$$

and

$$R^* = \{[\{B_s^2(\xi, \eta) + \beta^2\}\beta\sinh t + \{B_s(\xi, \eta)a_s(\xi) - B_s(\xi, \eta_s)[B_s^2(\xi, \eta) + \beta^2]\}\operatorname{sgn}(\xi - \xi_r)]^2 + \beta^2 a_s^2(\xi)\}^{\frac{1}{2}}. \tag{C-23}$$

C.2. The Singular Terms Arising from the Spanwise Integral

To isolate the singular terms arising from the spanwise integral, it is more convenient to consider the integral defined by equation (33d), i.e.

$${}_3L_{rs,j}(\xi) = \int_{\eta_1}^{\eta_2} \sqrt{1 - \eta^2}T_{2j}(\eta)H(x, \eta)\left(\frac{\partial x}{\partial \xi}\right)\cdot\frac{1}{(\eta - \eta_s)^2}\left[1 - \frac{(x - x_r)}{R}\right]d\eta. \tag{C-24}$$

The integral ${}_3L_{rs,j}(\xi)$ is evaluated in the form,

$${}_3L_{rs,j}(\xi) = \{1 - \operatorname{sgn}(\xi - \xi_r)\}{}_3{}_1L_{s,j}(\xi) + \frac{\{(\xi - \xi_r){}_3{}_2L_{rs,j}(\xi)\}}{(\xi - \xi_r)},$$

where $(\xi - \xi_r){}_3{}_2L_{rs,j}(\xi)$ is defined in (C-1) above. It may be shown that no singular terms arise from the integral ${}_3{}_1L_{s,j}(\xi)$, so that the singular content of ${}_3L_{rs,j}(\xi)$ and ${}_3{}_2L_{rs,j}(\xi)$ are identical. Introducing the functions $A_{rs}(\xi)$, $B_s(\xi, \eta)$, $C_s(\xi, \eta)$ defined by expressions (C-2), (C-3), (C-7), then by direct comparison with the corresponding expressions in Ref. 4, it may be shown that,

$$\begin{aligned}
&\int_{\eta_1}^{\eta_2} \sqrt{1 - \eta^2}T_{2j}(\eta)H(x, \eta)\left(\frac{\partial x}{\partial \xi}\right)\cdot\frac{1}{(\eta - \eta_s)^2}\left[1 - \frac{(x - x_r)}{R}\right]d\eta \\
&= 2\sqrt{1 - \eta_s^2}T_{2j}(\eta_s)H(x_r, \eta_s)\left(\frac{\partial x}{\partial \xi}\right)_{r,s}\frac{\sqrt{a_s(\xi_r)}}{A_{rs}(\xi_r)}\cdot\frac{1}{(\xi - \xi_r)} + \\
&+ \frac{2}{\sqrt{a_s(\xi_r)}}\left[\sqrt{1 - \eta_s^2}T_{2j}(\eta_s)H(x_r, \eta_s)\left(\frac{\partial x}{\partial \xi}\right)_{r,s}\cdot\frac{\beta^2 C_s(\xi_r, \eta_s)}{a_s(\xi_r)} + \right. \\
&\left. + B_s(\xi_r, \eta_s)\left\{\frac{\partial}{\partial \eta}\left[\sqrt{1 - \eta^2}T_{2j}(\eta)H(x, \eta)\left(\frac{\partial x}{\partial \xi}\right)\right]\right\}_{r,s}\right]\log|\xi - \xi_r| \\
&+ O\{(\xi - \xi_r)^n \log|\xi - \xi_r|\} + \{\text{Regular terms}\}, \quad (n \geqslant 1).
\end{aligned} \tag{C-25}$$

In equation (C-25), $(\partial x/\partial\xi)_{r,s}$ and $\{\partial/\partial\eta[\sqrt{1-\eta^2}T_{2j}(\eta)H(x,\eta)(\partial x/\partial\xi)]\}_{r,s}$ indicate that the appropriate expressions are evaluated at $(\xi = \xi_r, \eta = \eta_s)$.

Thus the singular content of ${}_{32}L_{rs,j}(\xi)$ is given by equation (C-25), and rearranging,

$$(\xi - \xi_r){}_{32}L_{rs,j}(\xi) = {}_{32}\bar{L}_{rs,j} + S_{rs,j}(\xi - \xi_r)\log|\xi - \xi_r| + O\{(\xi - \xi_r)^2 \log|\xi - \xi_r|\} + \{\text{Regular terms}\}, \quad \text{(C-26)}$$

where,

$${}_{32}\bar{L}_{rs,j} = 2\sqrt{1-\eta_s^2}H(x_r,\eta_s)\left(\frac{\partial x}{\partial\xi}\right)_{rs}\frac{\sqrt{a_s(\xi_r)}}{A_{rs}(\xi_r)}T_{2j}(\eta), \quad \text{(C-27)}$$

and

$$\begin{aligned} S_{rs,j} = \frac{2}{\sqrt{a_s(\xi_r)}}\Bigg[&\left\{\sqrt{1-\eta_s^2}H(x_r,\eta_s)\left(\frac{\partial x}{\partial\xi}\right)_{r,s}\cdot\beta^2\frac{C_s(\xi_r,\eta_s)}{a_s(\xi_r)} + \right. \\ &+ B_s(\xi_r,\eta_s)\frac{\partial}{\partial\eta}\left(\sqrt{1-\eta^2}H(x,\eta)\frac{\partial x}{\partial\xi}\right)_{r,s}\Bigg\}T_{2j}(\eta_s) + \\ &+ \left\{B_s(\xi_r,\eta_s)\sqrt{1-\eta_s^2}H(x_r,\eta_s)\left(\frac{\partial x}{\partial\xi}\right)_{rs}\right\}T'_{2j}(\eta_s)\Bigg] \end{aligned} \quad \text{(C-28)}$$

with $T'_{2j}(\eta) = (d/d\eta)T_{2j}(\eta)$.

Expressions for evaluating the quantities

$$\sqrt{1-\eta^2}H(x_r,\eta_s)\left(\frac{\partial x}{\partial\xi}\right),$$

and

$$\frac{\partial}{\partial\eta}\left\{\sqrt{1-\eta^2}H(x_r,\eta_s)\left(\frac{\partial x}{\partial\xi}\right)\right\}$$

are given in Appendix B. $A_{rs}(\xi_r)$ and $B_s(\xi,\eta_s)$ are defined by equations (C-4), (C-5) above. From equations (C-7) and (C-3),

$$C_s(\xi_r,\eta_s) = \left\{\frac{\partial}{\partial\eta}B_s(\xi_r,\eta)\right\}_{\eta_s} = \frac{1}{2}\left\{\frac{\partial^2}{\partial\eta^2}x(\xi_r,\eta)\right\}_{\eta_s}. \quad \text{(C-29)}$$

Explicit expressions for $\partial^2x/\partial\eta^2$ may be derived from the formulae for $\partial x/\partial\eta$, equation (B-24) in Appendix B. However, since the expressions for $\partial x/\partial\eta$ are evaluated using double length arithmetic in the evaluation of the finite part integral ${}_{31}L_{s,j}(\xi)$, then the double length procedure for $\partial x/\partial\eta$ may be used to provide single length accurate values for $\partial^2x/\partial\eta^2$ defined as,

$$\left(\frac{\partial^2x(\xi,\eta)}{\partial\eta^2}\right)_{\eta_s} = \frac{1}{\varepsilon}\left\{\left(\frac{\partial x}{\partial\eta}\right)_{\xi,\eta_s+\varepsilon} - \left(\frac{\partial x}{\partial\eta}\right)_{\xi,\eta_s}\right\}, \quad \text{(C-30)}$$

where ε is suitably small (typically 10^{-8} with 16 decimal place accuracy in double length working). The use of the expression (C-30) obviates the need for geometry routines incorporating the second derivatives of the leading and trailing edges.

APPENDIX D

The Analytic Integrals in the Chordwise Integration

From equation (42) the analytic integrals in the chordwise integration are,

$$I_i(\xi_r) = \oint_0^1 \sqrt{\frac{1-\xi}{\xi}} T_i(2\xi - 1) \frac{d\xi}{(\xi - \xi_r)} \tag{D-1}$$

and

$$J_i(\xi_r) = \int_0^1 \sqrt{\frac{1-\xi}{\xi}} T_i(2\xi - 1) \log|\xi - \xi_r| \, d\xi. \tag{D-2}$$

These integrals are readily evaluated on transforming to the variable θ, defined by

$$\cos\theta = (2\xi - 1)$$

so that $T_i(2\xi - 1) = \cos i\theta$.

Thus,

$$I_i(\xi_r) = \oint_0^\pi (1 - \cos\theta)\cos i\theta \frac{d\theta}{(\cos\theta - \cos\theta_r)}, \tag{D-3}$$

and

$$J_i(\xi_r) = \tfrac{1}{2}\int_0^\pi (1 - \cos\theta)\cos i\theta \log|\tfrac{1}{2}(\cos\theta - \cos\theta_r)| \, d\theta, \tag{D-4}$$

where $\cos\theta_r = (2\xi_r - 1)$, and using the results,

$$\oint_0^\pi \cos k\theta \frac{d\theta}{(\cos\theta - \cos\theta_r)} = \pi \frac{\sin|k|\theta_r}{\sin\theta_r},$$

$$\int_0^\pi \cos k\theta \log|\cos\theta - \cos\theta_r| \, d\theta = \frac{-\pi}{2}\cos k\theta_r, \quad \text{for} \quad k \neq 0$$

$$= -\pi \log 2, \quad \text{for} \quad k = 0,$$

$$\int_0^\pi \cos k\theta \, d\theta = 0, \quad \text{for} \quad k \neq 0$$

$$= \pi, \quad \text{for} \quad k = 0,$$

then, from integrals (D-3), (D-4),

$$I_i(\xi_r) = \pi(1 - \cos\theta_r)\frac{\sin i\theta_r}{\sin\theta_r}, \quad \text{for} \quad i \geqslant 1, \tag{D-5a}$$

$$= -\pi, \quad \text{for} \quad i = 0, \tag{D-5b}$$

and

$$J_i(\xi_r) = \frac{-\pi}{2}\left[\frac{\cos i\theta_r}{i} - \frac{1}{2}\left\{\frac{\cos(i+1)\theta_r}{(i+1)} + \frac{\cos(i-1)\theta_r}{(i-1)}\right\}\right] \quad \text{for} \quad i \geqslant 2, \tag{D-6a}$$

$$= \frac{\pi}{2}[\log 2 + \tfrac{1}{4}\cos 2\theta_r - \cos\theta_r], \quad \text{for} \quad i = 1, \tag{D-6b}$$

$$= -\pi[\log 2 - \tfrac{1}{2}\cos\theta_r], \quad \text{for} \quad i = 0. \tag{D-6c}$$

The quantities $\cos k\theta_r$, $\sin k\theta_r/\sin \theta_r$, may be evaluated from the following recurrence relations.

Let

$$C_k = \cos k\theta_r, \qquad S_k = \frac{\sin k\theta_r}{\sin \theta_r},$$

then

$$C_0 = 1, \qquad C_1 = (2\xi_r - 1),$$
$$C_k = 2(2\xi_r - 1)C_{k-1} - C_{k-2}, \qquad k \geqslant 2$$

and

$$S_0 = 0, \qquad S_1 = 1,$$
$$S_k = 2(2\xi_r - 1)S_{k-1} - S_{k-2}, \qquad k \geqslant 2.$$

TABLE 1

Convergence of Overall Values for Gothic Planform, Aspect Ratio 1

	m/n	5	8	9
C_L	8	1·3969	1·3967	1·3967
	12	1·4019	1·4015	1·4015
	16	1·4048	1·4044	1·4044

	m/n	5	8	9
$Xac/\bar{c}$	8	0·6899	0·6899	0·6899
	12	0·6892	0·6893	0·6893
	16	0·6889	0·6889	0·6889

	m/n	5	8	9
$\bar{\bar{\eta}}$	8	0·4258	0·4258	0·4258
	12	0·4253	0·4253	0·4253
	16	0·4250	0·4250	0·4250

TABLE 2

Comparison of Overall Values for Gothic Planforms Calculated by Slender Wing Theory and Lifting Surface Theory (Present Method)

C_L

AR	SWT	LST
0·5	0·785	0·747
1·0	1·571	1·405
2·0	3·142	2·426
3·0	4·712	3·148

$Xac/\bar{c}$

AR	SWT	LST
0·5	0·700	0·697
1·0	0·700	0·689
2·0	0·700	0·679
3·0	0·700	0·674

$\bar{\eta}$

AR	SWT	LST
0·5	0·424	0·426
1·0	0·424	0·425
2·0	0·424	0·424
3·0	0·424	0·422

AR—Aspect Ratio
SWT—Slender Wing Theory
LST—Lifting Surface Theory

TABLE 3

Comparison of Overall Values for a Cambered Mild Gothic Planform

	m/n	8	9	*Datum*
C_L	8	0·1078	0·1076	0·1
	16	0·1054	0·1058	

	m/n	8	9	
$Xac/\bar{c}$	8	0·8822	0·8816	0·9138
	16	0·8852	0·8831	

	m/n	8	9	
$\bar{\eta}$	8	0·3854	0·3854	0·3889
	16	0·3875	0·3868	

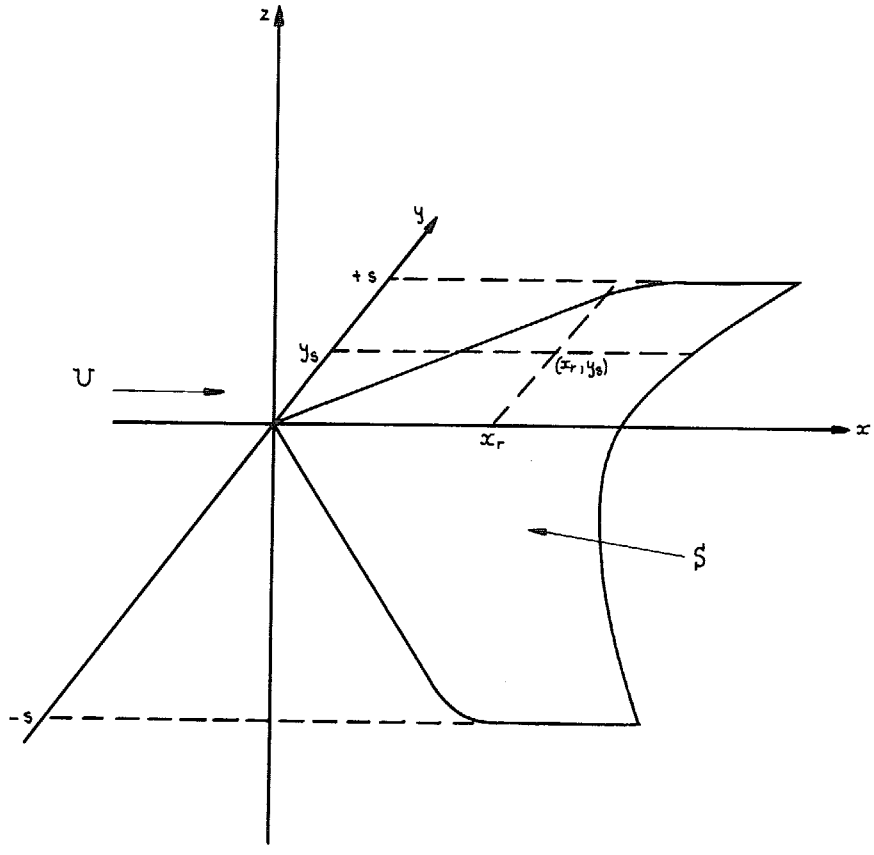

FIG. 1. The co-ordinate axes.

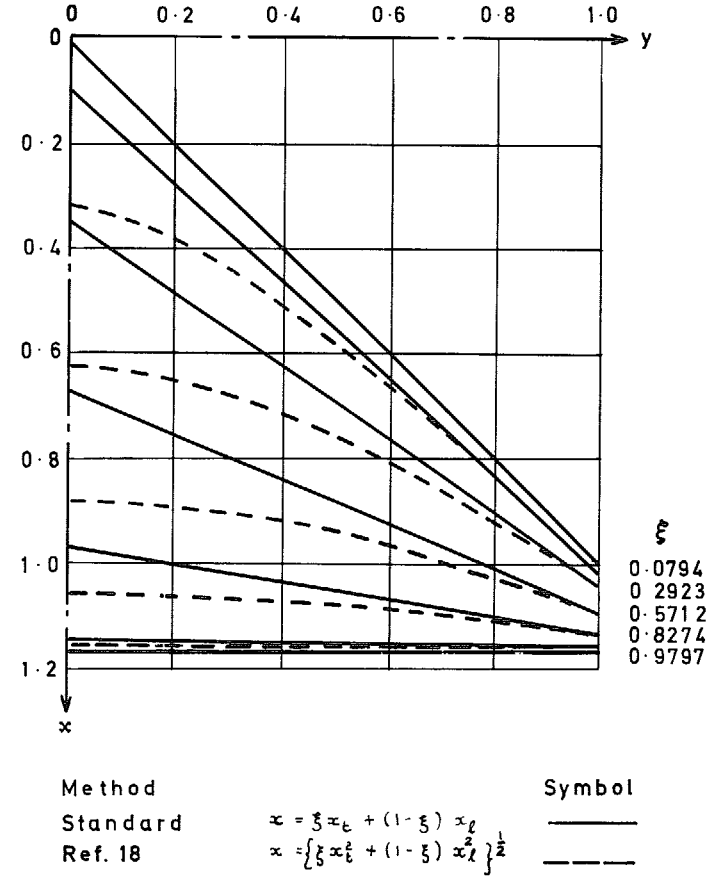

FIG. 2. A comparison of chordwise coordinates for a 45° cropped delta of AR = 3

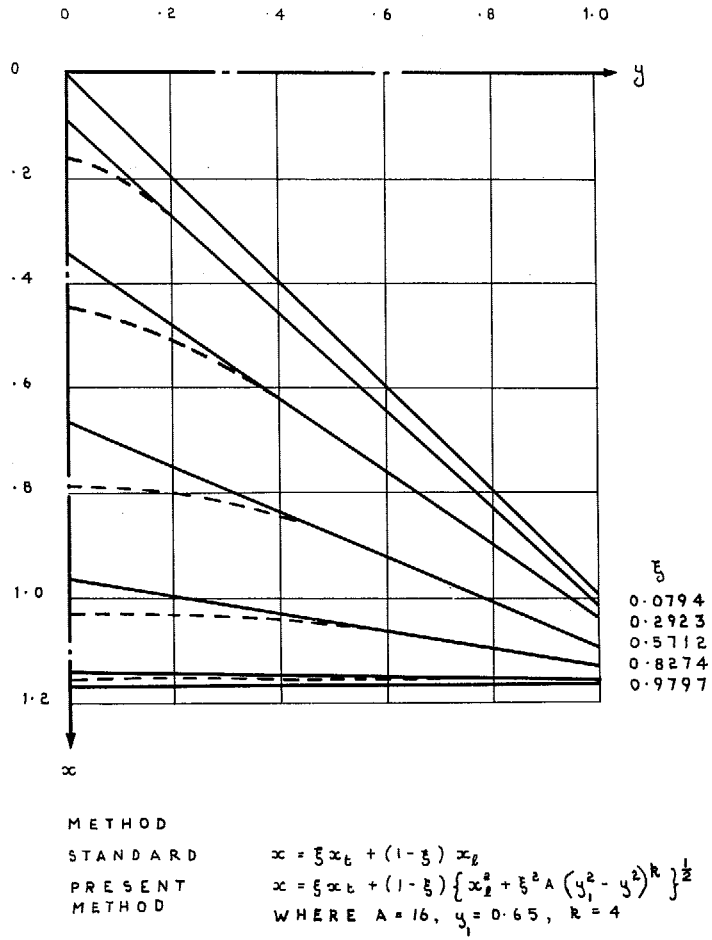

FIG. 3. A comparison of chordwise coordinates for a 45° cropped delta of AR = 3.

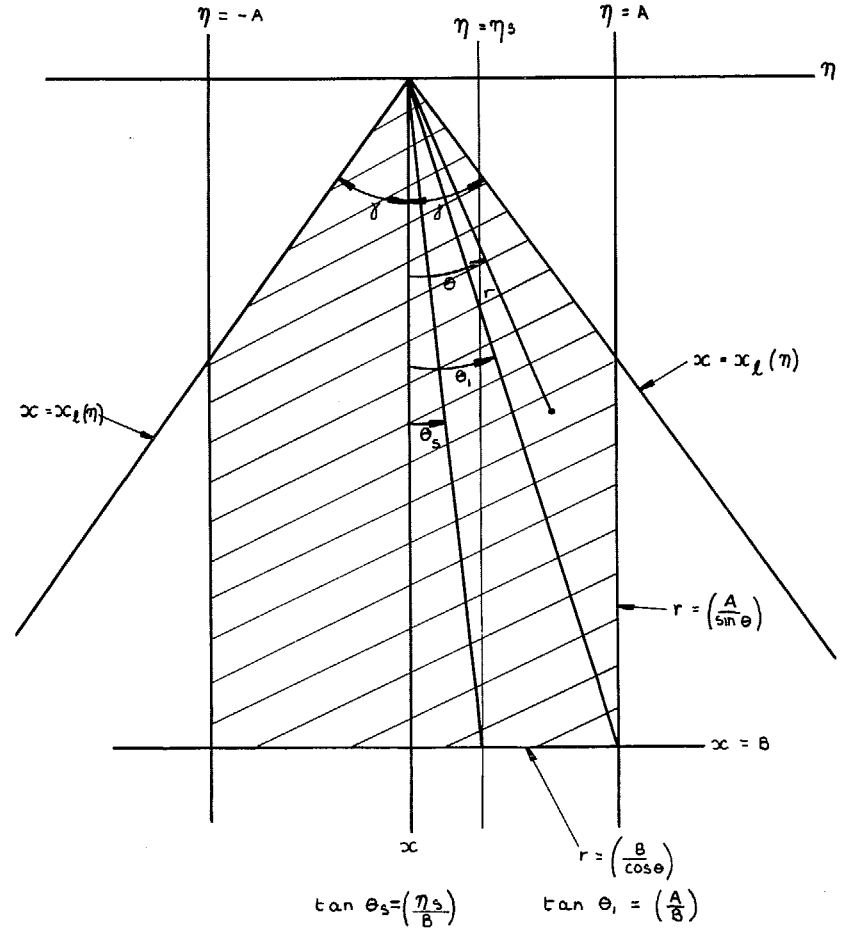

FIG. 4. The integration region in the analysis of the downwash on the centreline.

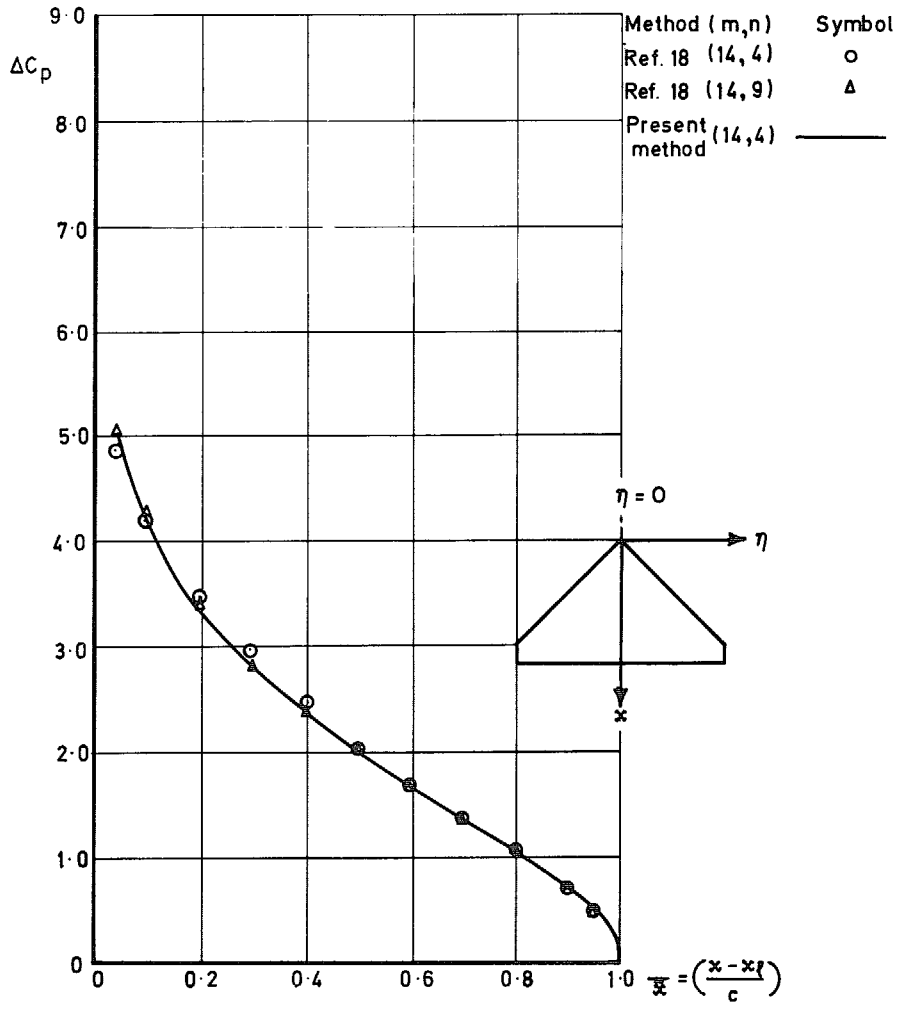

FIG. 5. Comparison of ΔCp distributions for a cropped delta planform at $\eta = 0{\cdot}0$.

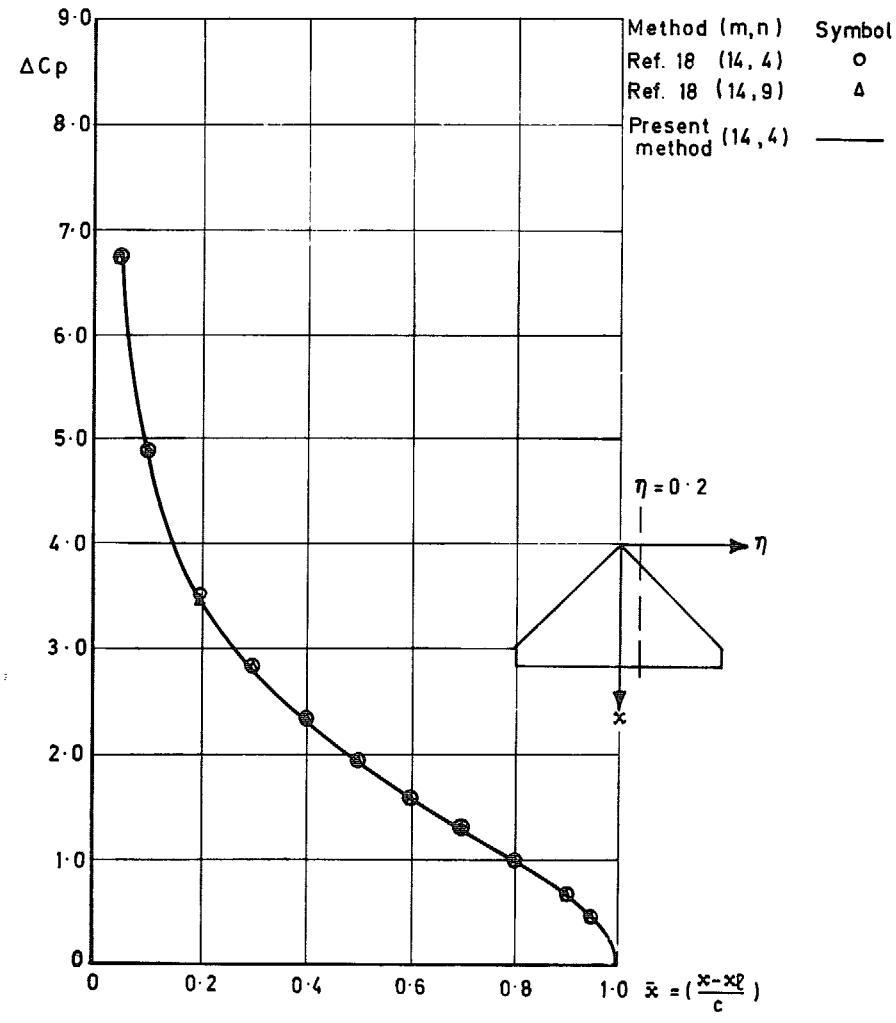

FIG. 6. Comparison of ΔCp distributions for a cropped delta planform at $\eta = 0{\cdot}2$.

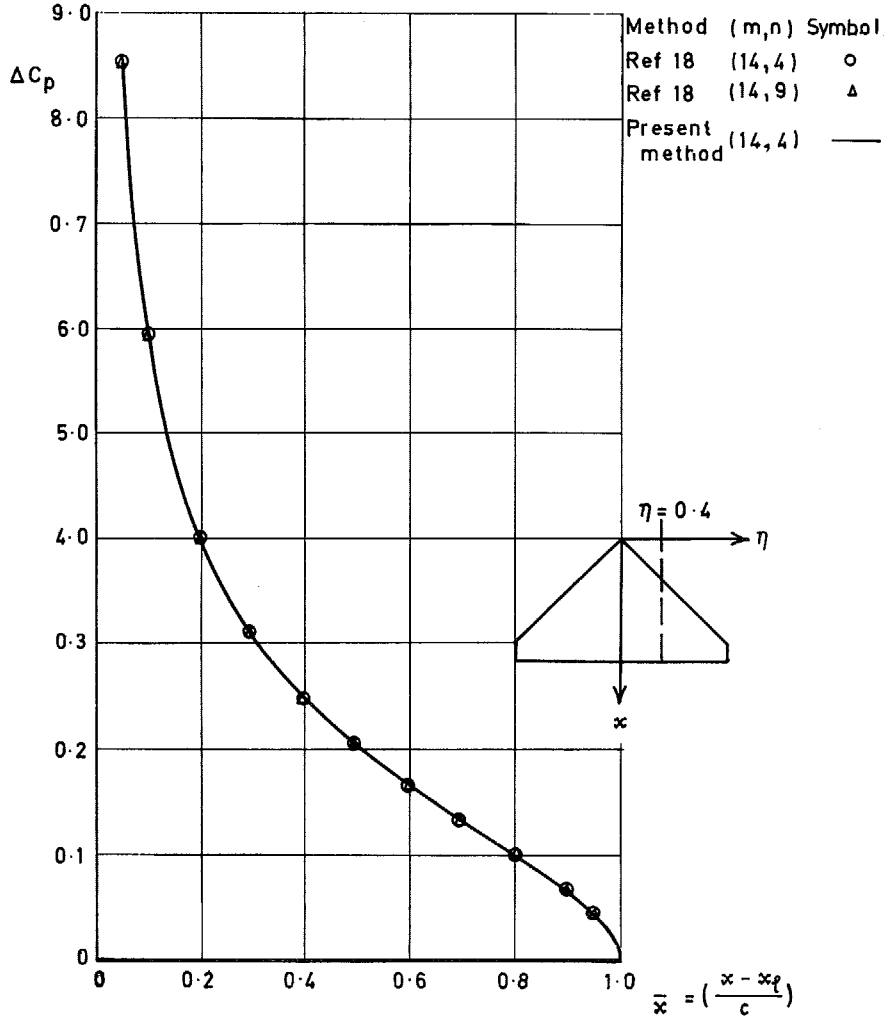

FIG. 7. Comparison of ΔCp distributions for a cropped delta planform at $\eta = 0{\cdot}4$.

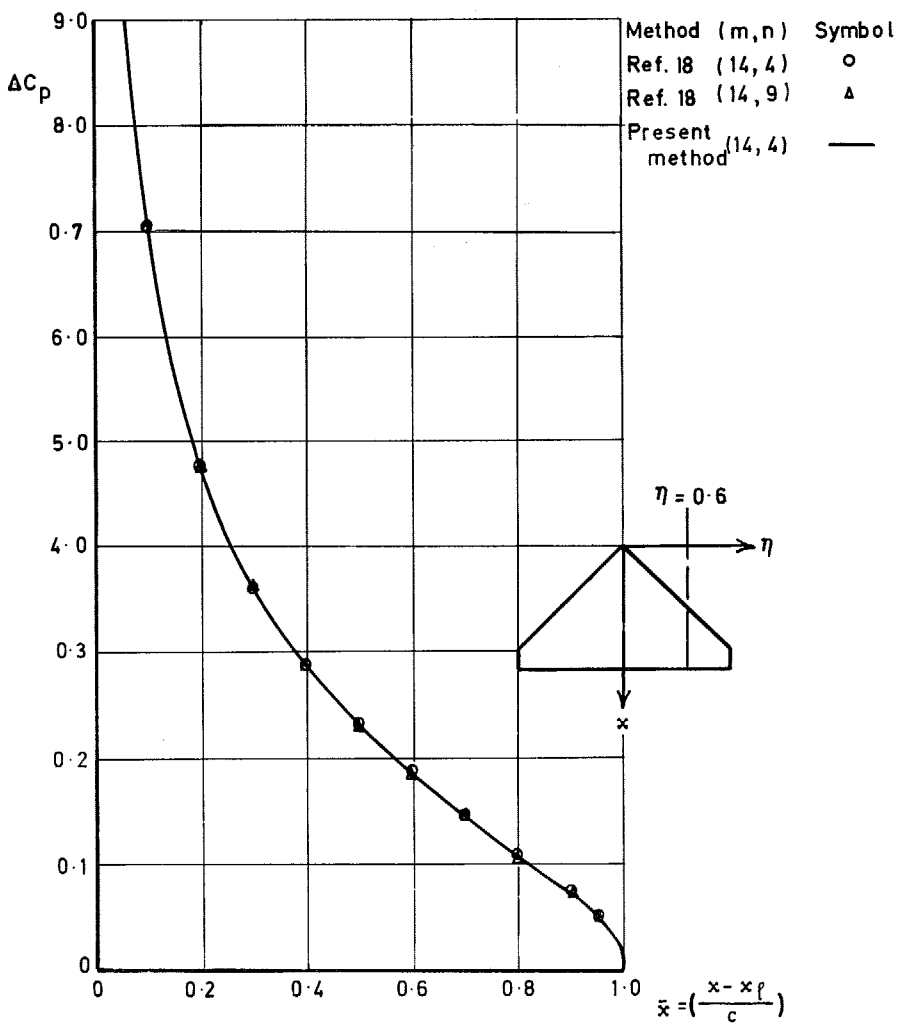

FIG. 8. Comparison of ΔCp distributions for a cropped delta planform at $\eta = 0{\cdot}6$.

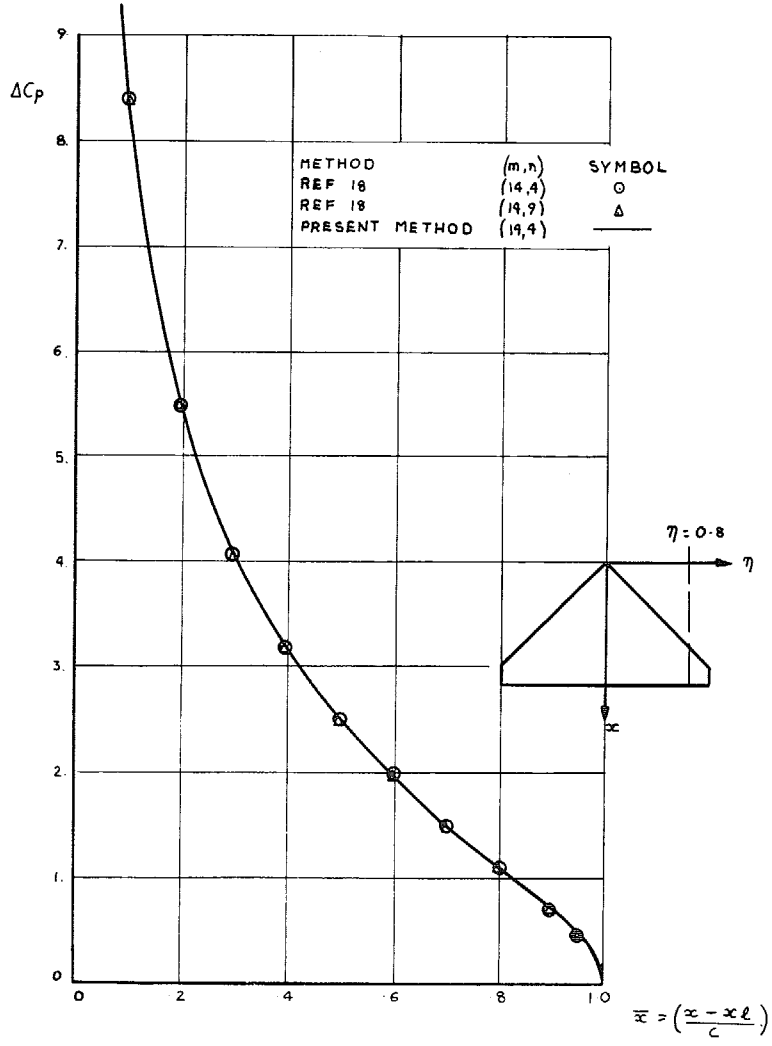

FIG. 9. Comparison of ΔCp distributions for a cropped delta planform at $\eta = 0{\cdot}8$.

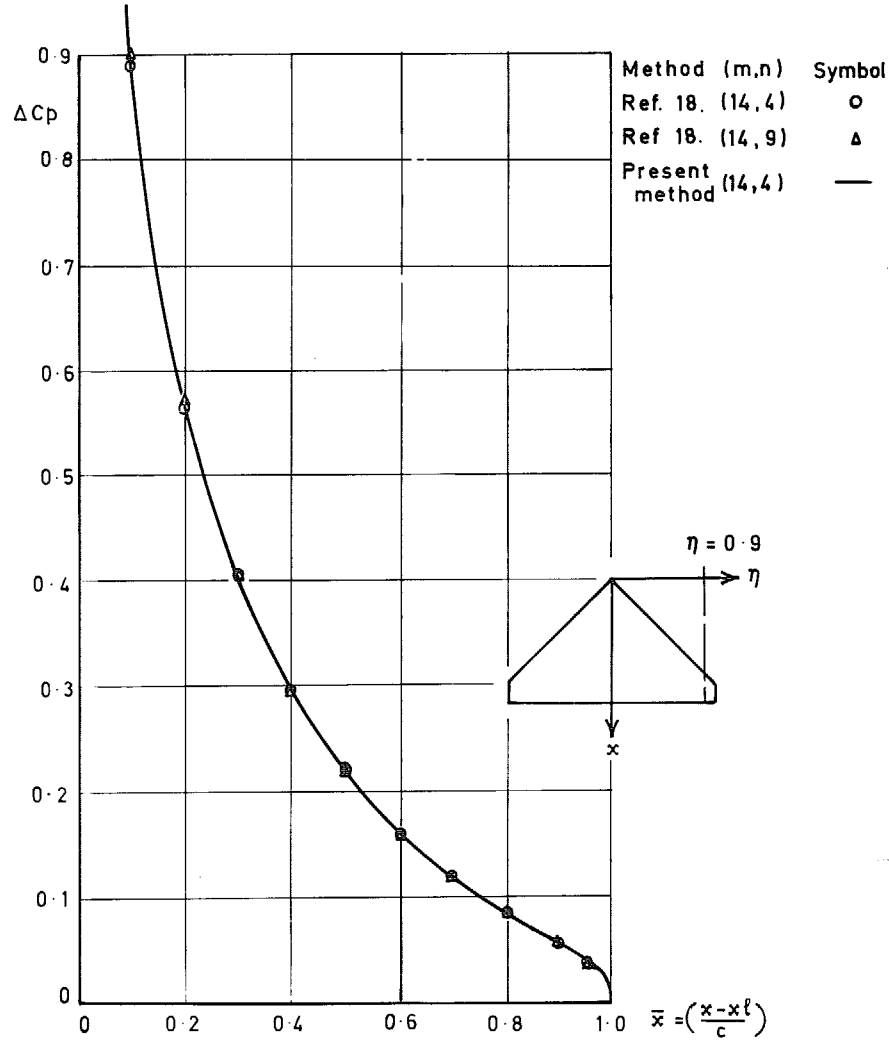

FIG. 10. Comparison of ΔCp distributions for a cropped delta planform at $\eta = 0{\cdot}9$.

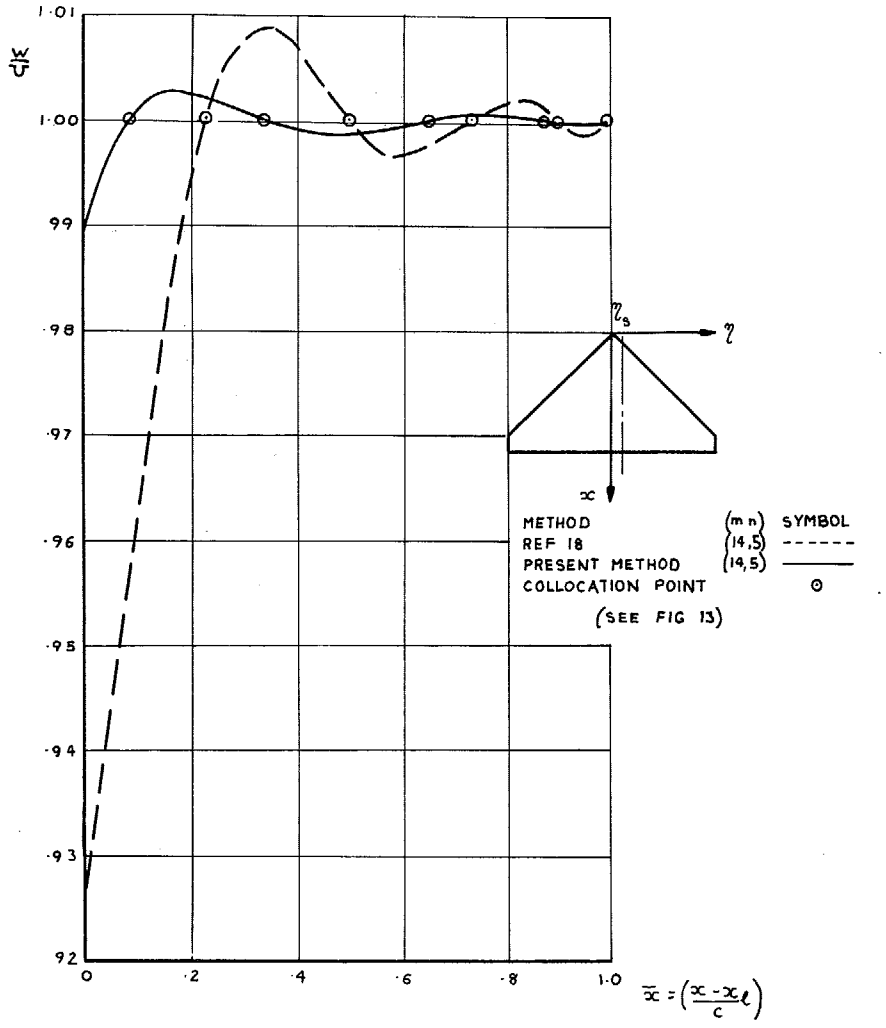

FIG. 11. Comparison of chordwise downwash interpolations for a cropped delta planform at spanwise collocation station $\eta_s = 0{\cdot}1045$.

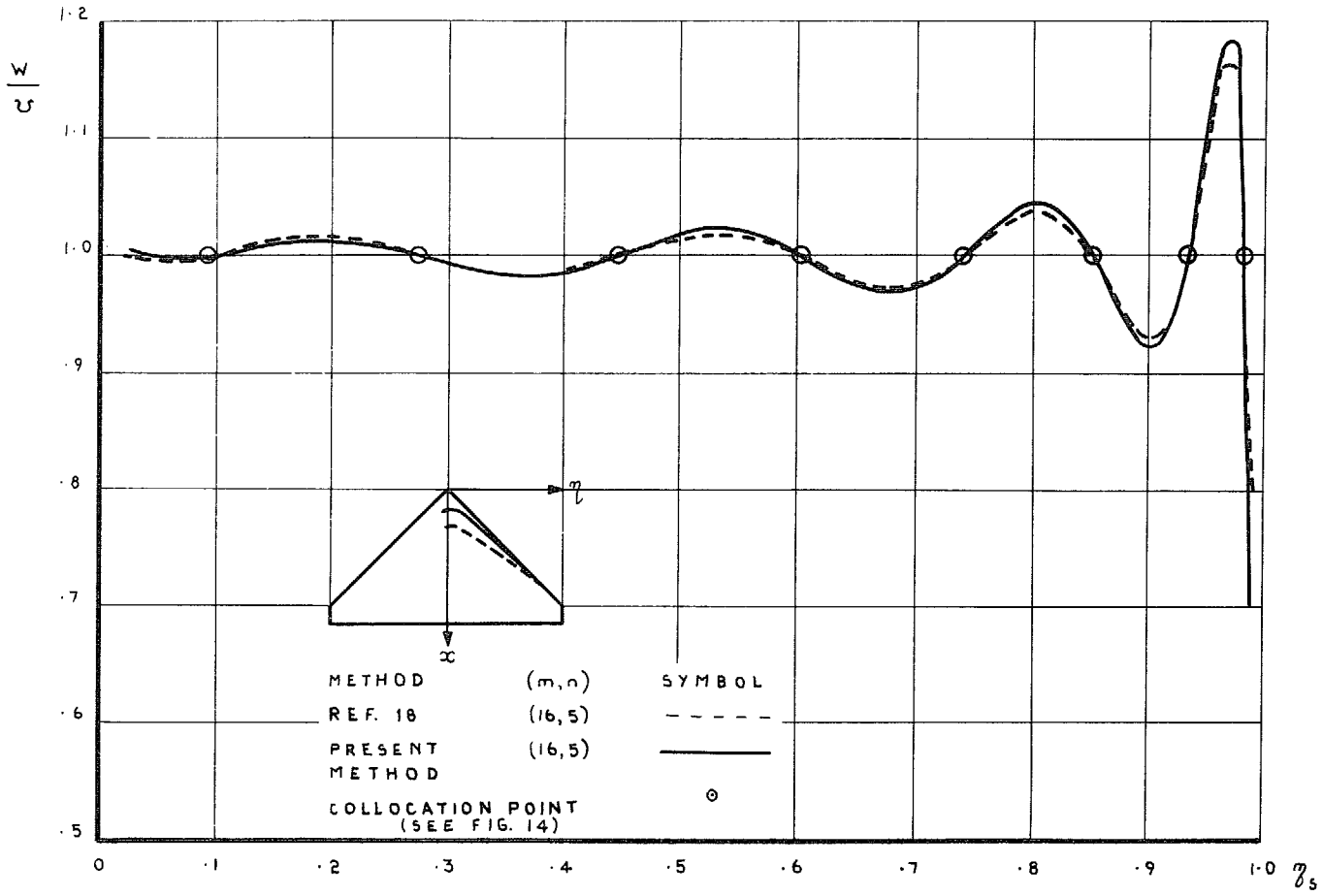

FIG. 12. Comparison of spanwise downwash interpolations for a cropped delta planform at chordwise collocation station $\xi_r = 0{\cdot}0794$.

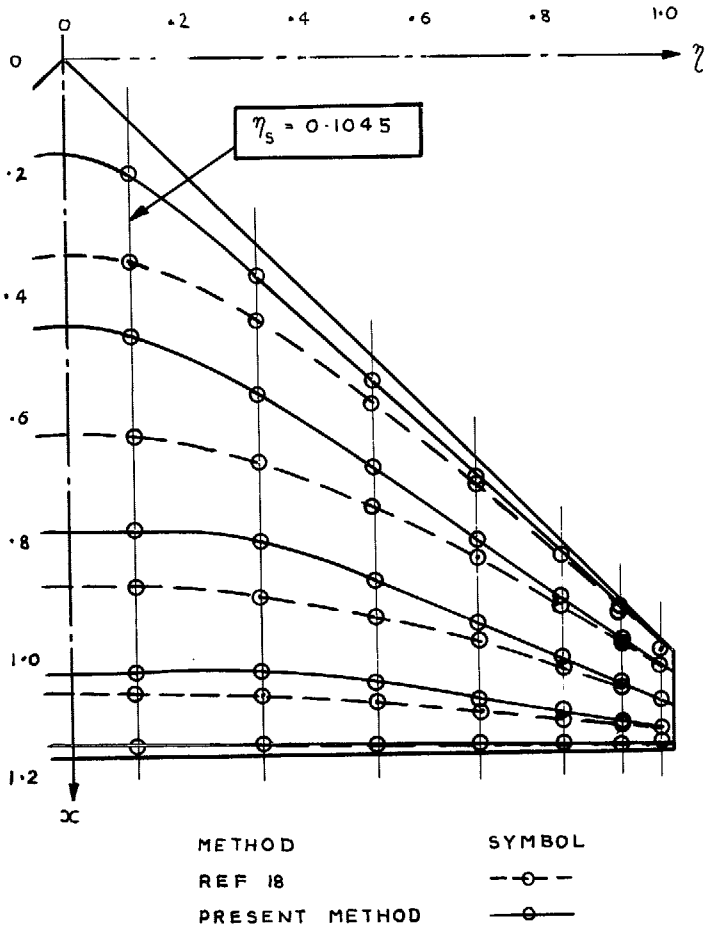

FIG. 13. Comparison of collocation distributions for a cropped delta planform with $(m, n) = (14, 5)$.

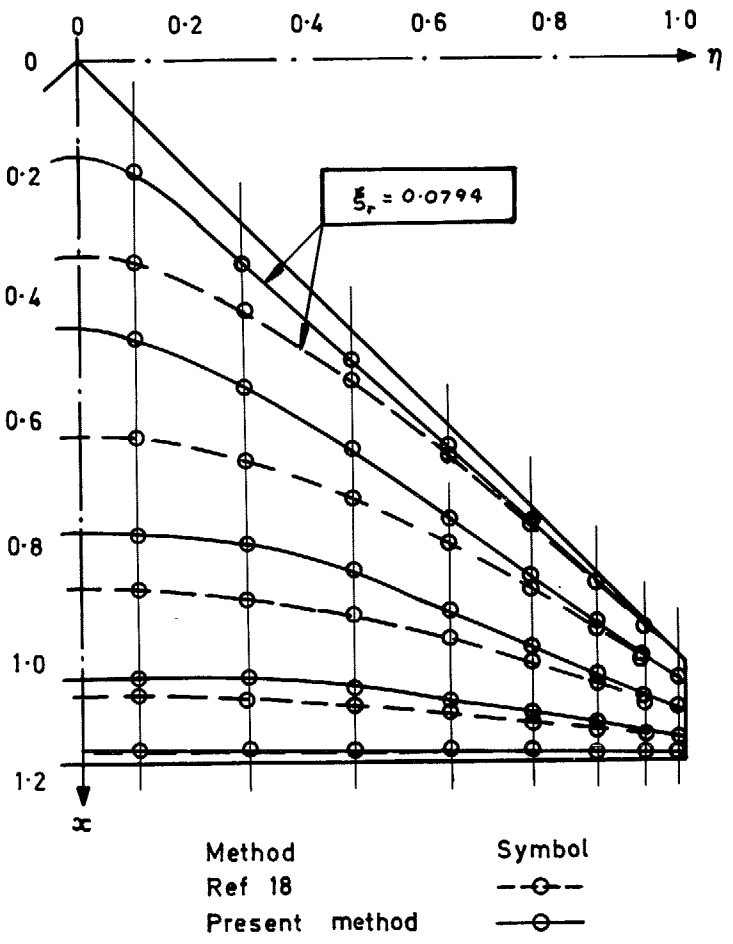

FIG. 14. Comparison of collocation distributions for a cropped delta planform with $(m, n) = (16, 5)$.

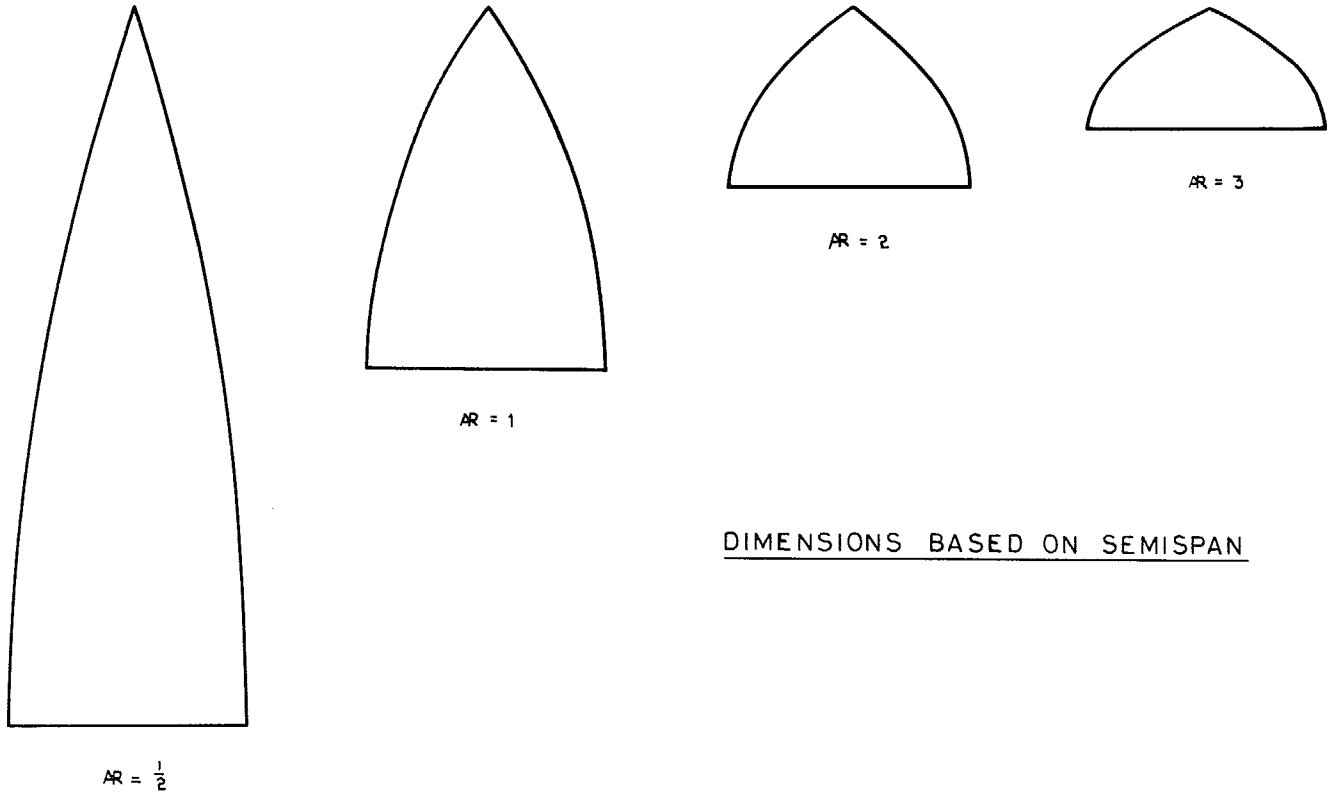

FIG. 15. Gothic planforms.

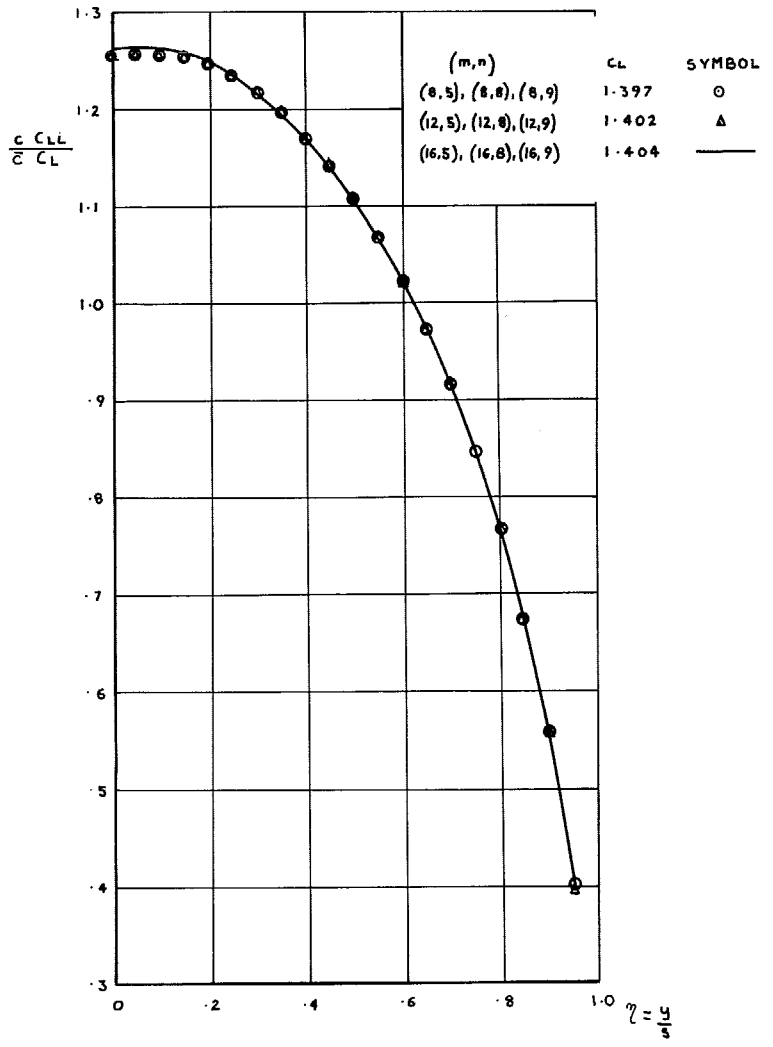

FIG. 16. Spanwise loading for a gothic planform $AR = 1$.

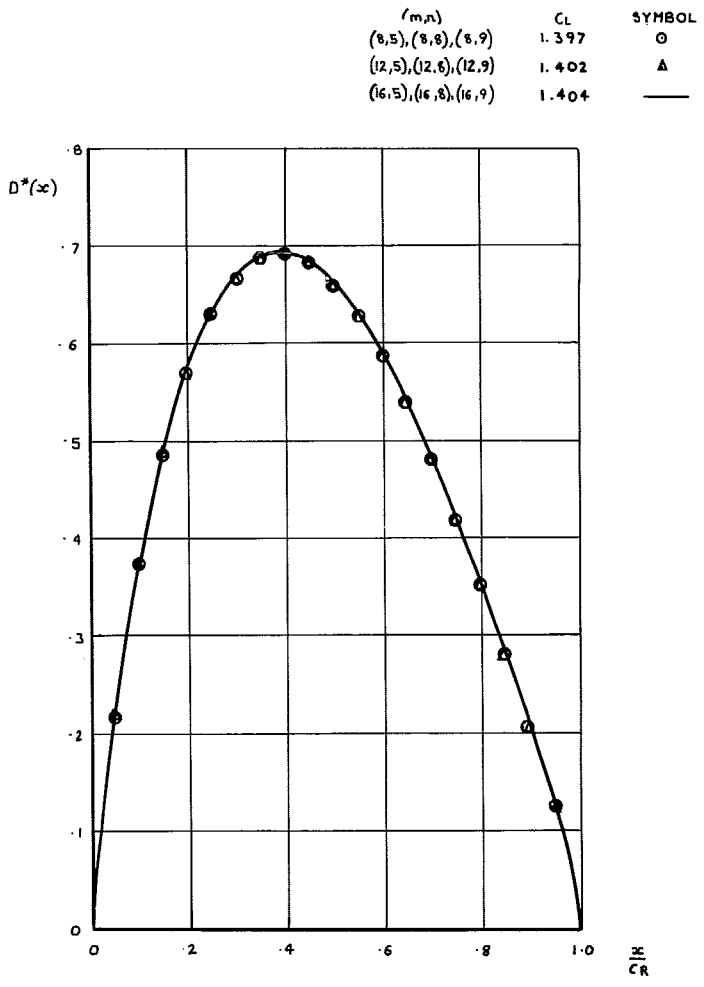

FIG. 17. Cross loading for a gothic planform $AR = 1$.

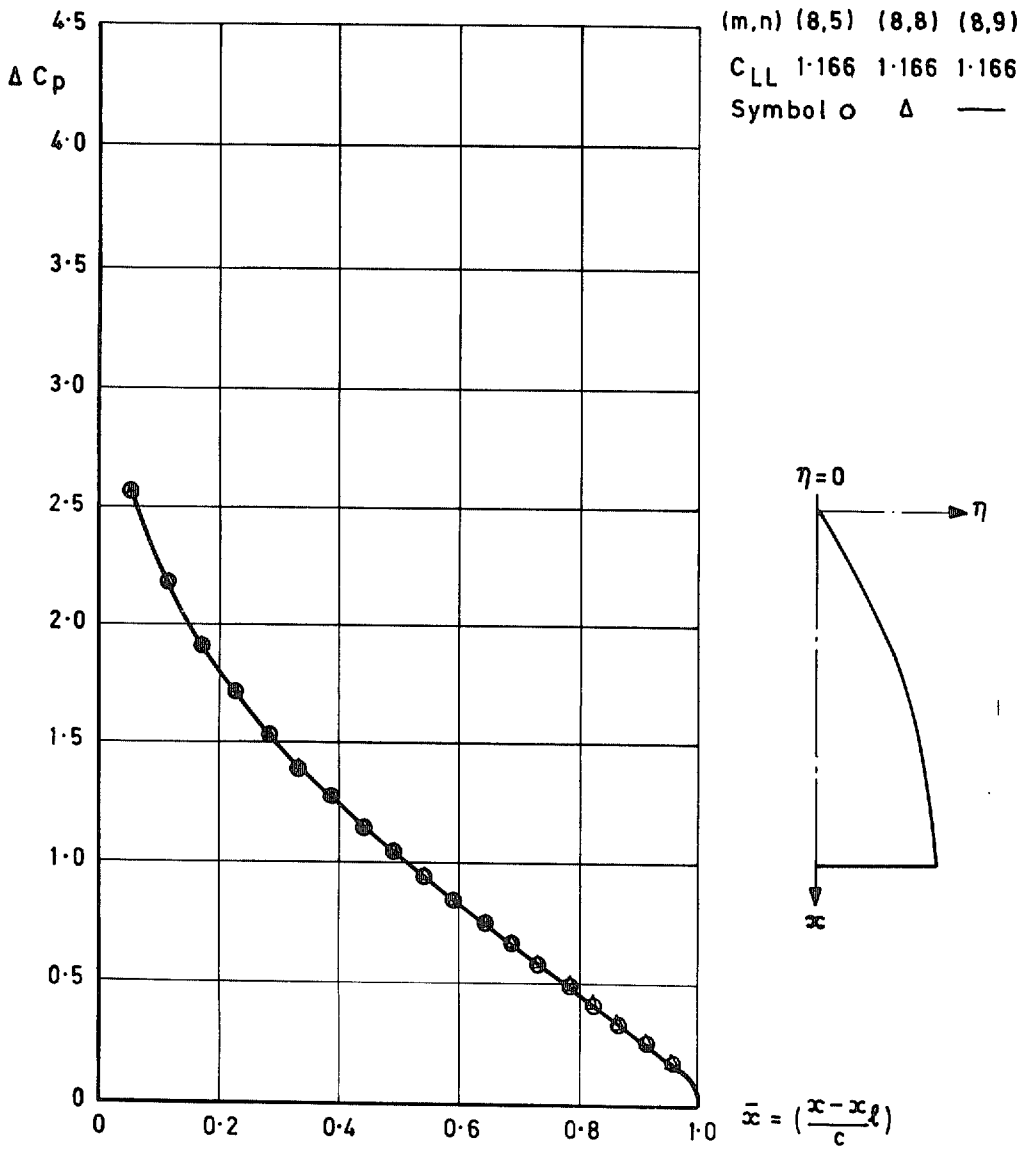

FIG. 18. Chordwise convergence of ΔCp at $\eta = 0$ with $m = 8$ for a gothic planform $AR = 1$.

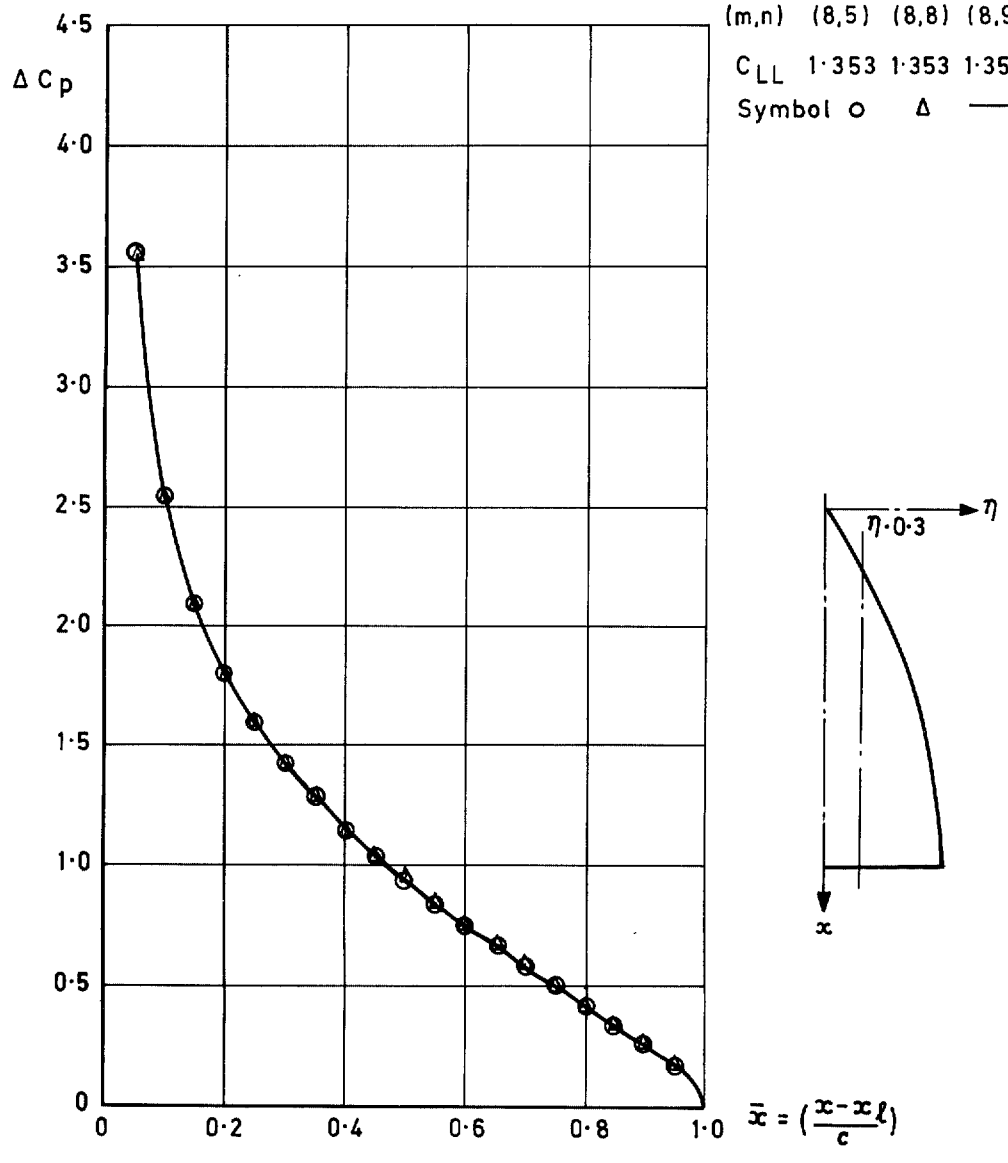

FIG. 19. Chordwise convergence of ΔCp at $\eta = 0{\cdot}3$ with $m = 8$ for a gothic planform $AR = 1$.

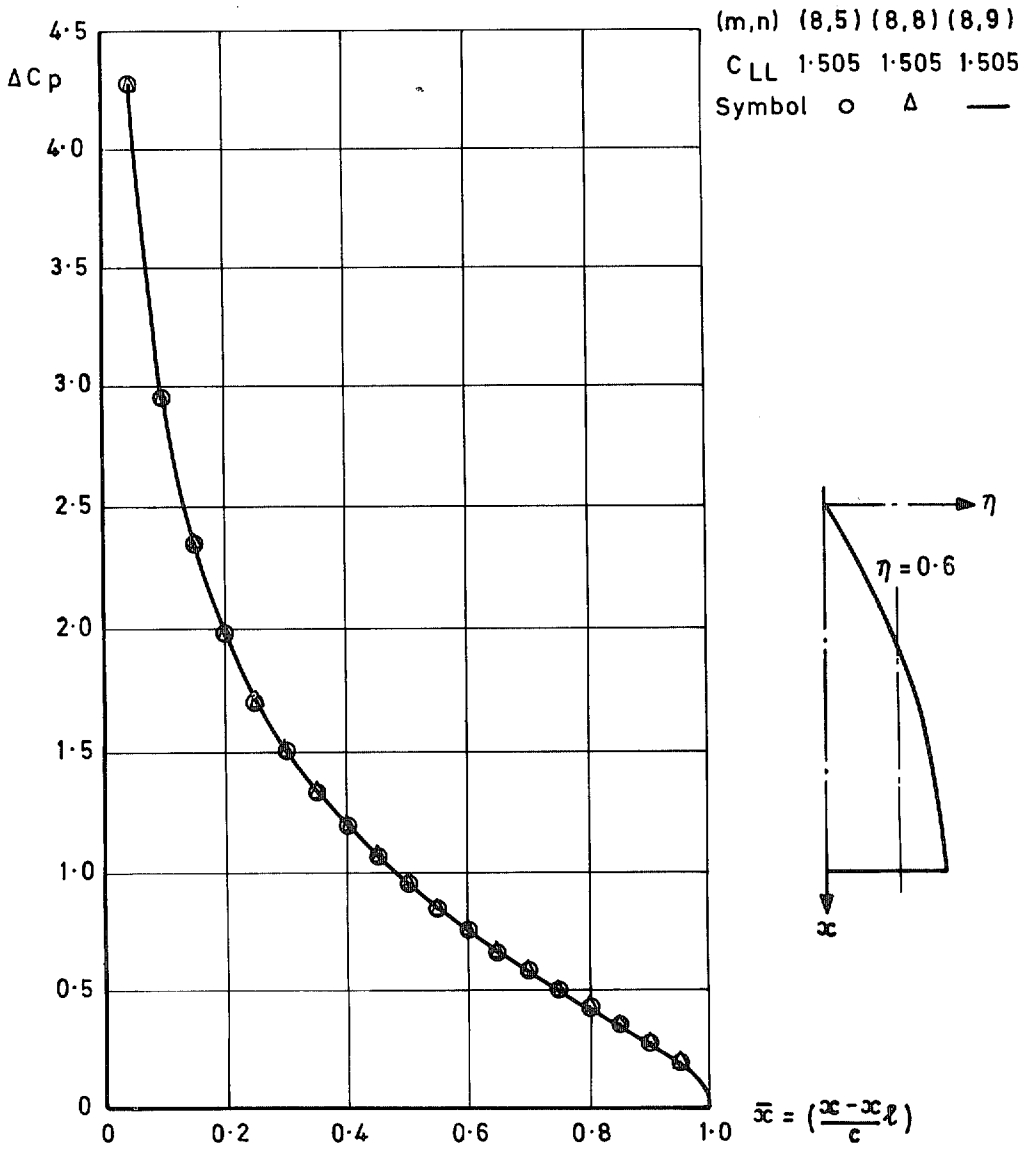

FIG. 20. Chordwise convergence of ΔCp at $\eta = 0{\cdot}6$ with $m = 8$ for a gothic planform $AR = 1$.

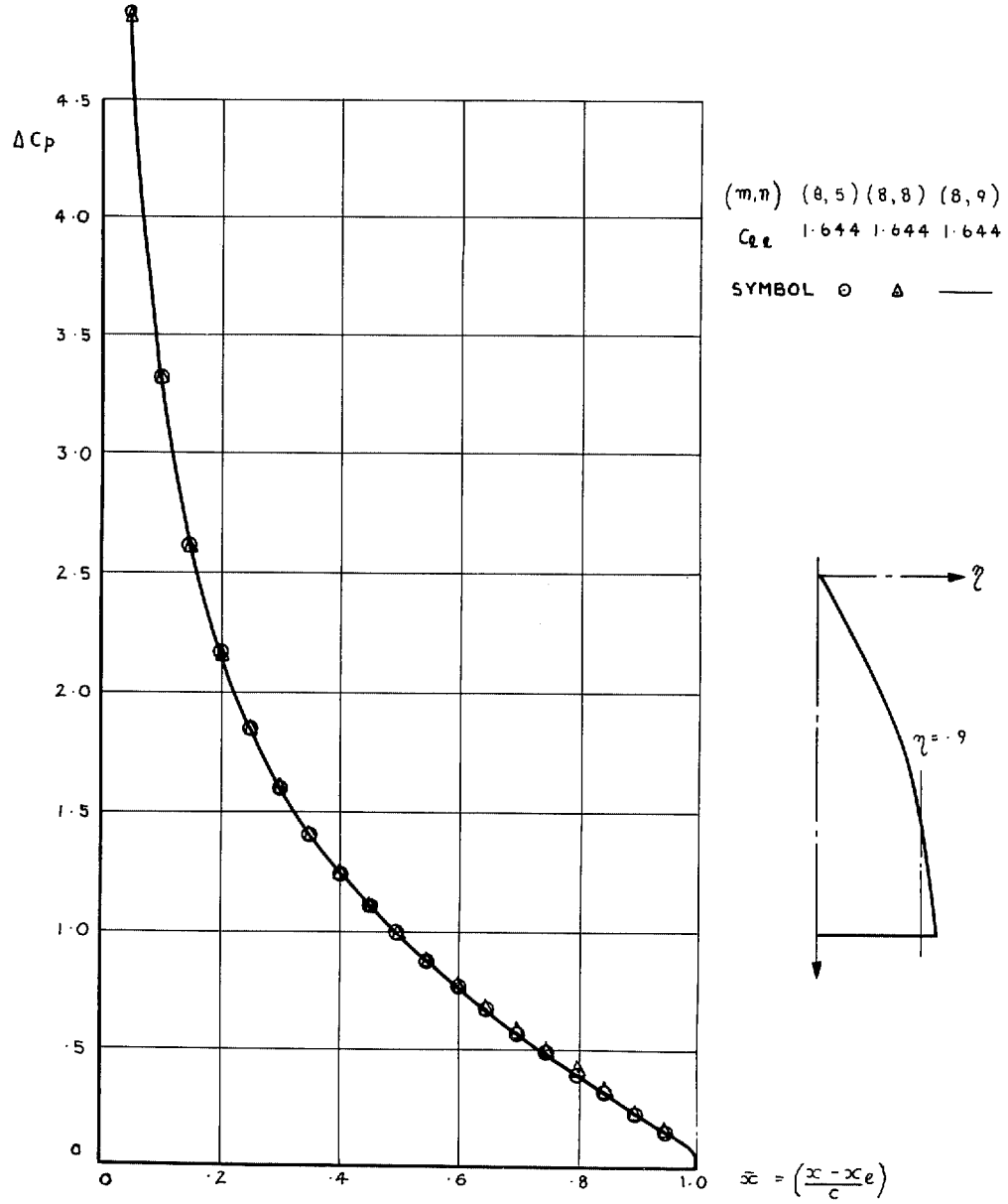

FIG. 21. Chordwise convergence of ΔCp at $\eta = 0{\cdot}9$ with $m = 8$ for a gothic planform $AR = 1$.

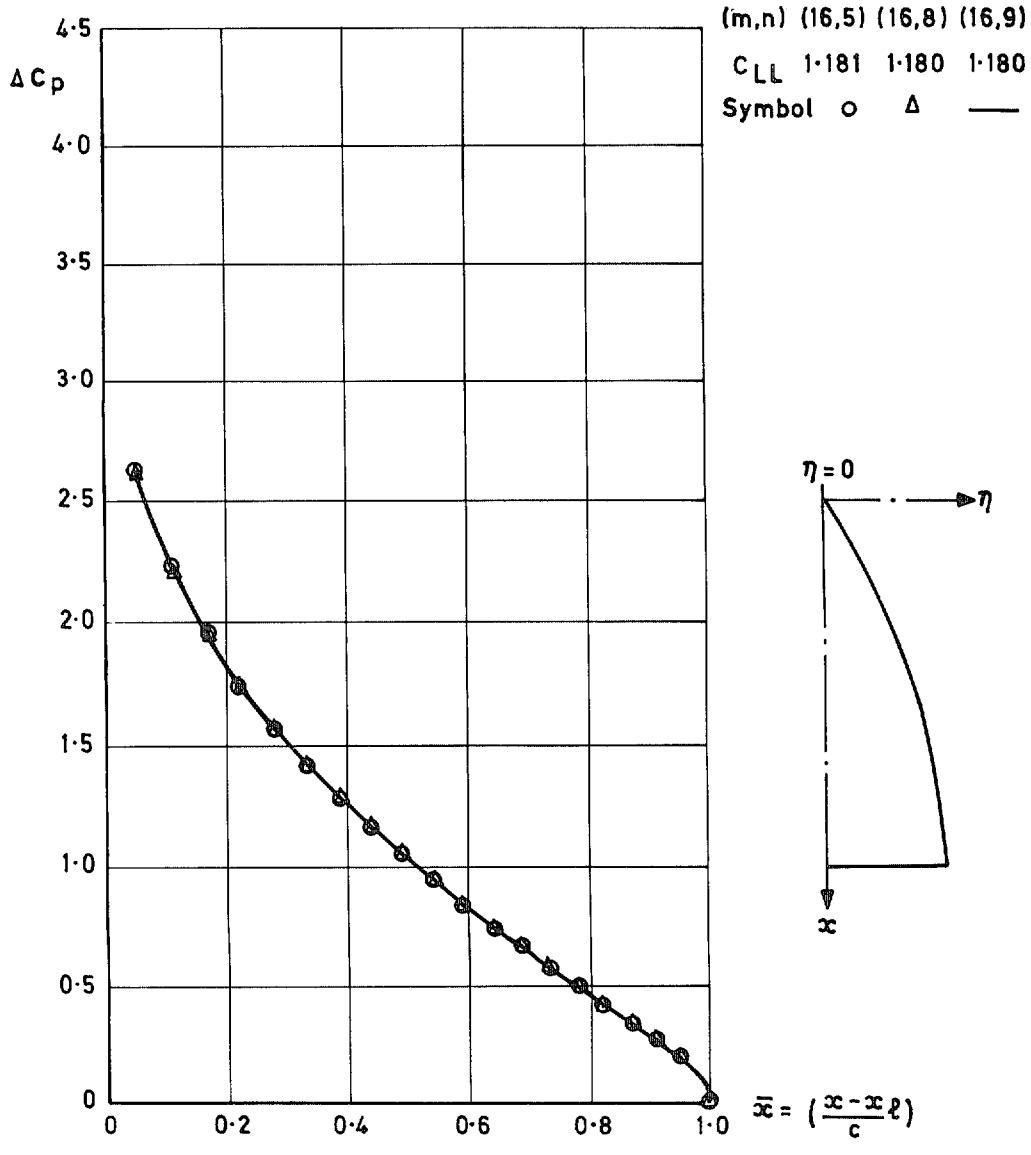

FIG. 22. Chordwise convergence of ΔCp at $\eta = 0$ with $m = 16$ for a gothic planform $AR = 1$.

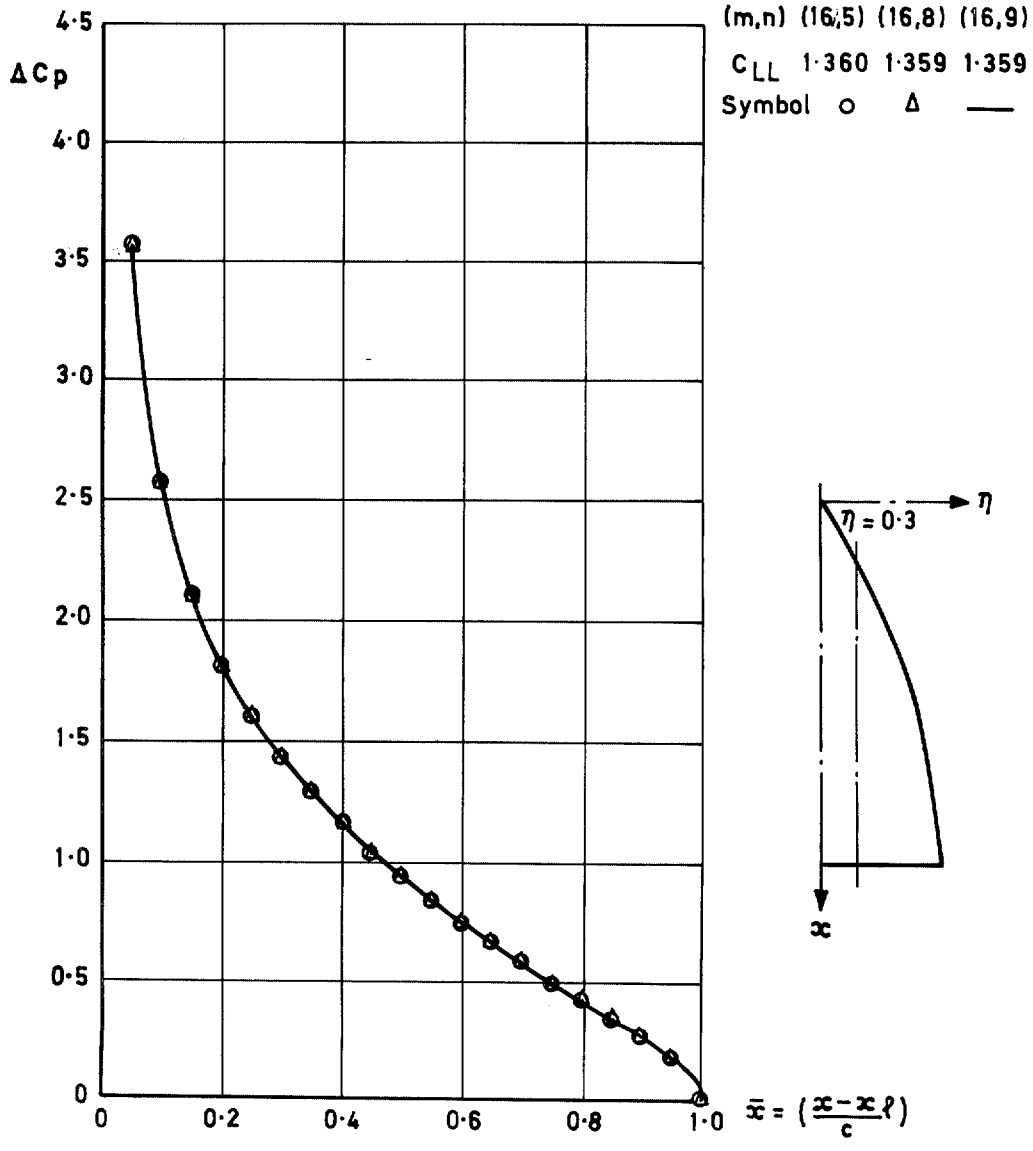

FIG. 23. Chordwise convergence of ΔCp at $\eta = 0{\cdot}3$ with $m = 16$ for a gothic planform $AR = 1$.

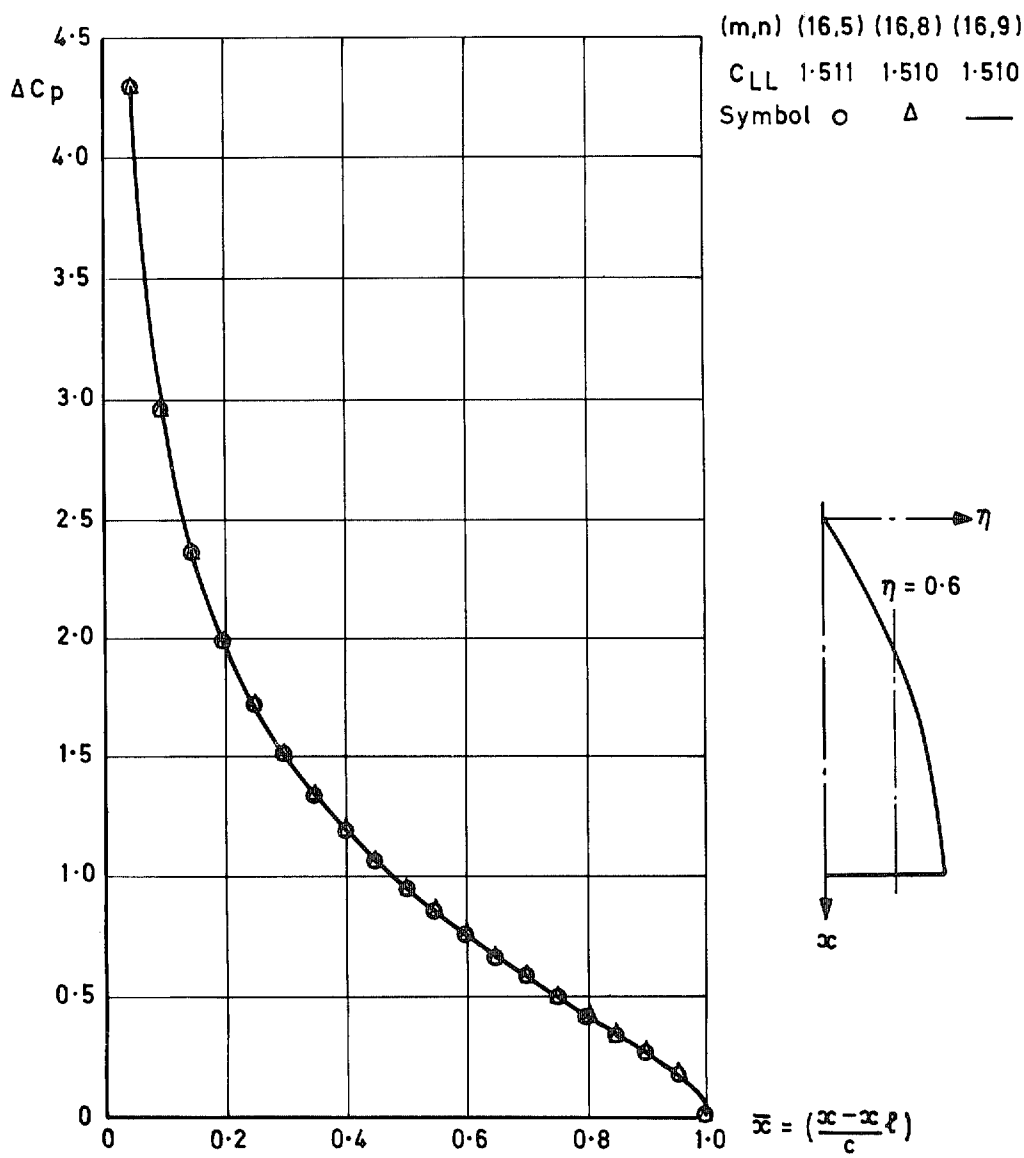

FIG. 24. Chordwise convergence of ΔCp at $\eta = 0{\cdot}6$ with $m = 16$ for a gothic planform $AR = 1$.

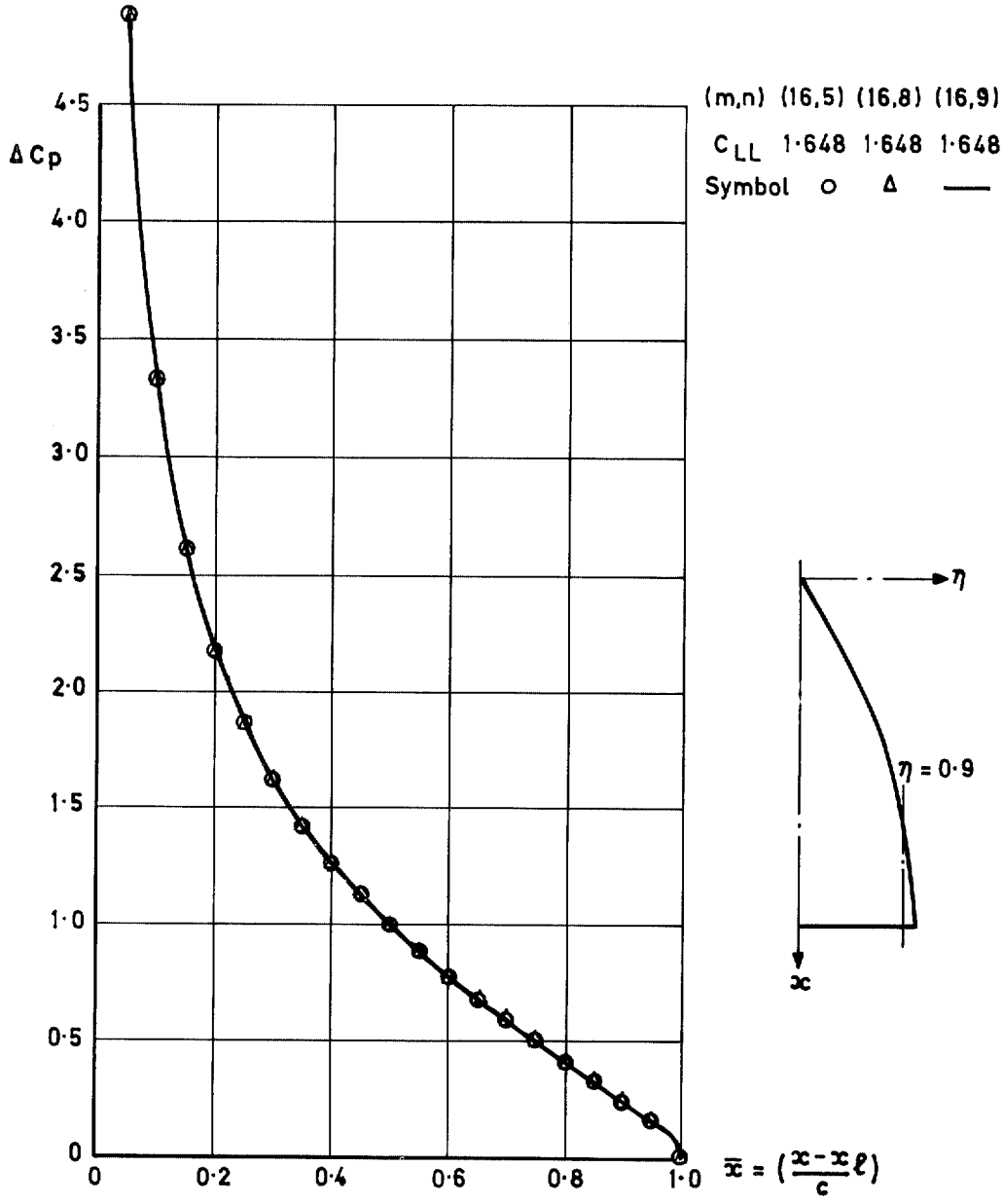

FIG. 25. Chordwise convergence of ΔCp at $\eta = 0{\cdot}9$ with $m = 16$ for a gothic planform $AR = 1$.

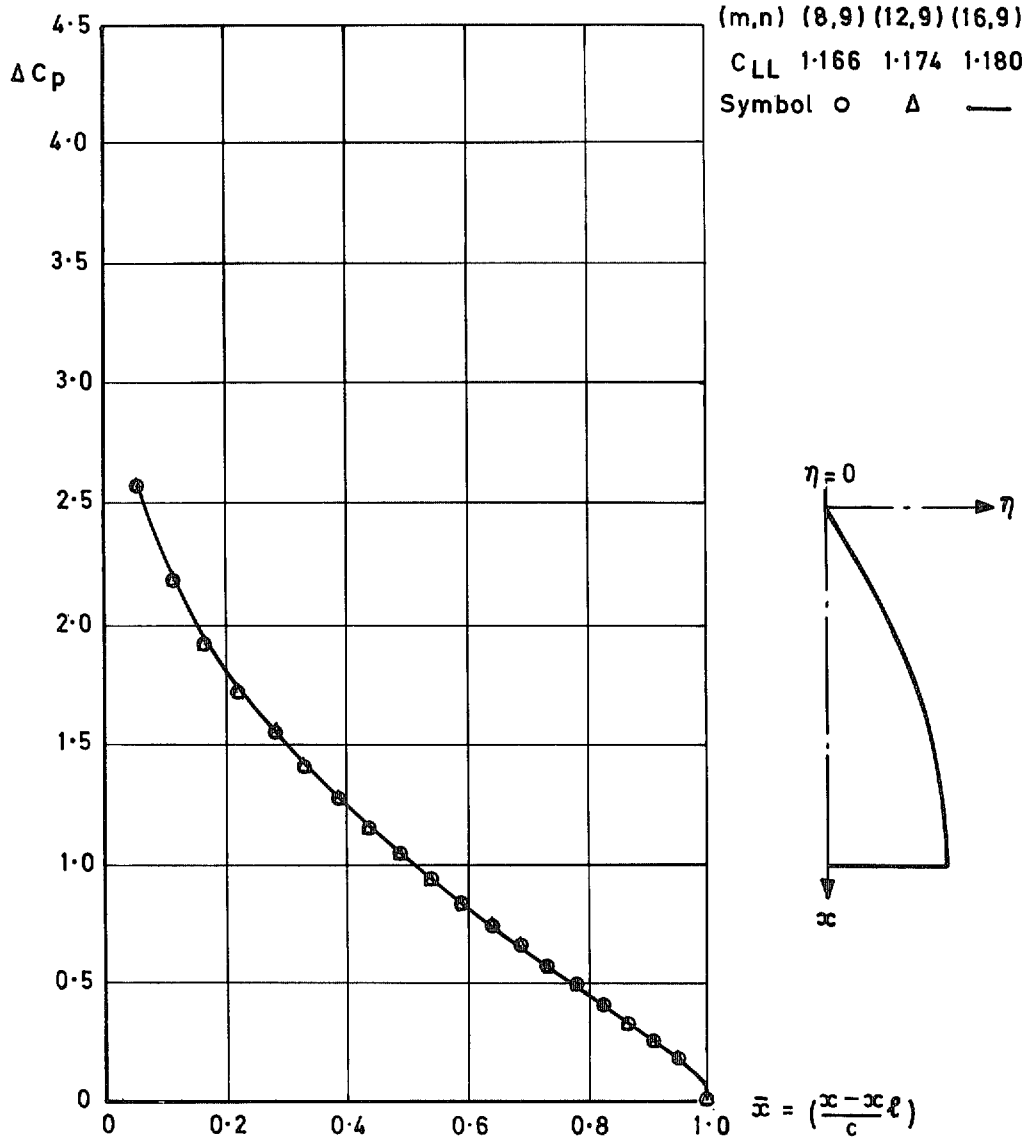

FIG. 26. Comparison of ΔCp distributions at $\eta = 0$ with $n = 9$ for a gothic planform $AR = 1$.

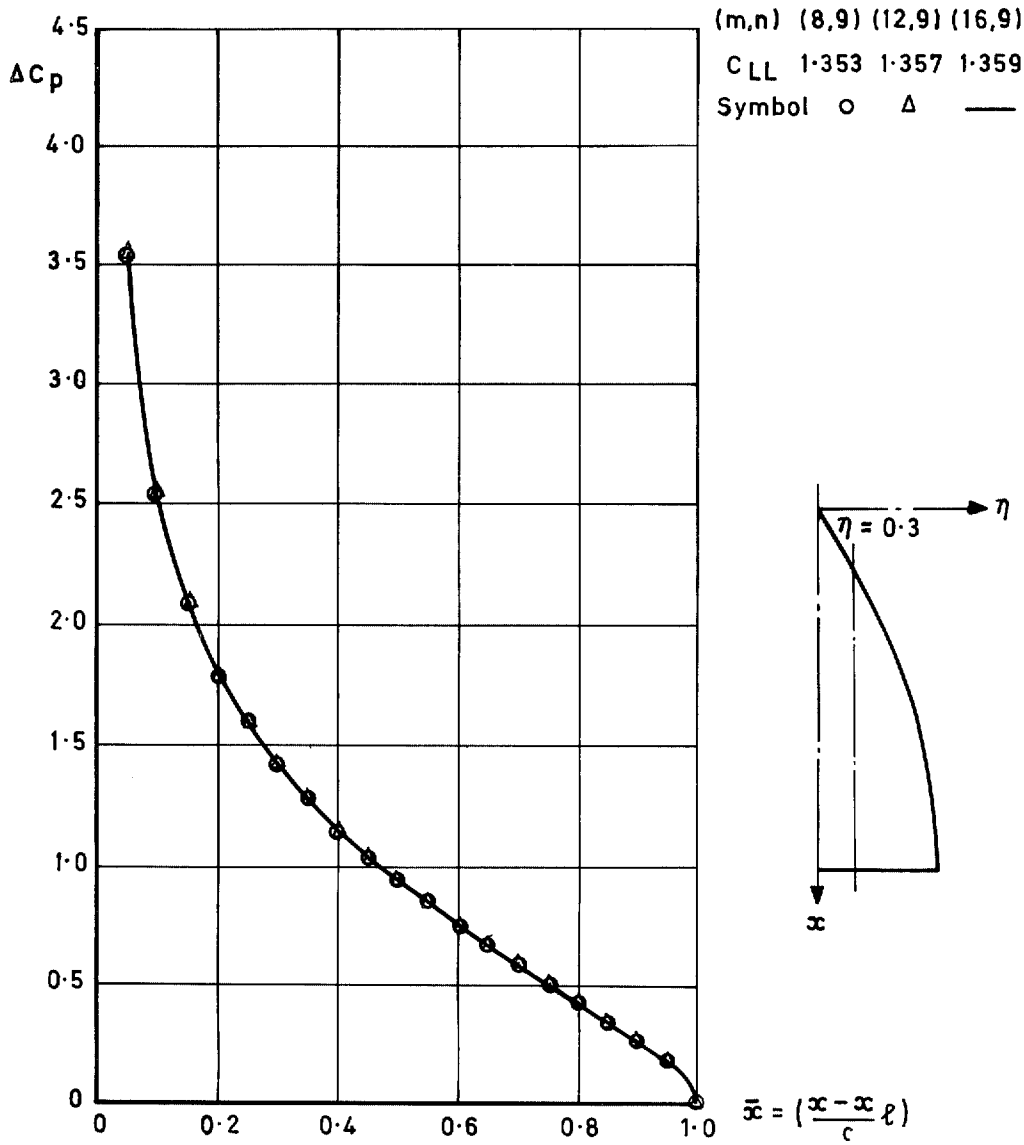

FIG. 27. Comparison of ΔCp distributions at $\eta = 0{\cdot}3$ with $n = 9$ for a gothic planform $AR = 1$.

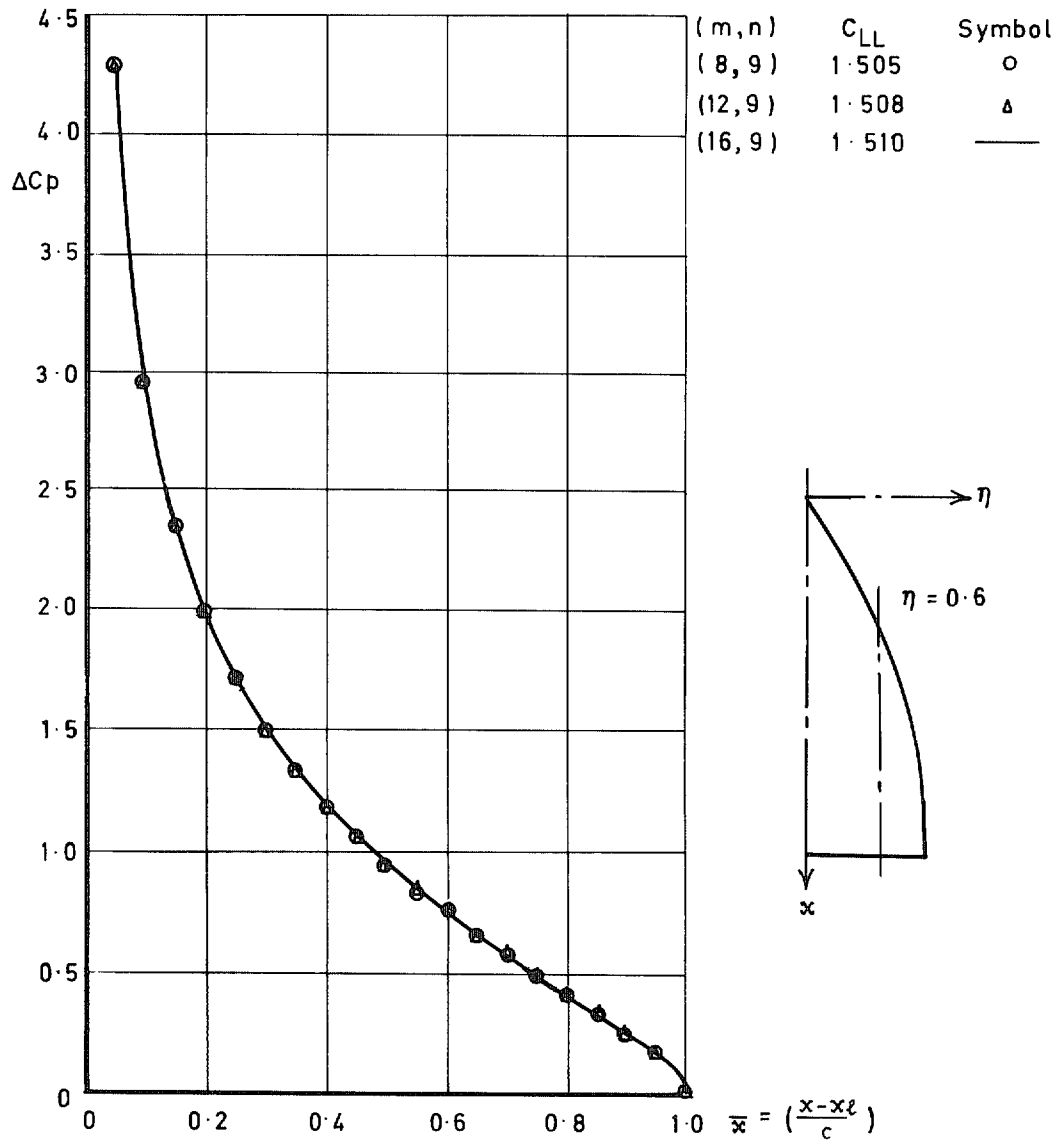

FIG. 28. Comparison of ΔCp distributions at $\eta = 0{\cdot}6$ with $n = 9$ for a gothic planform $AR = 1$.

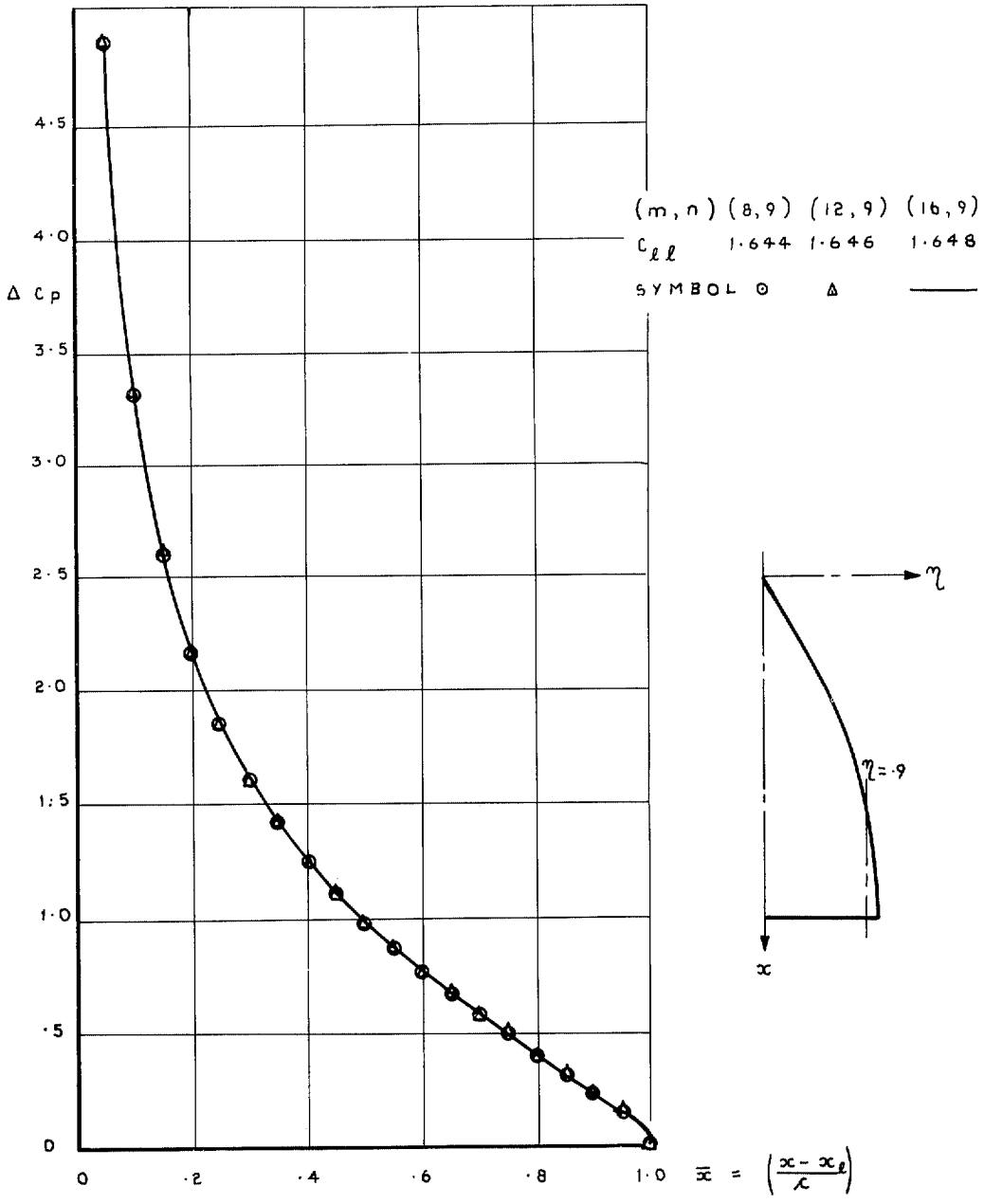

FIG. 29. Comparison of ΔCp distributions at $\eta = 0{\cdot}9$ with $n = 9$ for a gothic planform $AR = 1$.

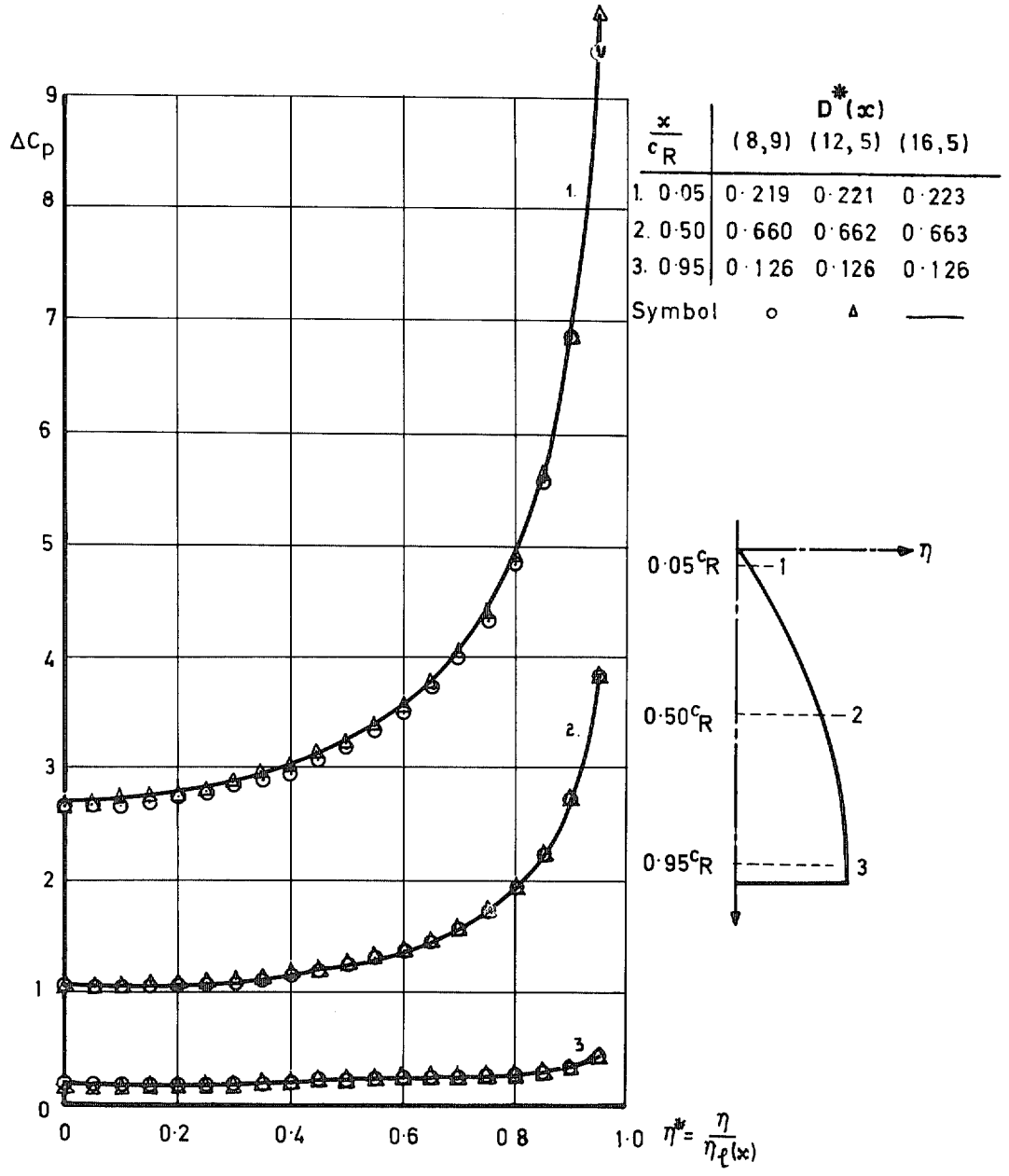

FIG. 30. Spanwise convergence of ΔCp with $n = 5$ for a gothic planform $AR = 1$.

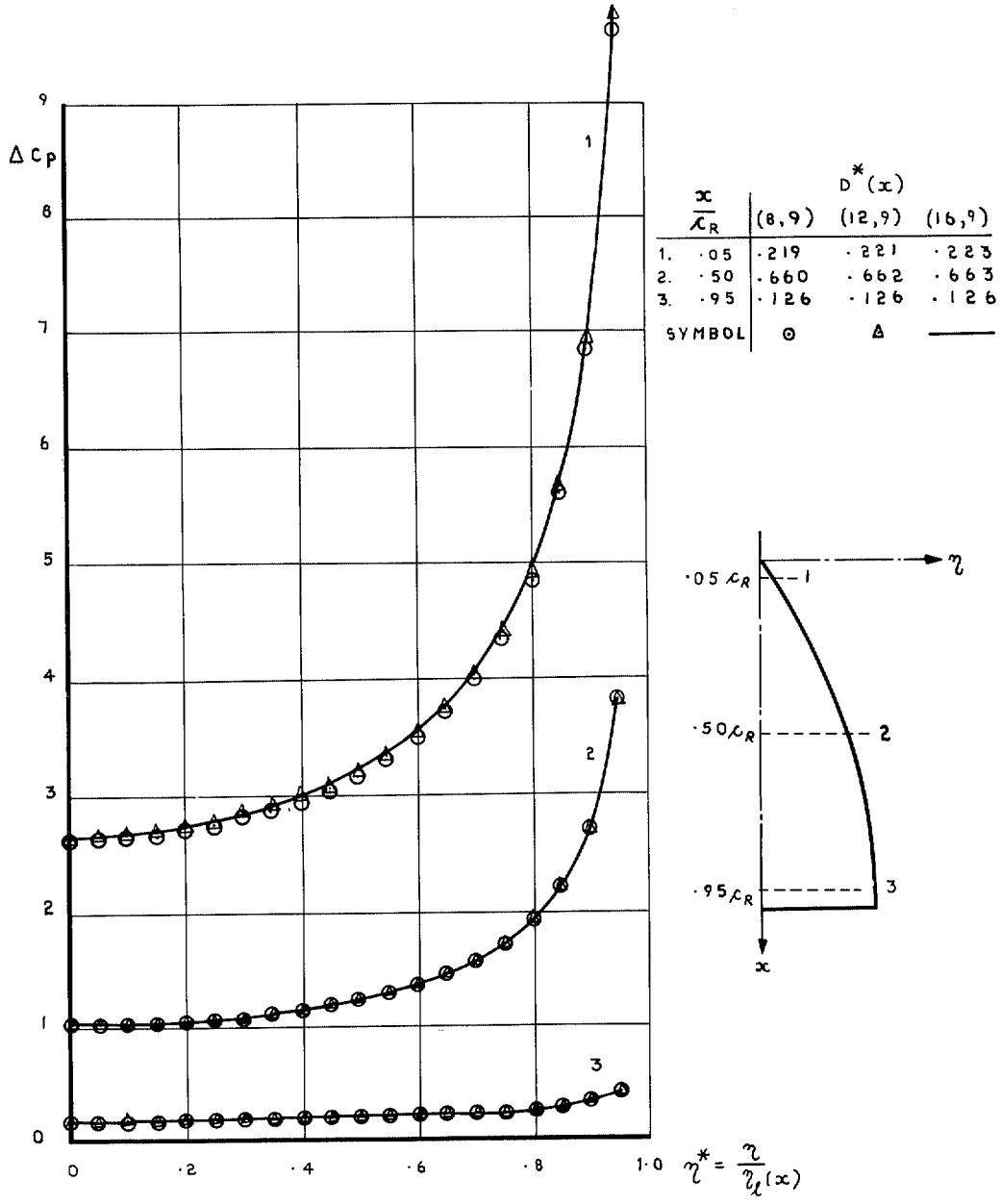

FIG. 31. Spanwise convergence of ΔCp with $n = 9$ for a gothic planform $AR = 1$.

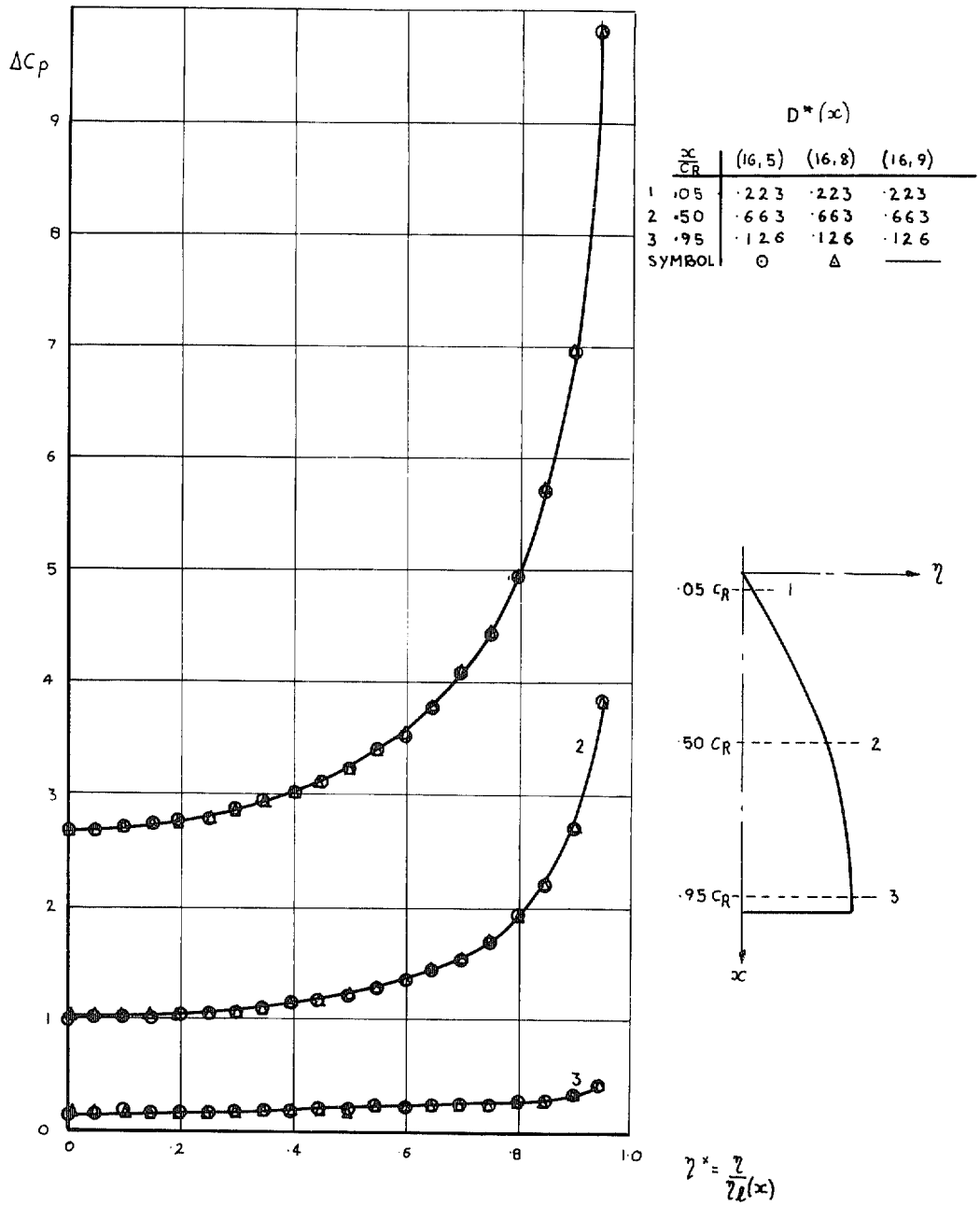

FIG. 32. Comparison of ΔCp distributions with $m = 16$ for a gothic planform $AR = 1$.

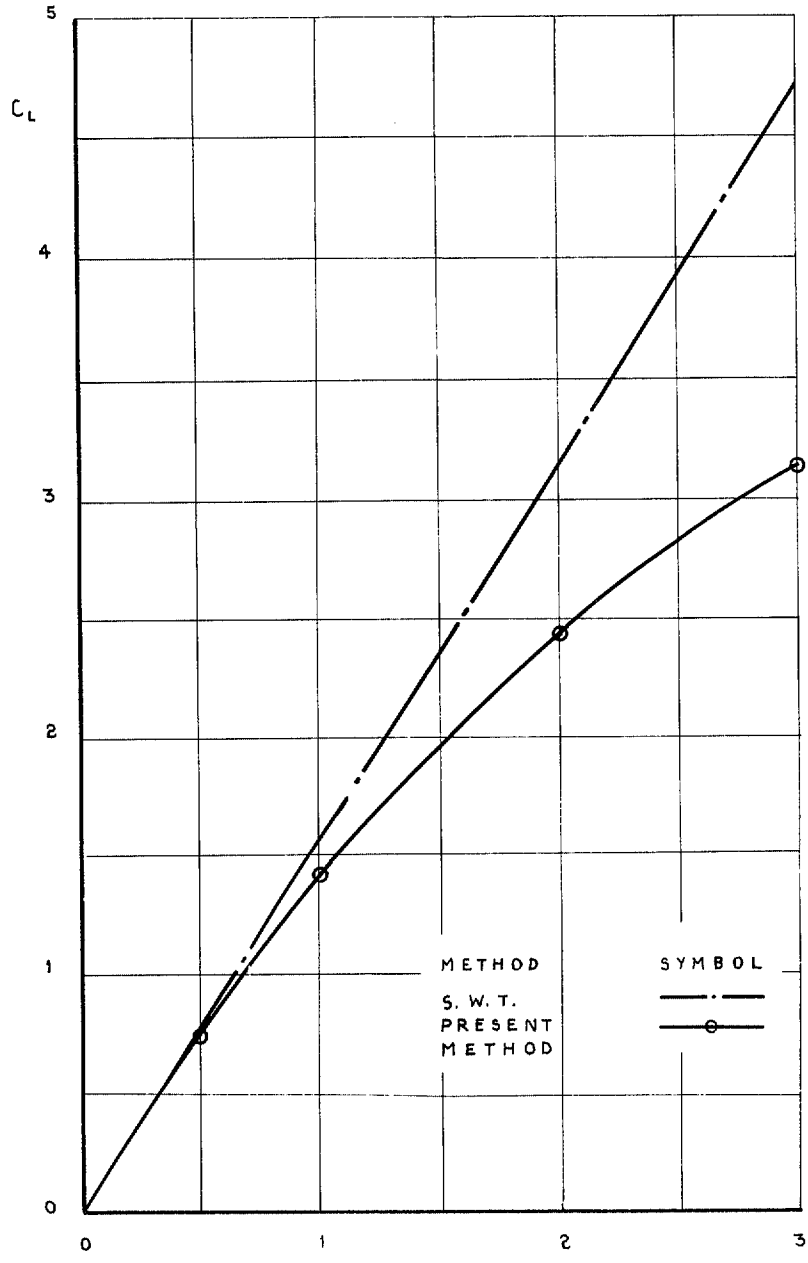

FIG. 33. Variation of lift coefficient with aspect ratio for gothic wing planforms.

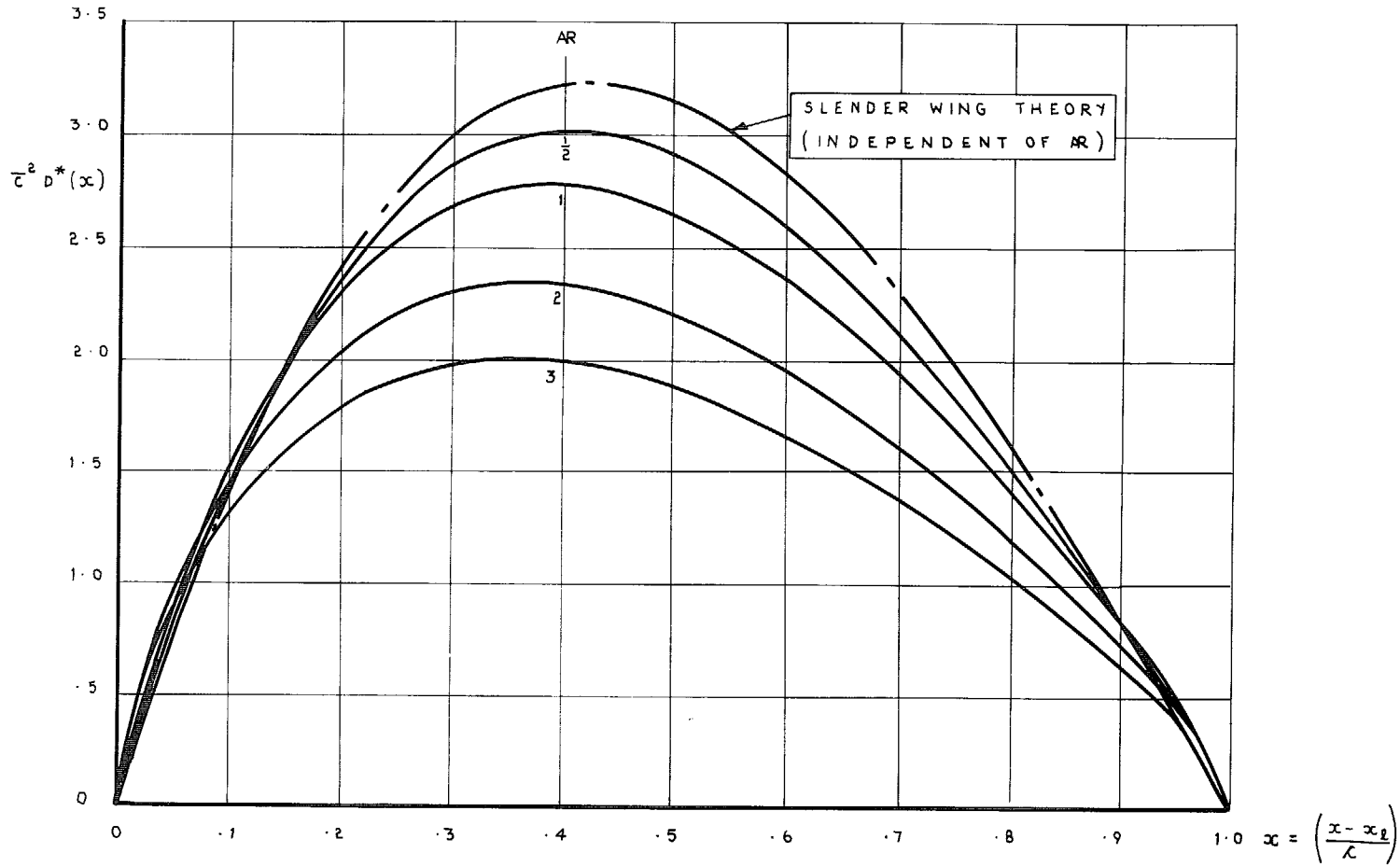

FIG. 34. Comparison of cross loading scaled by $\bar{C}^2$ with slender wing theory gothic wing planforms.

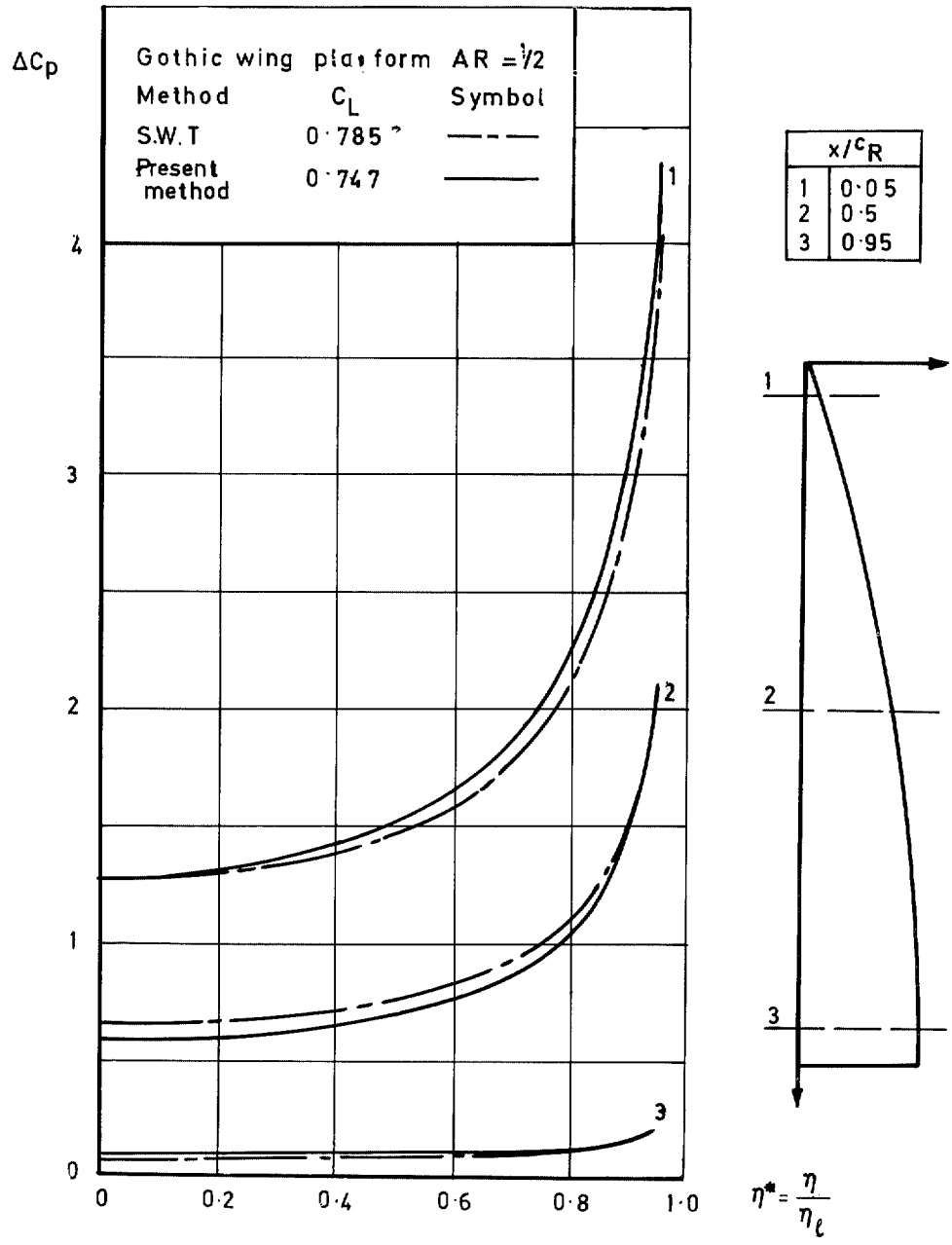

FIG. 35. Comparison of ΔCp with slender wing theory gothic planform $AR = \frac{1}{2}$.

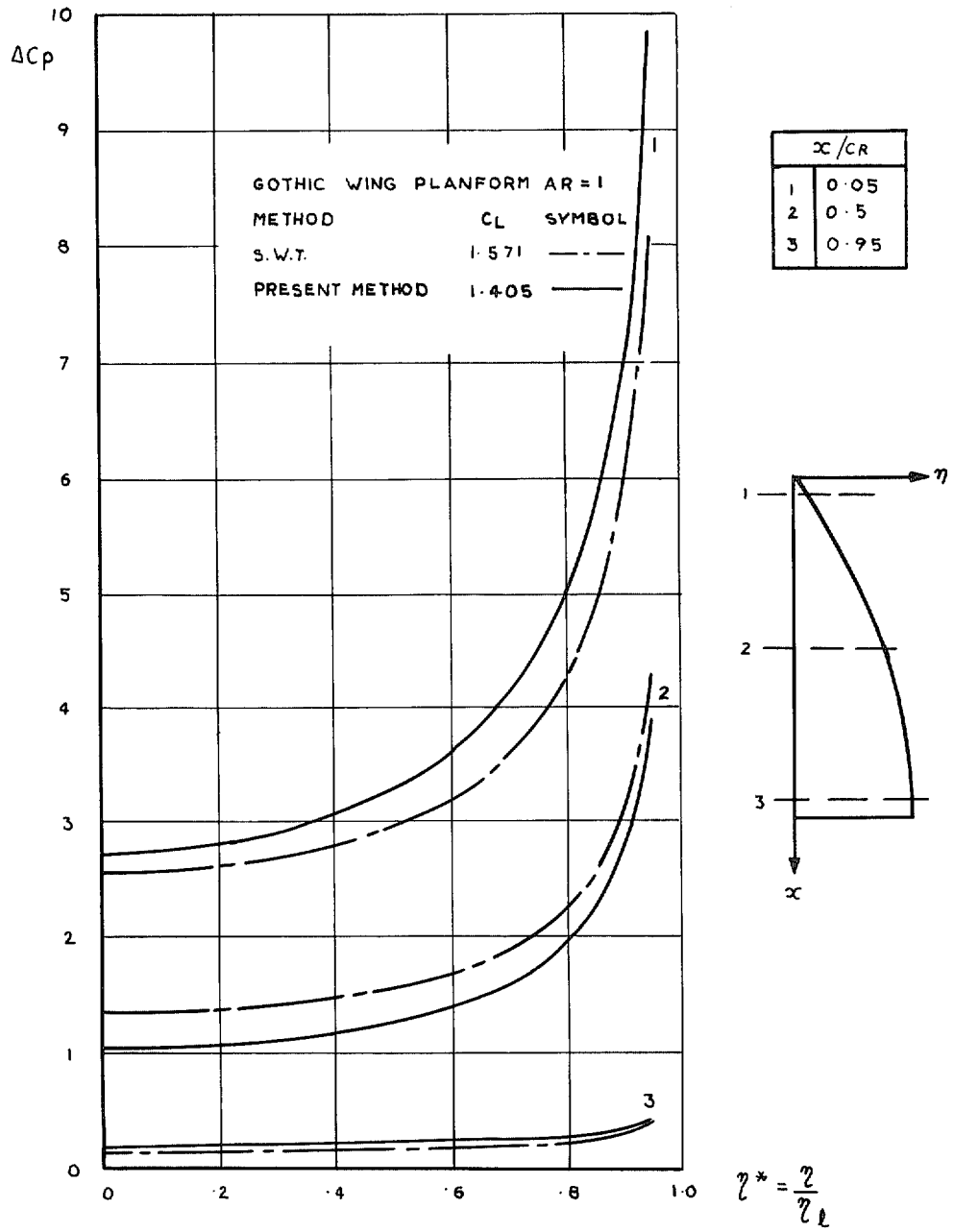

FIG. 36. Comparison of ΔCp with slender wing theory gothic planform $AR = 1$.

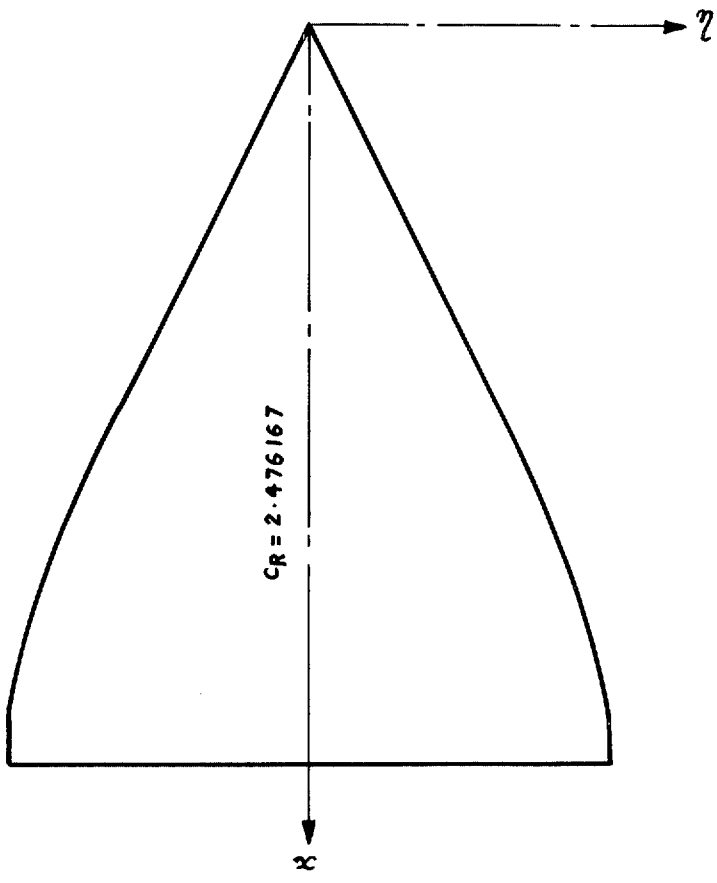

FIG. 37. The mild gothic planform.

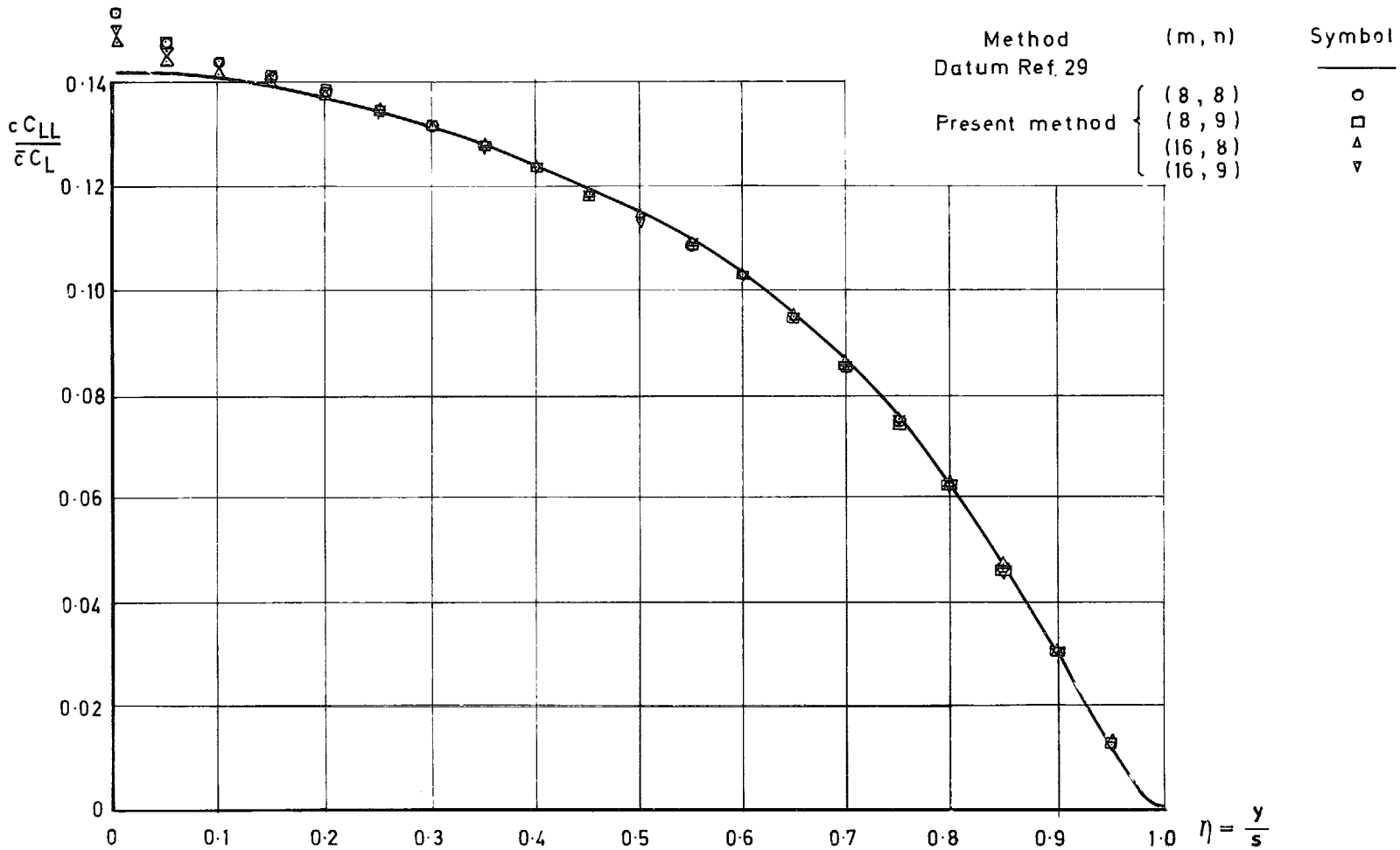

FIG. 38. Spanwise loading for a mild gothic cambered planform.

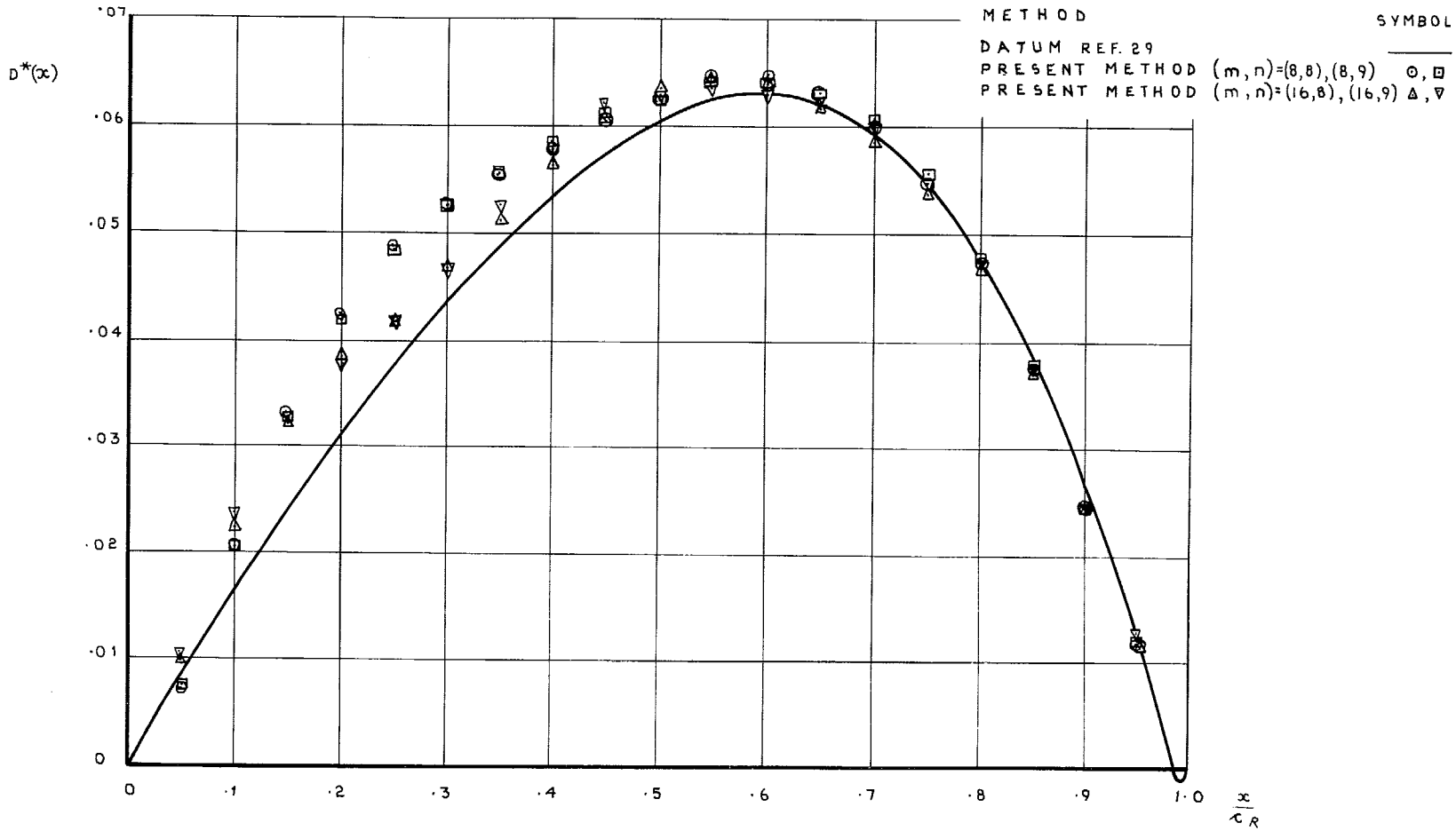

FIG. 39. Cross loading for a mild gothic cambered planform.

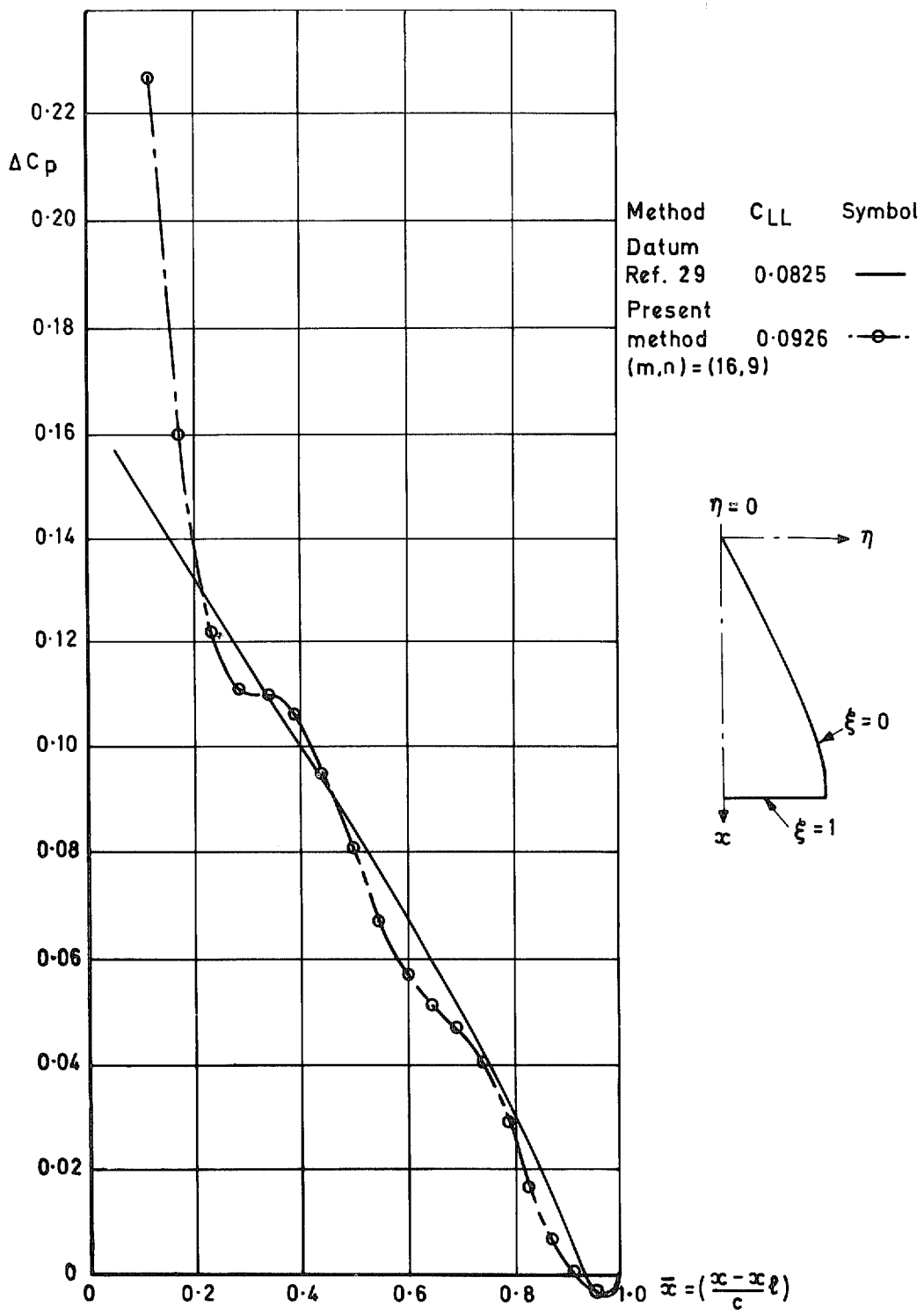

FIG. 40. Chordwise distribution of ΔCp at $\eta = 0$ for a mild gothic cambered planform.

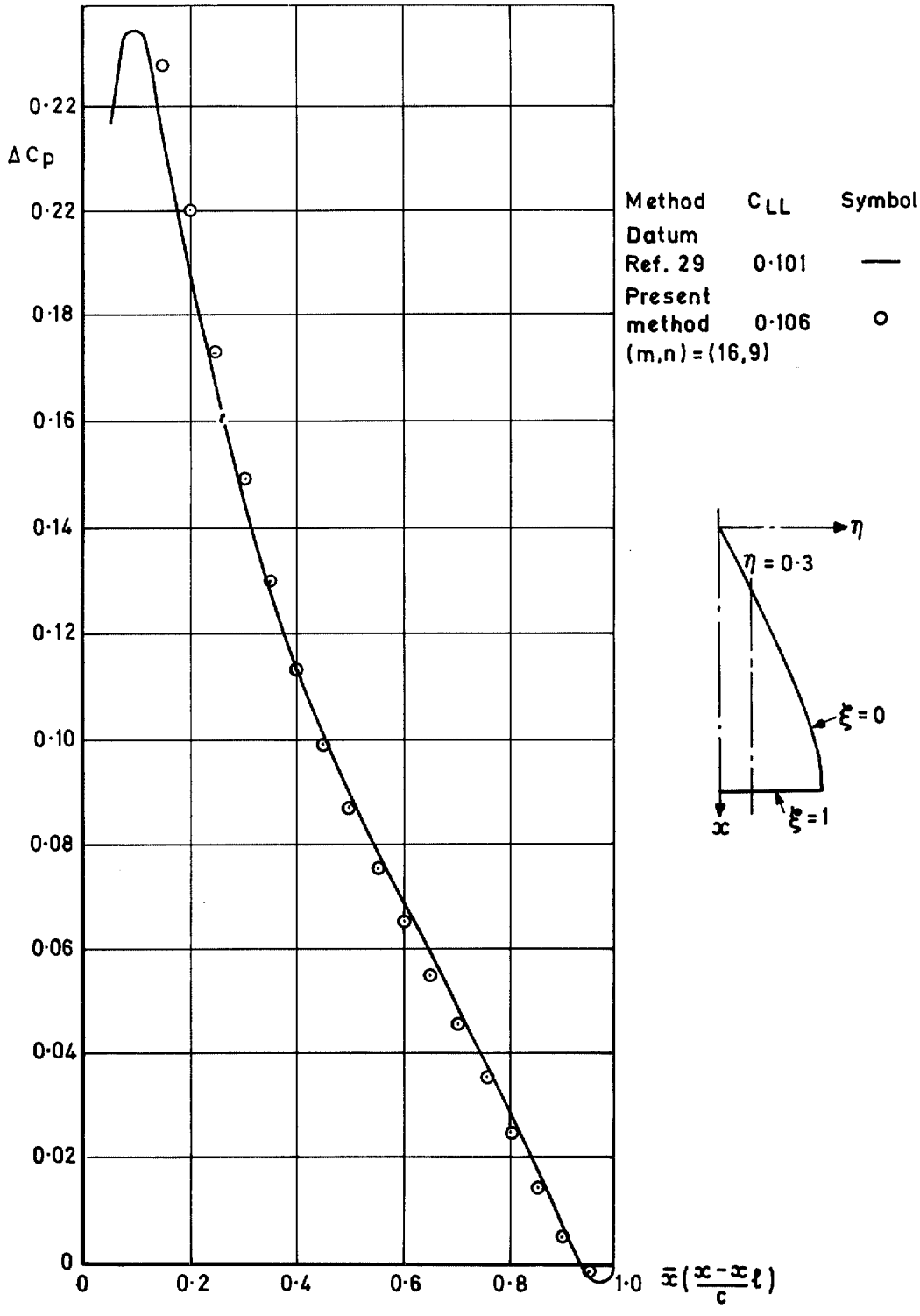

FIG. 41. Chordwise distribution of ΔCp at $\eta = 0{\cdot}3$ for a mild gothic cambered planform.

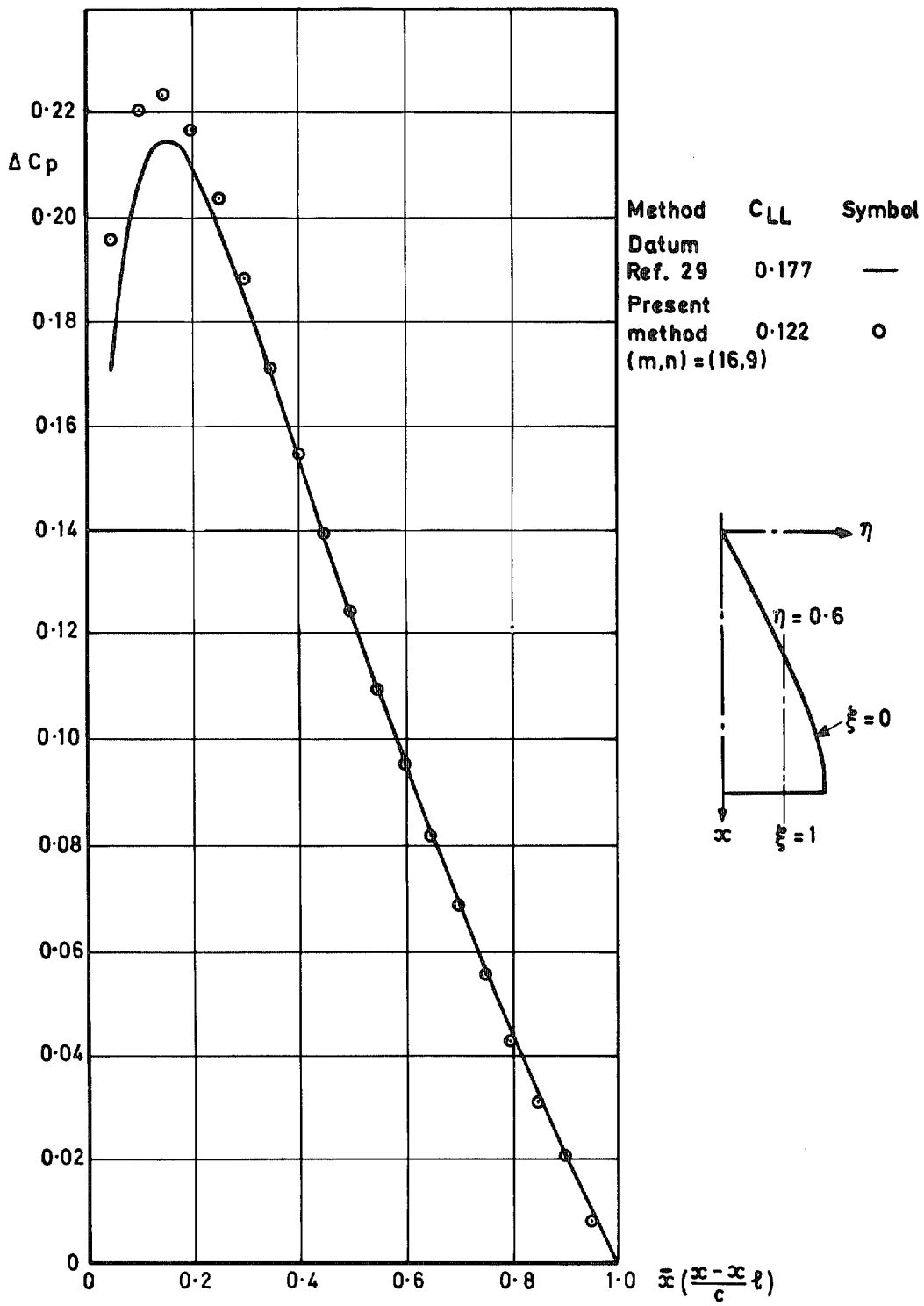

FIG. 42. Chordwise distribution of ΔCp at $\eta = 0{\cdot}6$ for a mild gothic cambered planform.

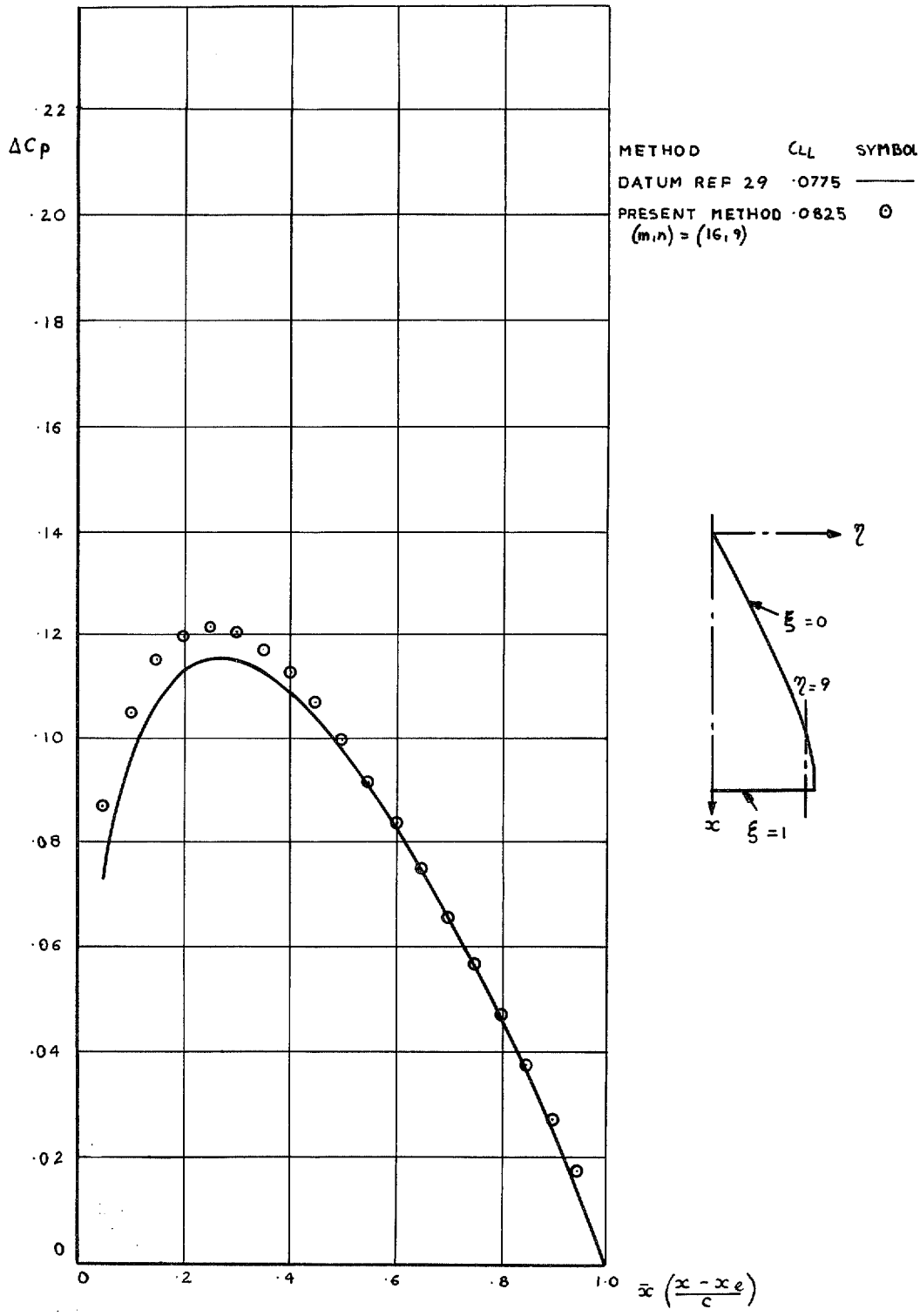

FIG. 43. Chordwise distribution of ΔCp at $\eta = 0{\cdot}9$ for a mild gothic cambered planform.

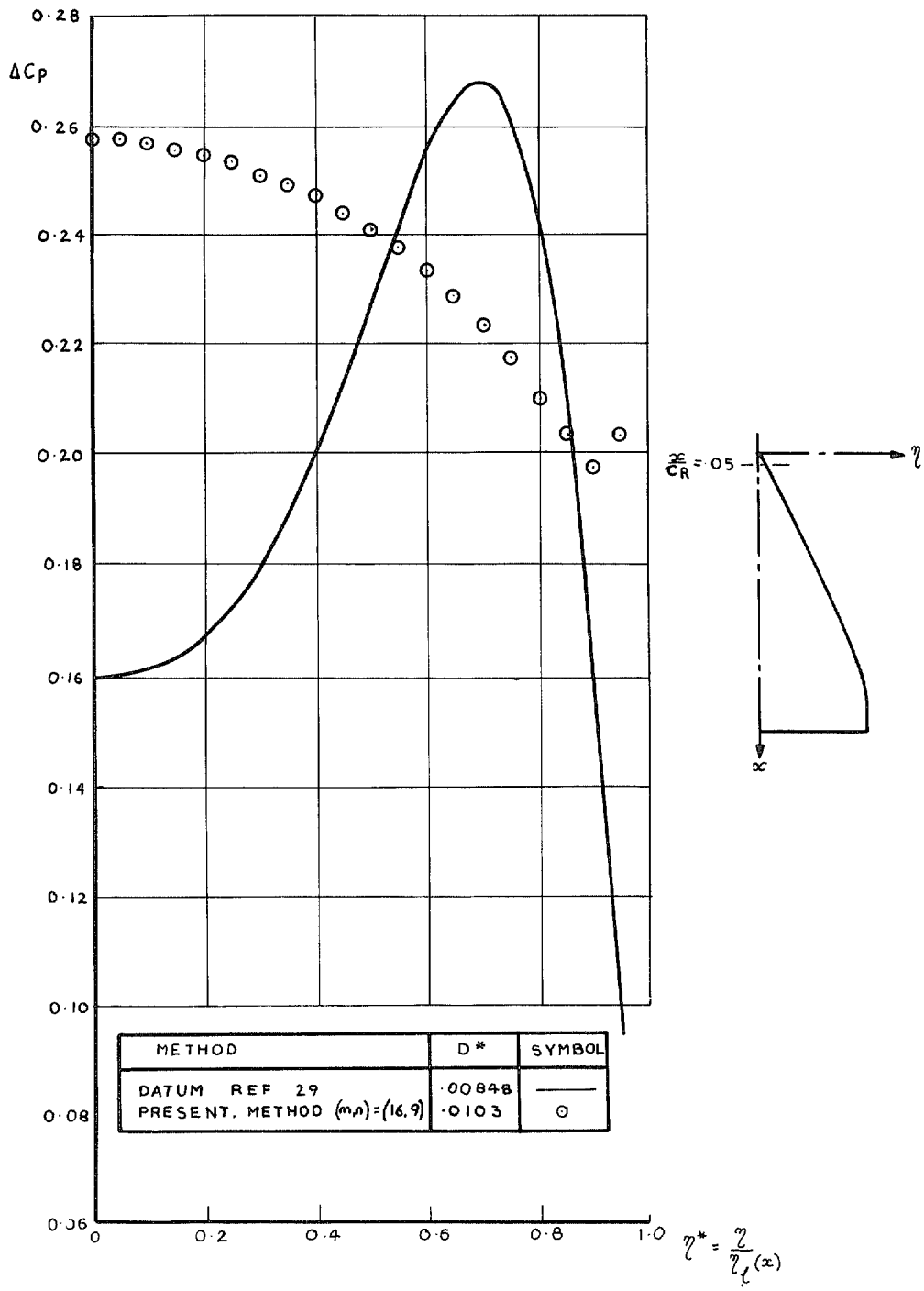

FIG. 44. Spanwise distribution of ΔCp at $x/c_R = 0{\cdot}05$ for a mild gothic cambered planform.

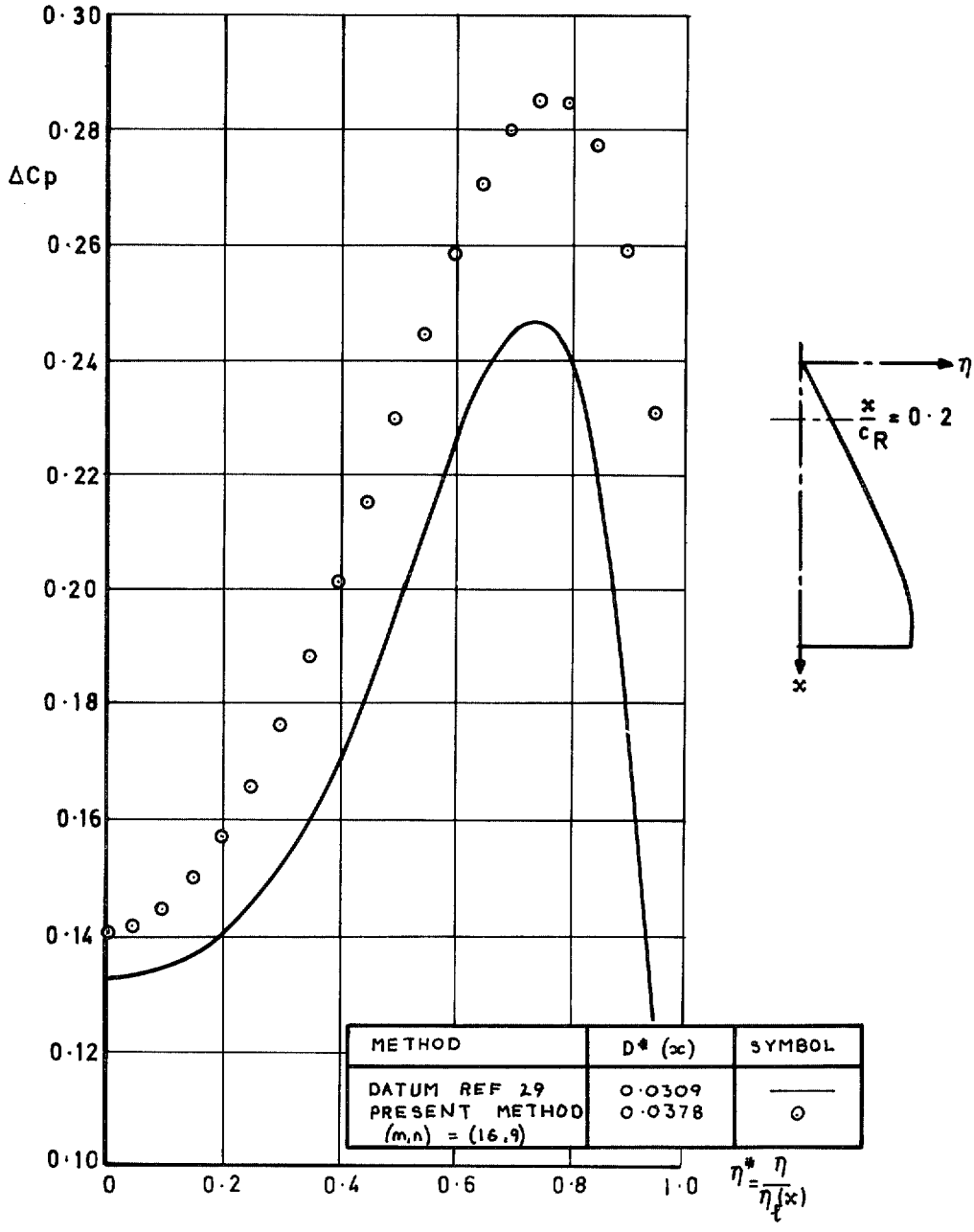

FIG. 45. Spanwise distribution of ΔCp at $x/c_R = 0{\cdot}2$ for a mild gothic cambered planform.

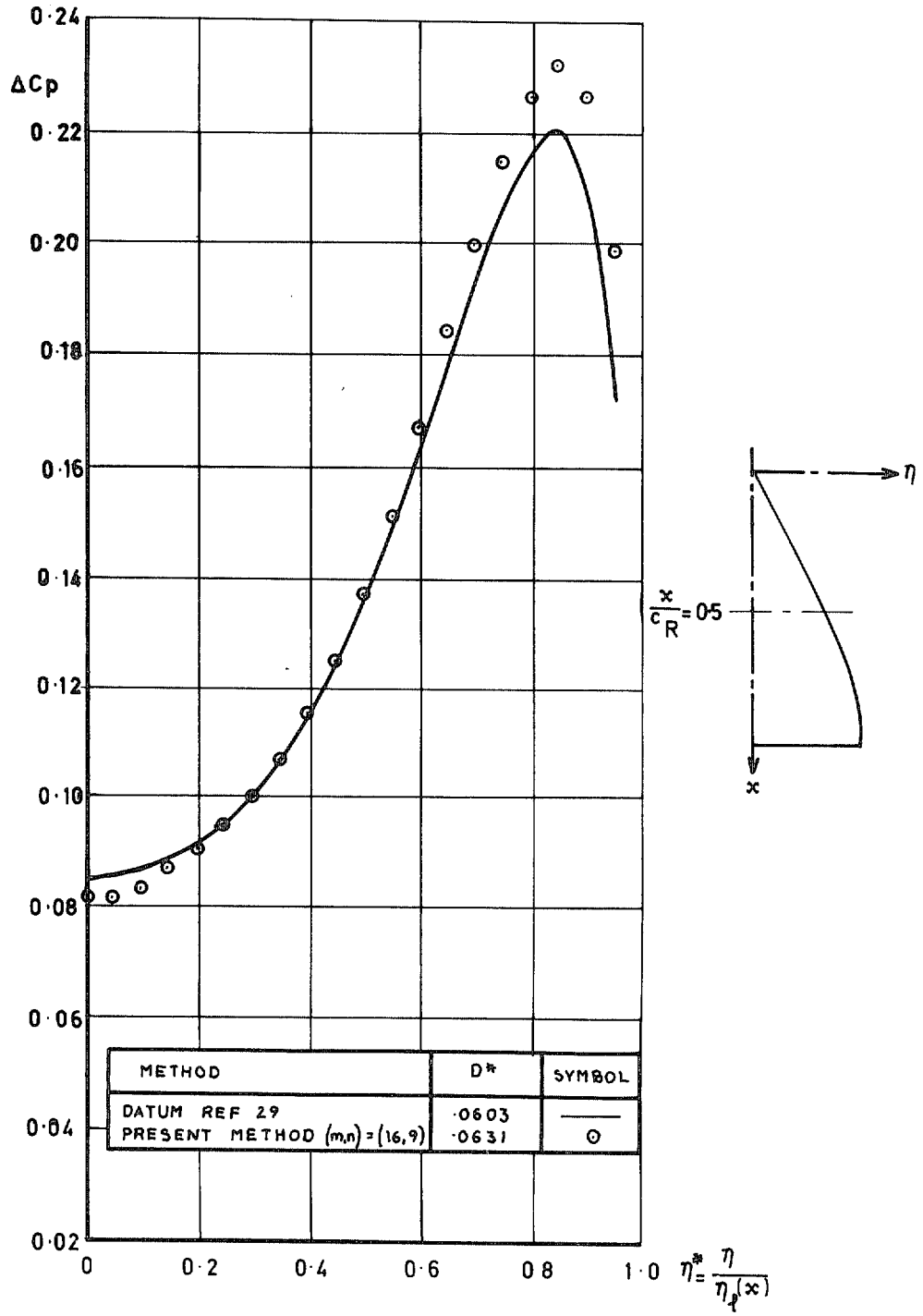

FIG. 46. Spanwise distribution of ΔCp at $x/c_R = 0{\cdot}5$ for a mild gothic cambered planform.

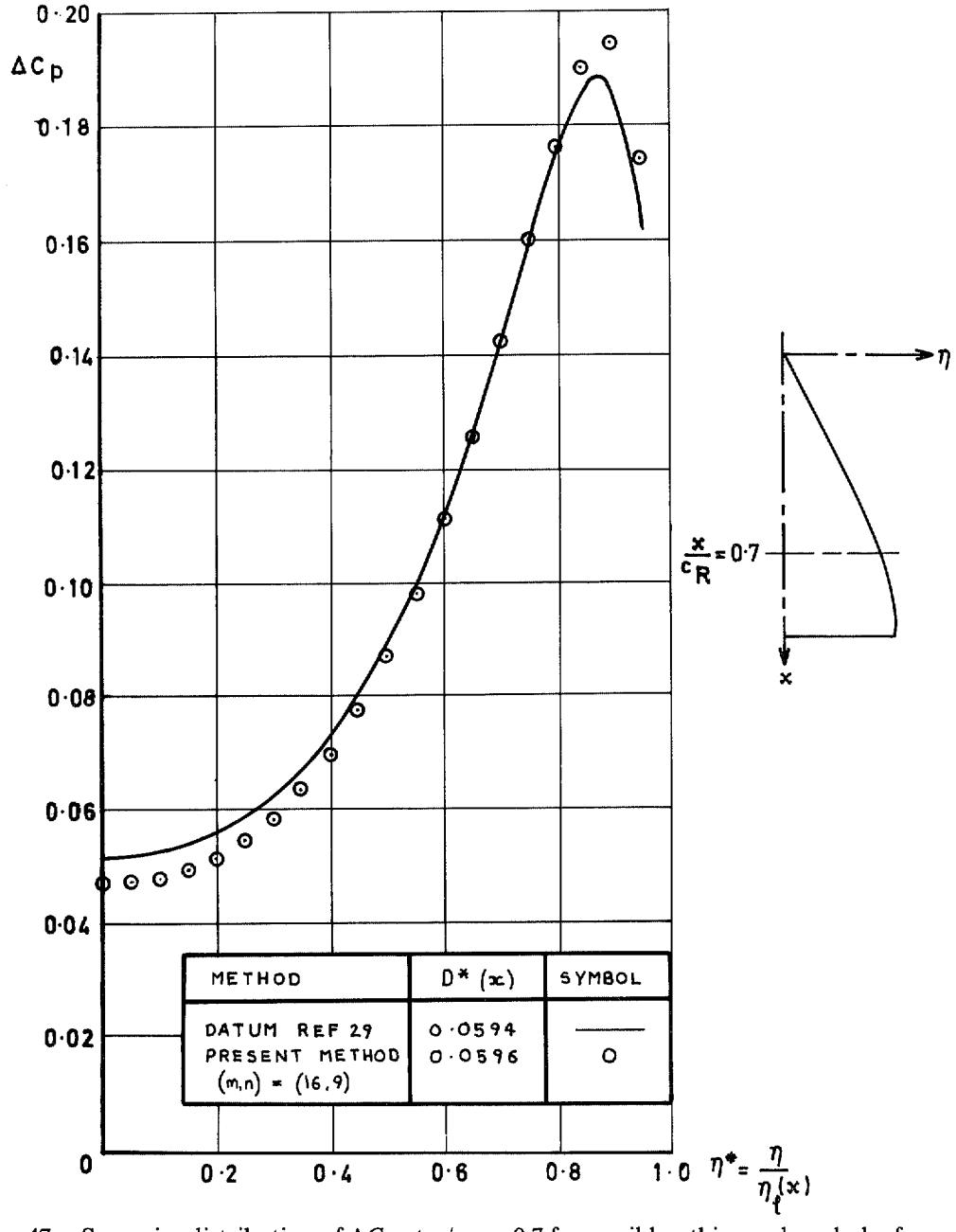

FIG. 47. Spanwise distribution of ΔCp at $x/c_R = 0{\cdot}7$ for a mild gothic cambered planform.

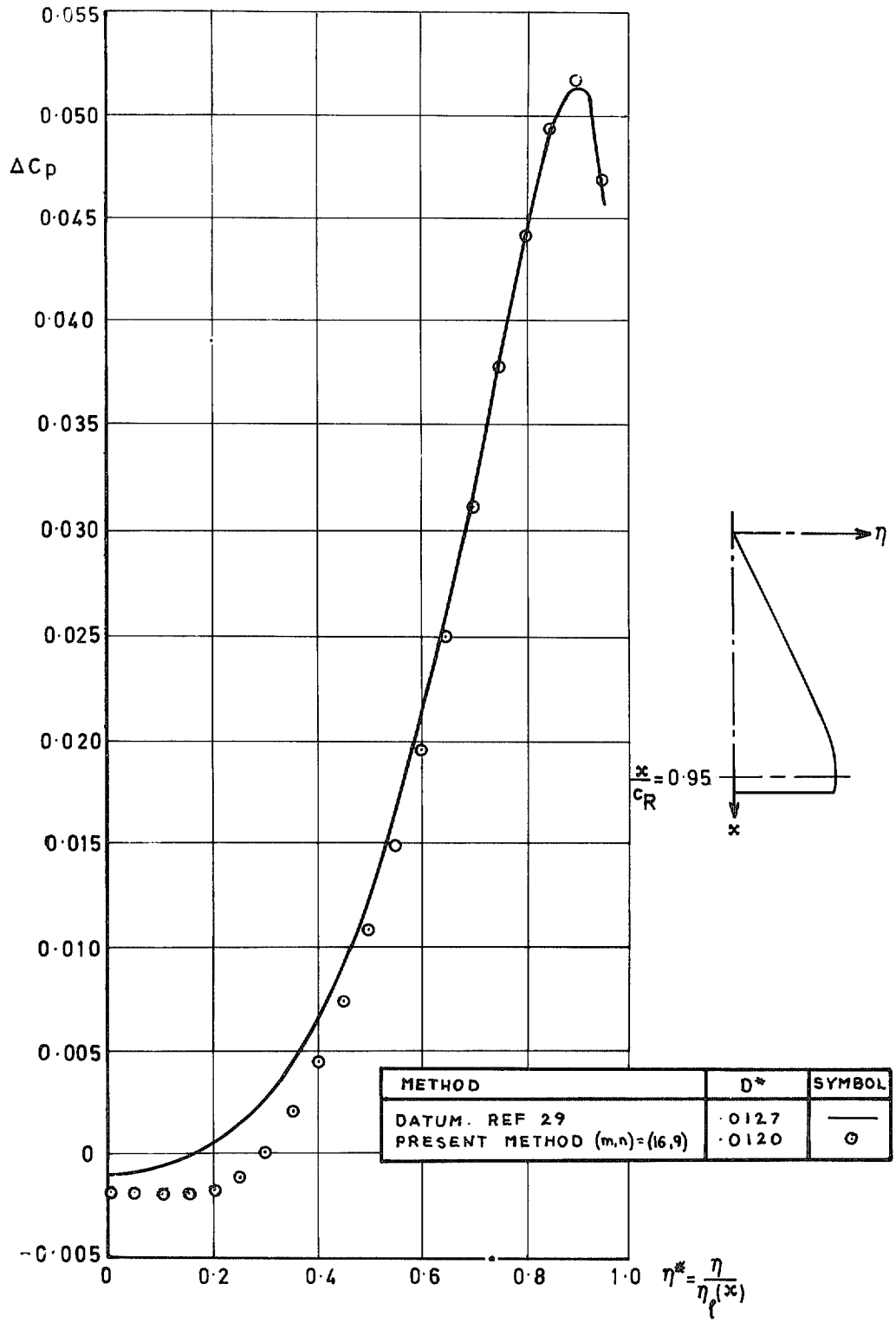

FIG. 48. Spanwise distribution of ΔCp at $x/c_R = 0{\cdot}95$ for a mild gothic cambered planform.

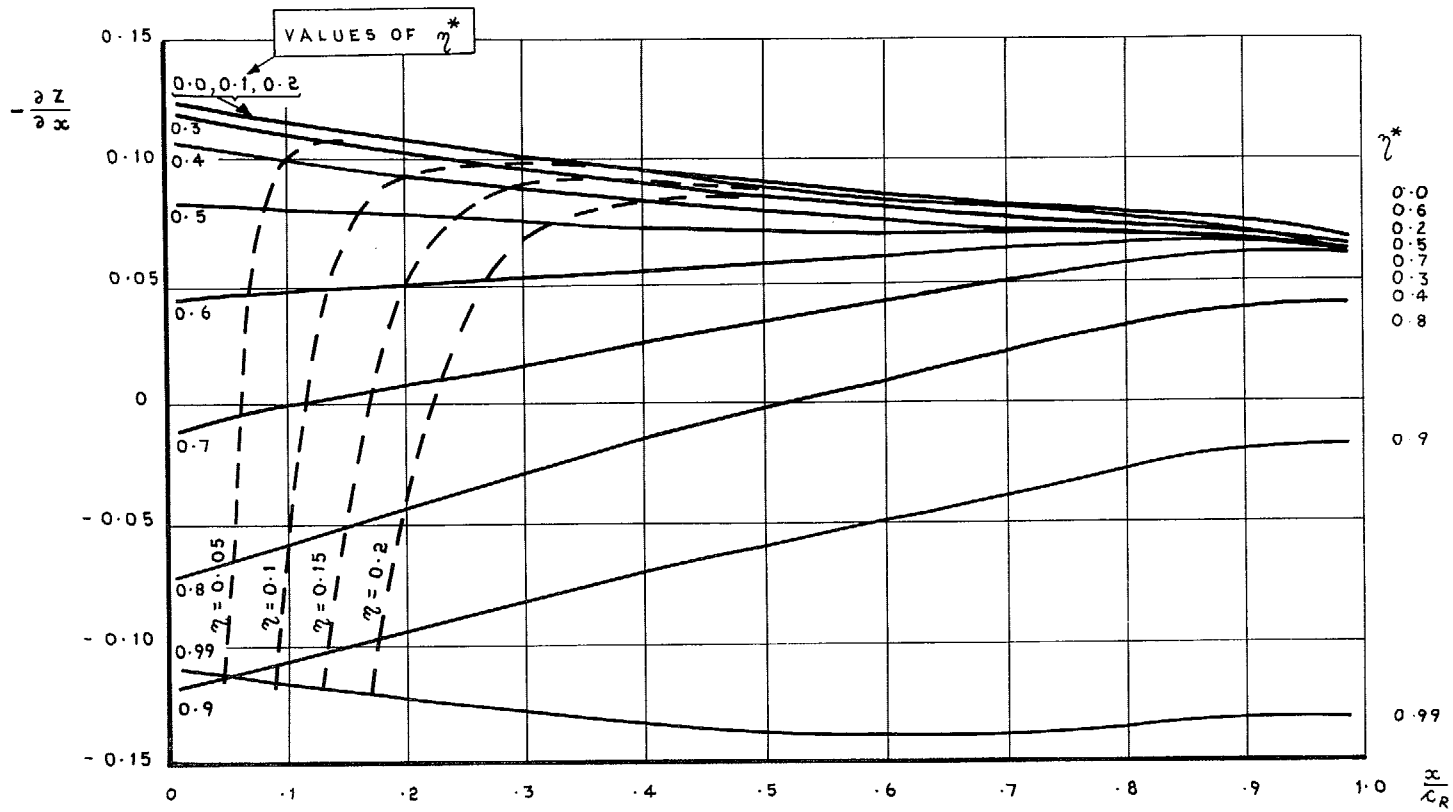

FIG. 49. The downwash distribution on the mild gothic cambered planform.

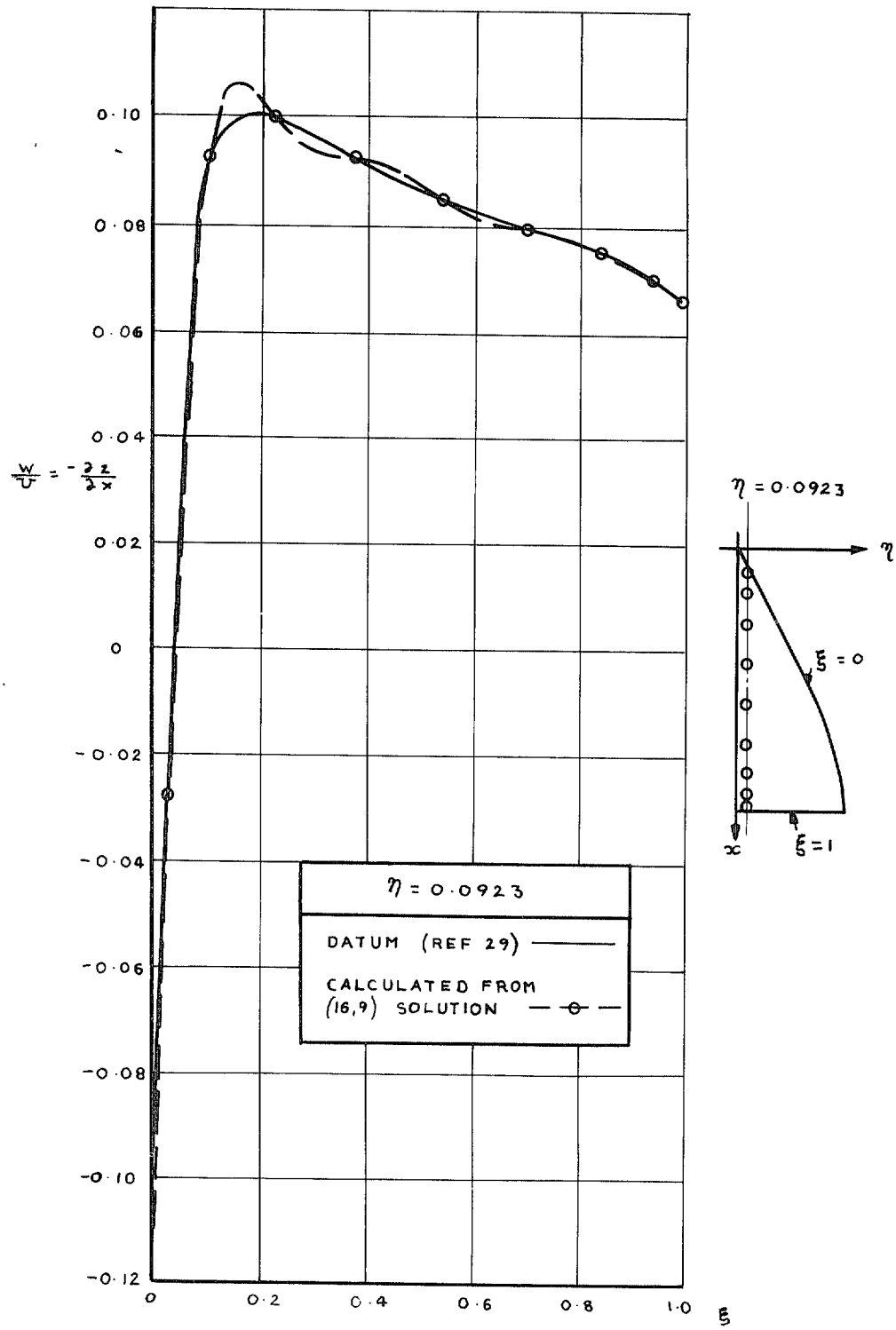

FIG. 50. Comparison of downwash variations at the first spanwise collocation station for the cambered mild gothic planform.

Printed in England for Her Majesty's Stationery Office by J. W. Arrowsmith Ltd., Bristol BS3 2NT.
Dd. 505374 K5 2/75.

HER MAJESTY'S STATIONERY OFFICE

Government Bookshops

49 High Holborn, London WC1V 6HB
13a Castle Street, Edinburgh EH2 3AR
41 The Hayes, Cardiff CF1 1JW
Brazennose Street, Manchester M60 8AS
Southey House, Wine Street, Bristol BS1 2BQ
258 Broad Street, Birmingham B1 2HE
80 Chichester Street, Belfast BT1 4JY

Government publications are also available through booksellers

ISBN 0 11 470905 X*